THE LOW FREQUENCY MICROWAVE SPECTRA OF $^{14}NH_3$ AND CARBONYL SULPHIDE

BAKSHI VIDYANAND SINHA

THE LOW FREQUENCY MICROWAVE SPECTRA OF $^{14}NH_3$ AND CARBONYL SULPHIDE

by

Bakshi Vidyanand Sinha, B.Sc.(Hons.), M.Sc.(Patna)

Submitted in partial fulfillment of
the requirements for the degree of
Master of Science

Department of Physics
Memorial University of Newfoundland
August 1978

St. John's Newfoundland

ACKNOWLEDGEMENTS

I wish to express my deep sense of gratitude to my supervisor, Professor P.D.P. Smith for his guidance and help during the course of work.

I am indebted to Dr. R. Tipping for suggesting the idea of shifting the reflection resonances within the guide.

I acknowledge the use of the computational work done by Dr. G. Pedersen and Mr. Paul Gillard of MUN to predict the $^{14}NH_3$ spectrum.

The financial support in the forms of the Memorial University of Newfoundland Graduate Fellowship and teaching assistantship is gratefully acknowledged.

ABSTRACT

Fifteen new ground state inversion lines of $^{14}NH_3$ were observed at 80^0 to 90^0C, accurately measured and assigned. The electric dipole moment computed from the Stark shifts is 1.472 ± 0.002 D, which compares well with the value 1.475 ± 0.006 D reported recently by Fujio Shimizu. Corrections were applied to K = 3 and K = 6 lines.

Nine 0→1 rotational transitions of Carbonyl Sulphide, including one Fermi pair and one triplet due to quadrupole interaction of ^{33}S nucleus were observed, accurately measured and assigned. The relative electric dipole moments of OCS in the (10^00) and (02^00) states and those of ^{18}OCS, $O^{13}CS$, $OC^{33}S$ and $OC^{34}S$ in the ground state were computed from the Stark shifts. The relative electric dipole moments for $O^{13}CS$ and $OC^{34}S$ are respectively 1.0057 and 1.0155.

A new technique to distinguish and shift the reflection resonances within the guide from the absorption lines of the gas was developed and successfully employed.

TABLE OF CONTENTS

LIST OF TABLES

LIST OF FIGURES

CHAPTER I

INTRODUCTION

Because of the intensity and richness of its spectrum, ammonia has played a major role in the development of microwave spectroscopy. It has provided a large number of easily observable lines on which to try both experimental technique and theory.

The investigation of rotational Raman and IR spectra of ammonia has shown that this molecule has pyramidal structure with the nitrogen atom at the apex and three hydrogen atoms in a triangle forming the base. The height of the pyramid, the N-H equilibrium distance, and the H-N-H angle are 0.3816×10^{-8} cm, 1.0124×10^{-8} cm, and 106.67 degrees, respectively. The moments of inertia have very small values $I^B = I^A = 2.088 \times 10^{-40}$ gm-cm^2, and $I^C = 4.4141 \times 10^{-40}$ gm-cm^2. Thus this molecule is an oblate symmetric top belonging to the C_{3v} point group. Four normal modes of vibrations are associated with this geometrical conformation. Two of them are totally symmetric non-degenerate (A_1 species) and the other two are doubly degenerate (E species) vibrations (1). They are illustrated in Fig. 1.1.

The fact that there exist two equilibrium positions of the N-atom on either side of the base, separated by a potential, gives rise to a doubling of each energy level of the whole system of rotational and vibrational states. The transitions from one of the pair of energy levels to the other for all rotational states give rise to what is called the "Inversion Spectrum" of ammonia.

Although this inversion spectrum is well studied at frequencies above 12 gHz, and good measurements continue down to 7286 MHz, yet there remain hundreds of lines below the last frequency, and some above it, which have not been observed, most probably because of their low absorptions. This situation becomes apparent on examining Fig. 2.8, which plots the frequencies predicted by an empirical formula first introduced by Costain, and shows the approximate frequencies of a multitude of lines, whose absorptions should decrease as the frequency decreases, or the angular momentum quantum number J increases.

Although there are theories, which will be mentioned in this chapter, concerned with the penetration of the ammonia molecule's central potential barrier, yet none of them are sufficiently accurate in their predictions to be really useful in microwave spectroscopy, where measurements are readily made to accuracies of a few hundredths of a Magahertz. Further, since the spectrum is crowded with lines, these theories are unable to indicate the quantum numbers of observed lines by simple comparison of the observed frequencies with their predictions. For example, the frequencies predicted by the theory of Spirko, Stone and Papousek for the lines with J = 7 differ from the observed frequencies by amounts ranging from 5% to 10% of the observed frequency, while spacing between adjacent lines varies from 3% to 11.5% of the line frequency.

Formulas of the type introduced by Costain, fitted to a group of known lines that have been accurately measured give much closer agreement with new observed lines, but it is generally found that the accuracy decreases as the quantum numbers of the line move away from those of the known group. Costain's original formulation is

not useful at these microwave frequencies below 12 gHz, but later modifications of the procedure, such as that by Schnabel et al., are useful for line identification in this range. However, without measurements such as these, there is no critique either of such theories, or of empirical approximations.

One hundred and nineteen fairly strong inversion lines of $^{14}NH_3$ in the ground state have been reported in the NBS monograph, 70, Volume IV. The absolute intensities of these lines are $\sim 10^{-8} cm^{-1}$ or greater. By raising the temperature of the gas the high rotational levels can be populated, and thus the comparatively weaker lines can also be observed. The object of the present work is to observe, assign and measure some new lines of $^{14}NH_3$. These lines are plotted on the graphs of Figs. 2.8 and 2.9. The search for lines was also extended beyond the area marked "New Lines", but it was found impossible to observe more lines with the present apparatus, because in all cases the intensity was below the limit of $2 \times 10^{-9} cm^{-1}$.

Although the ground state strongest rotational (0→1) transition line of OCS has been used in double resonance experiments (Battaglia, Gozzini and Polacco and others (25)+), there is little reference in the literature on the weaker components of the 0→1 rotational transitions arising out of other vibrational states or other isotopic species of carbonyl sulphide. Also there is no reference to the dipole moments of different isotopic species of the molecule in different vibrational states being determined. For this reason, while using the (000) 0→1 OCS line for calibration purposes, it appeared well to observe some of the adjacent lines of carbonyl sulphide and to compute the dipole moments in each case from Stark spectroscopy.

+ The author apologises that the reference (25) to (30) were introduced at the last moment, and are not in the regular numerical sequence.

MOLECULAR THEORY

1.1 Inversion

If the potential energy is plotted as a function of the distance of the N-atom from the H_3-plane, a curve of the form given is Fig. 1.2 is obtained. There is barrier of height V_1 between the two potential-wells. The nitrogen atom can tunnel through the potential barrier and so invert the molecular pyramid. The effective magnitude of the potential barrier to inversion depends on the normal mode of vibration excited and the degree of excitation. If this barrier is finite (as in NH_3) each vibrational levle G(v) is split into two component levels G(v+) and G(v-). The splitting of the levels is very much dependent on the barrier height V_1, becoming zero as the barrier becomes infinite. Because the lowest vibrational level is always symmetric, the lower member of each pair of sub-levels is symmetric and the upper is anti-symmetric to inversion. The transition between the sub-levels of the same vibrational state is called inversion. The inversion frequency can be further explained by consideration of the proper potential function.

1.2 Some Potential Functions of the Two Fold Inversion Barrier

Various potential functions for the nitrogen atom as it goes through the plane of the hydrogen atoms have been suggested by different authors, with an assumption that the inversion motion is associated with the v_2 bending mode of amonia and that the inversion problem can be formulated in terms of a single particle, moving under the influence of two fold potential, but restrained to a single co-ordinate.

Numerous theoretical papers dealing with inversion splitting differ in both the form of the potential functions used and approximations made, whi

solving the Schrödinger's equation. Thus, Dennison and Uhlenbeck (2) treated the double minimum potential problem through W.K.B. approximations for the ground as well as ν_2 excited vibrational state. The agreement for the ground state was very good and it was to within 20% for the first excited state.

Manning (3) did a complete analysis for the energy levels of NH_3 and ND_3 with the potential function

$$V(x) = -C \operatorname{sech}^2 \left(\frac{x}{2\rho}\right) + D \operatorname{sech}^4 \left(\frac{x}{2\rho}\right)$$

where C, D, and ρ are constants. The variable x is the distance of the N-atom from the plane of the H-atoms. The energy level differences obtained by him are in good agreement with experimentally observed values for NH_3. Approximate barrier heights for NH_3 and ND_3 obtained thereby were 2072 cm^{-1} and 2068 cm^{-1} respectively.

Newton and Thomas (4) chose a different potential function

$$V(y) = K(a + by^2)^2 / (1 + y^2)^2$$

where K, a and b are constants, and y is proportional to x. The W.K.B. method was used for the solution of the Schrödinger's equation. This gives results which are comparable in accuracy with those from Manning's potential. But the values calculated for the first excited state are not satisfactory.

Costain and Sutherland (5) have used a potential function which is more obviously and directly related to the molecular motion in a simple way

$$V = \frac{3}{2} k_r (\Delta r)^2 + \frac{3}{2} k_\delta (\Delta\delta)^2,$$

where Δr and $\Delta\delta$ are changes in the bond length and bond angle respectively, and k_r and k_δ are the corresponding force constants. This form of potential gives good values of the potential barrier and the inversion frequencies.

Swalen and Ibers (6) used a potential of the form

$$V(q) = \frac{1}{2} aq^2 + \frac{1}{2} bq^4 + v \exp(-cq^2),$$

where a, b, c and v are the potential constants and q is the normal coordinate of motion. The agreement between the calculated and observed values for the energy levels of NH_3 and ND_3 is far better than previously achieved.

Damburg and Propin (7) used the one-dimensional potential

$$V(x) = K (R^2 - x^2)^2 / 8R^2,$$

where 2R is the distance between the minima of the two potential wells.

Davis and Christoffersen (8) obtained the exact solution for a one-dimensional time-independent Schrödinger's equation with a symmetric double minimum potential constructed from two Morse potentials.

1.3 Vibration-Inversion Interaction

All the theoretical papers listed above have aimed at predicting the dependence of the inversion splitting on the quantum number n_2 associated with the ν_2 mode in which the pyramid height changes most drastically. The relative success of the one-dimensional treatment comes from the fact that the ν_2-normal mode is primarily involved in inversion. But other normal modes of vibration also affect the inversion considerably. This was first realised by Weeks et al (9). They used potential energy consisting of a double minimum potential involving the inversion-coordinate, plus the potential of a system of five uncoupled oscillators representing the remaining five vibrational degrees of freedom.

$$V = V_0(x) + \frac{1}{2} \sum_{i=1}^{5} C_i q_i^2$$

The summation is over the remaining five vibrational modes and q_i is the appropriate vibrational coordinate. The form of the potential used by them is

$$V_o(x) = -2F \cos\left(\frac{x}{L}\right) + 2G \cos\left(\frac{2x}{L}\right)$$

for $|x| \leq \pi L$

and $V_o(x) = 2(F + G)$

for $\pi L < |x| < \infty$ **

F, G and L are positive, and the two minima occur at $\cos\left(\frac{x_o}{L}\right) = \frac{F}{4G}$. F and G are assumed to be mild functions of the remaining vibrational coordinates and can be expressed in a Taylor series for small vibrational amplitude.

The current available data on the inversion-splitting in $^{14}NH_3$ (10) are summarised in Table 1.1. An energy level diagram for low lying vibrations is shown in Fig. 1.3.

V. Spirko et al (11) have also developed an effective inversion rotation Hamiltonian to describe the centrifugal distortion and Coriolis interactions in the ground and excited vibration-inversion states of ammonia, but that does not work well in the microwave region.

1.4 Effects of Rotation on the Inversion Spectrum of Ammonia

The fact that the molecule is rotating causes the pure inversion spectrum to be split into a large number of lines, each line corresponding with a given J,K state of a symmetric top molecule. J is the quantum number which represents the total angular momentum of the molecule and the quantum number K represents the component of the total angular momentum along the symmetry axis.

The rotational structure was first resolved by Bleany and Penrose (12), and theoretically explained by Sheng et al (13). They expressed

---

** In the paper by Weeks et al ∞ was given as $\frac{\pi}{2}$; a misprint.

the observed frequencies in the form

$$\nu = \nu_o + aJ(J+1) + bK^2 + cJ^2(J+1)^2 + dJ(J+1)K^2 + eK^4 + \ldots$$

This fits the low J and K values better than the high.

Costain (14), applying the exponential dependence of inversion splittings in the Uhlenbeck-Dennison potential, was able to fit a large number of lines to a six-constant semi-empirical formula of the form

$$\nu = \nu_o \exp [AJ(J+1) + BK^2 + CJ^2(J+1)^2 + DJ(J+1)K + EK^4]$$

This formula always gives ν positive, contrary to Sheng's formula. This fits all lines in the ground state with $J \leq 16$ to within 1.3 MHz except for the lines with $K = 3n$, where $n = 1, 2, 3, \ldots$.

Schnabel *et al* (15) extended Costain's formula upto higher powers viz., $J^5(J+1)^5$ and K^{10} and were able to fit 95 lines of $^{14}NH_3$ and 46 lines of $^{15}NH_3$ with an accuracy within 0.48 MHz and 0.39 MHz respectively.

The anomalous deviations of $K = 3$ lines from the above formulae have been explained by Nielsen and Dennison (16) on the basis of splitting of $|K| = 3$ levels by a vibration-rotation interaction. They derived a formula for the doublet splitting of $|K| = 3$ levels.

$$\Delta\nu = (-1)^J \alpha J(J+1)[J(J+1) - 2][J(J+1) - 6]$$

where α was called a rotation-vibration constant, but it is really a function of $J(J+1)$.

1.5 Selection Rules

The selection rules for pure inversion transitions in a symmetric top molecule are

$\Delta J = 0$ $\qquad$ $\Delta K = 0$

$+ \longrightarrow -$ $\qquad$ $+ \not\longrightarrow +$ $\qquad$ $- \not\longrightarrow -$

1.6 Stark Effect

When an electric field is applied to a polar gas, it interacts with the electric dipole, causing a splitting of the rotational energy levels,

which results in the appearance of fine structure of the rotational level spectrum. This is known as Stark effect.

The electric dipole moment can be represented by a vector $\vec{\mu}$ whose magnitude is measured by the distribution of charge in the molecule and the distance between the centres of the charges, i.e.

$$\vec{\mu} = \sum_i e_i \vec{r}_i$$

where e_i is the charge on the i^{th} particle and $\vec{r}_i$ is the vector distance of the i^{th} particle from the origin of a coordinate system fixed in the molecule. The summation is over all the nuclei and the electrons in the molecule.

If the stark effect perturbation is considerably smaller than the rotational energy level spacing, perturbation theory can be used to calculate the Stark splittings. The perturbation term $H^{(1)}$ is the interaction energy between the electric field $\vec{E}$ and the molecular dipole moment $\vec{\mu}$. The interaction-energy is expressed as

$$H^{(1)} = -\vec{\mu} \cdot \vec{E}$$

The first order perturbation energies are obtained from an average of the perturbation term $H^{(1)}$ in the Hamiltonian

$$H = H^{(0)} + H^{(1)}$$

over the unperturbed state, i.e.,

$$E_J^{(1)} = \int \Psi_J^{(0)} \, H^{(1)} \, \Psi_J^{(0)*} \, d\tau,$$

where the $\Psi_J^{(0)}$ is the wave function for the unperturbed rotor, and $H^{(0)}$ is the Hamiltonian for the field-free rotor.

The second-order energies are

$$E_J^{(2)} = \sum_{J \neq J'} \frac{[\int \Psi_J^{(0)} \, H^{(1)} \, \Psi_{J'}^{(0)*} \, d\tau] \, [\int \Psi_{J'}^{(0)} \, H^{(1)} \, \Psi_J^{(0)*} \, d\tau]}{E_J^{(0)} - E_{J'}^{(0)}}$$

The transitions involving inversion obey the selection rule

$$\Delta J = 0, \quad \Delta K = 0, \quad \Delta M = 0. \quad K \neq 0$$

where M is the quantum number pertaining to the projection of J in the E-direction. The Stark effect of the inversion doubling of ammonia represents a special case in the sense that the dipole-moment of ammonia is only "semi-permanent" because of the inversion splitting. Hence it does not show the first order Stark effect. The second order Stark shift of ammonia is given by (17)

$$\Delta\nu = \frac{0.5065\ \mu^2\ E^2}{\nu_Q} \quad [\frac{KM}{J(J+1)}]^2$$

where ν is in MHz, μ in Debye units, and E in volts per cm. Because the E^2 contributions to energy are degenerate in $\pm E$, only J+1 resolvable Stark lines result. All levels for $M \neq 0$ are doubly degenerate in $\pm M$. The maximum splitting occurs for M = J.

The expression for the Stark shift for 0→1 rotational transitions of OCS is given by (27)

$$\Delta\nu = \frac{0.1351\ \mu^2 E^2}{\nu_o}$$

For this transition there is only one Stark component, whose integrated intensity equals that of the normal line. This is an advantage in the measurements of the dipole and quadrupole moments of the carbonyl sulphide molecule.

1.7 Rotational Spectra of Linear Polyatomic Molecules

Molecules with permanent electric dipole moments give rotational spectra, and for these the selection rule is $\Delta J = \pm 1$. This gives for the change J → J+1

$$\nu = 2\ B_v(J+1) - 4\ D_v(J+1)^3$$

B_v, the effective rotational parameter for the vibrational state v, is given by

$$B_v = B_e - \sum_i \alpha_i (v_i + \frac{d_i}{2})$$

where B_e is the rotational constant for equilibrium configuration. The summation extends over all vibrations with the degenerate ones included only once. v_i is the vibrational quantum number and d_i is the degree of degeneracy for the i^{th} mode of vibration. For a non-degenerate mode $d_i = 1$, for a doubly degenerate mode $d_i = 2$, etc. D_v is the centrifugal distortion constant for the vibrational state.v. α_i is a small constant which measures the correction in B for that mode.

1.8 Fermi Resonance

In a polyatomic molecule it may happen that two vibrational levels belonging to different vibrations (or combinations of vibrations) may have nearly the same energy, that is, may be accidently degenerate. As was first recognized by Fermi in the case of CO_2, such "resonance" leads to a perturbation of the energy levels. The calculation of these perturbations is a standard method of quantum mechanics provided that the perturbation function is known.

The perturbation depends on the value of the matrix element W_{ni} of the perturbation function W,

$$W_{ni} = \int \psi_n^{o} \, W \, \psi_i'^{o} \, d\tau \qquad (1)$$

The perturbation function W is here essentially given by the anharmonic terms in the potential energy, while ψ_n^o and $\psi_i'^o$ are the zero approximation eigen functions of the two vibrational levels that perturb each

other. Since W is totally symmetric, W_{ni} will be zero unless ψ_n^o and ψ_i^o are of the same species (i.e., of the same symmetry type).

If the resonance is fairly close, the magnitude of the shift can be obtained according to the first-order perturbation theory from the secular determinant

$$\begin{vmatrix} E_n^o - E & W_{in} \\ W_{ni} & E_i^o - E \end{vmatrix} = 0 \qquad (2)$$

where E_n^o and E_i^o are the unperturbed energies.

The separation of the perturbed levels is given by

$$\Delta W = (4|W_{ni}|^2 + \delta^2)^{\frac{1}{2}} \qquad (3)$$

where $\delta = E_n^o - E_i^o$ is the separation between the unperturbed levels.

Most of the pairs of OCS levels which pertrub each other are those with quantum numbers $(v_1, v_2^{/\ell/}, v_3)$ and $(v_1-1, v_2+2^{/\ell/}, v_3)$. Such a pair of levels will be designated by subscript 1 and 2, respectively. The first pair of perturbing levels in OCS are $(1,0^o,0)$ and $(0,2^o,0)$. It can be shown that

$$W_{12} = k\{v_1[(v_2+2)^2-\ell^2]\}^{\frac{1}{2}} \qquad (4)$$

where W_{12} is the interaction energy and k is a constant for a given molecule. The perturbed wave functions are a mixture of the unperturbed wave functions and are given by

$$\psi_1 = a\,\psi_1^o - b\psi_2^o, \quad \psi_2 = b\psi_1^o + a\psi_2^o, \qquad (5)$$

where $$a = \frac{[[\delta^2 + 4|W_{12}|^2]^{\frac{1}{2}} + \delta]^{\frac{1}{2}}}{2[\delta^2 + 4|W_{12}|^2]^{\frac{1}{2}}}$$

$$b = \frac{\left[[\delta^2 + 4|W_{12}|^2]^{\frac{1}{2}} - \delta\right]^{\frac{1}{2}}}{2[\delta^2 + 4|W_{12}|^2]^{\frac{1}{2}}} \qquad (6)$$

The actual B values of the interacting levels are given by

$$B_1 = a^2 B_1^o + b^2 B_2^o, \qquad B_2 = b^2 B_1^o + a^2 B_2^o \qquad (7)$$

since $a^2 + b^2 = 1$

$$B_1 + B_2 = B_1^o + B_2^o \qquad (8)$$

The unperturbed value of α_2 is found from the separation between the rotational levels of states (000) and ($01^{\circ}0$). The frequency shift of the ($02^{\circ}0$) level due to Fermi resonance may be obtained from the known value of α_2. The unperturbed value of α_1 may be determined since the frequency change of the (100) state must be equal and opposite to that of ($02^{\circ}0$). Then from equation (7) a^2 and b^2 can be calculated and W_{12} obtained using equation (6).

1.9 Quadrupole Interaction by a Single Coupling Nucleus

If a system contains a quadrupole nucleus, the interaction of the quadrupole with the external electrons couples together the nuclear spin $\vec{I}$ and the rotational angular momentum $\vec{J}$ to form a resultant $\vec{F}$, where the quantum number F takes one of the values

$$F = J + I, \quad J + I - 1, \quad \ldots \quad |J - I|.$$

From quantum mechanical considerations the first-order quadrupole coupling energies for a single coupling nucleus in a linear molecule are shown to be

$$E_q = - (eqQ)\, Y\, (J, I, F)$$

where (eqQ) is referred to as the quadrupole coupling constant, and

and Y(J, I, F) as the Casimer function.

$$Y(J, I, F) = \frac{3/4\ C(C+1) - I(I+1)\cdot J(J+1)}{2(2J-1)\ (2J+3)\ I(2I-1)}$$

and $C = F(F+1) - I(I+1) - J(J+1)$.

The selection rules for hyperfine transitions in rotational absorption spectra are

$$\Delta J = +1, \quad \Delta F = 0, \pm 1, \quad \Delta I = 0.$$

The rotational frequencies perturbed by quadrupole coupling are given by

$$\nu = \nu_o - (eqQ)\ [Y(J+1, I, F') - Y(J, I, F)]$$

where ν_o is the unperturbed rotational frequency, and F' corresponds to the lower state relative to the rotational level without hyperfine structure.

Note- The sections 1.6 through 1.9 are condensed from the following books :

Microwave Spectroscopy , C.H. Townes and A.L. Schawlow, Mc Graw-Hill Book Co., 1955

Rotational Spectra and Molecular Structure, James E. Wollrab, Academic Press, 1967

Microwave Molecular Spectra, W.Gordy and R. Cook, Interscience Publishers, 1970

TABLE 1.1 Vibration-Inversion-Rotation Dependence in $^{14}NH_3$

$$\Delta_n = \Delta_n^{o} + (B_n^{-} - B_n^{+})\,[J(J+1) - K^2] + (C_n^{-} - C_n^{+})\,K^2$$

Level				Inversion splitting		
v_1	v_2	$v_3^{\ell_3}$	$v_4^{\ell_4}$	Δ_n^{o} (cm^{-1})	$B_n^{-} - B_n^{+}$	$C_n^{-} - C_n^{+}$
0	0	0^{o}	0^{o}	0.793	-0.005054	0.001998
0	1	0^{o}	0^{o}	35.81	-0.1817	0.0721
0	2	0^{o}	0^{o}	284.56	-0.535	0.231
0	3	0^{o}	0^{o}	512.02	-0.3041	0.1034
0	0	1^{1}	0	0.35	-0.0036	0.0007
0	0	0	1^{1}	1.01	+0.048	0.011
1	0	0^{o}	0^{o}	0.99	-0.012	0.003
0	0	2^{2}	0^{o}	0.43	---	---
0	0	1^{1}	1^{1}	0.57	---	---
1	0	0^{o}	1^{1}	0.86	---	---

Ref. (10).

The inversion splitting in cm^{-1} correspond to the energy differences of $hc\Delta_n$ in ergs.

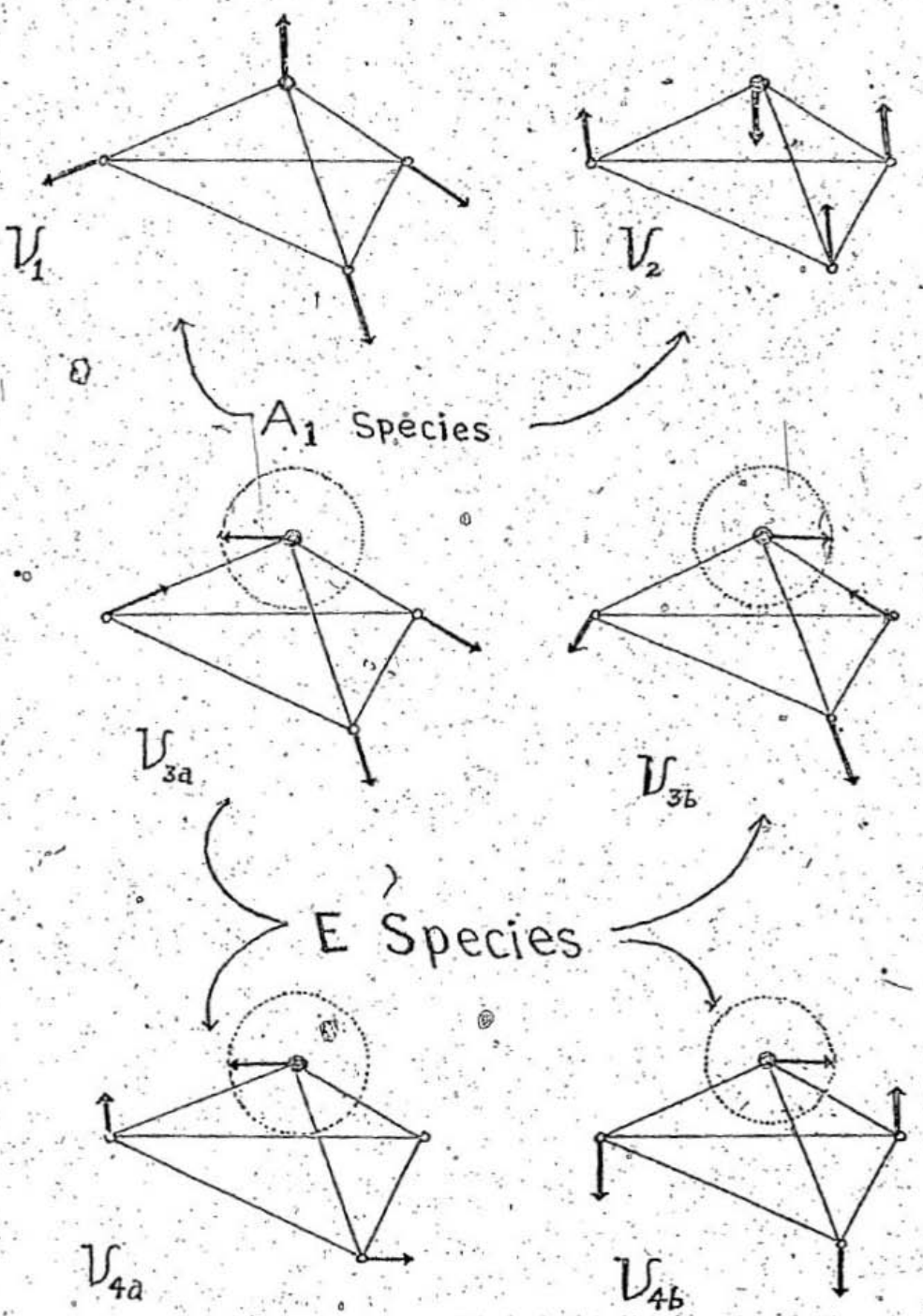

Fig. 1.1 Normal modes of vibration of $^{14}NH_3$ molecule

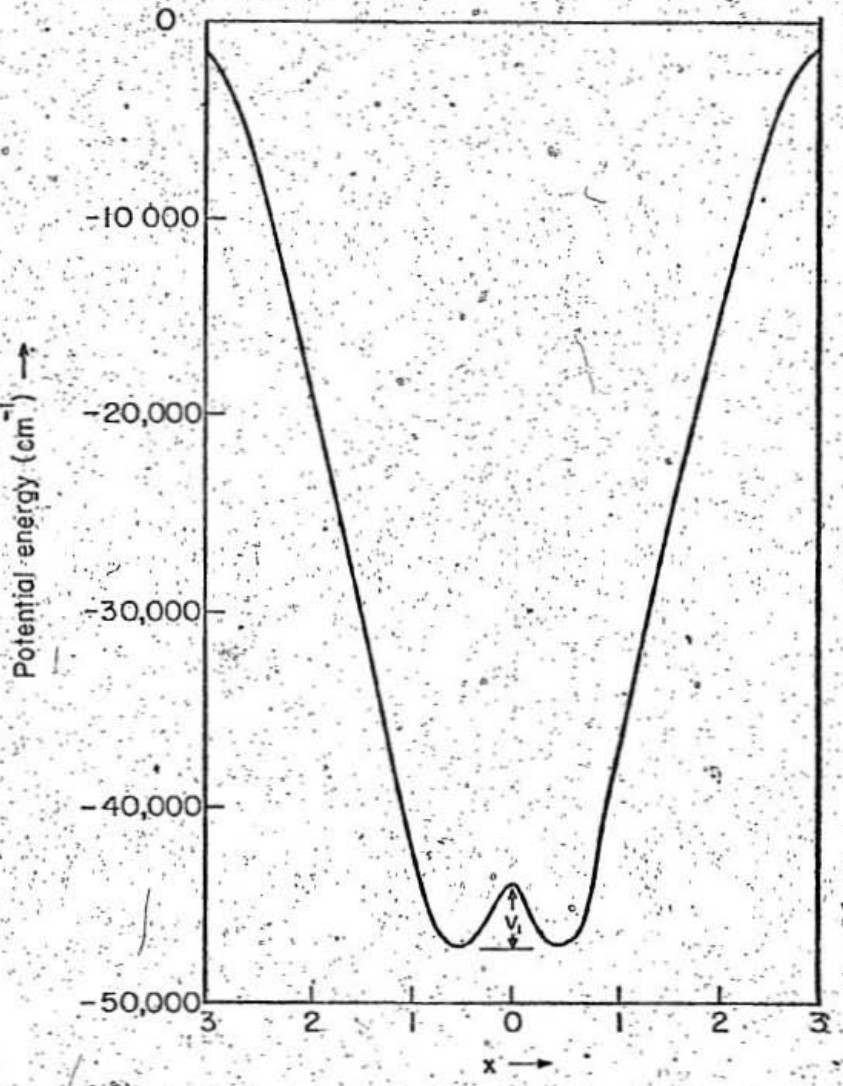

Fig. 1.2 Potential Curve for NH_3

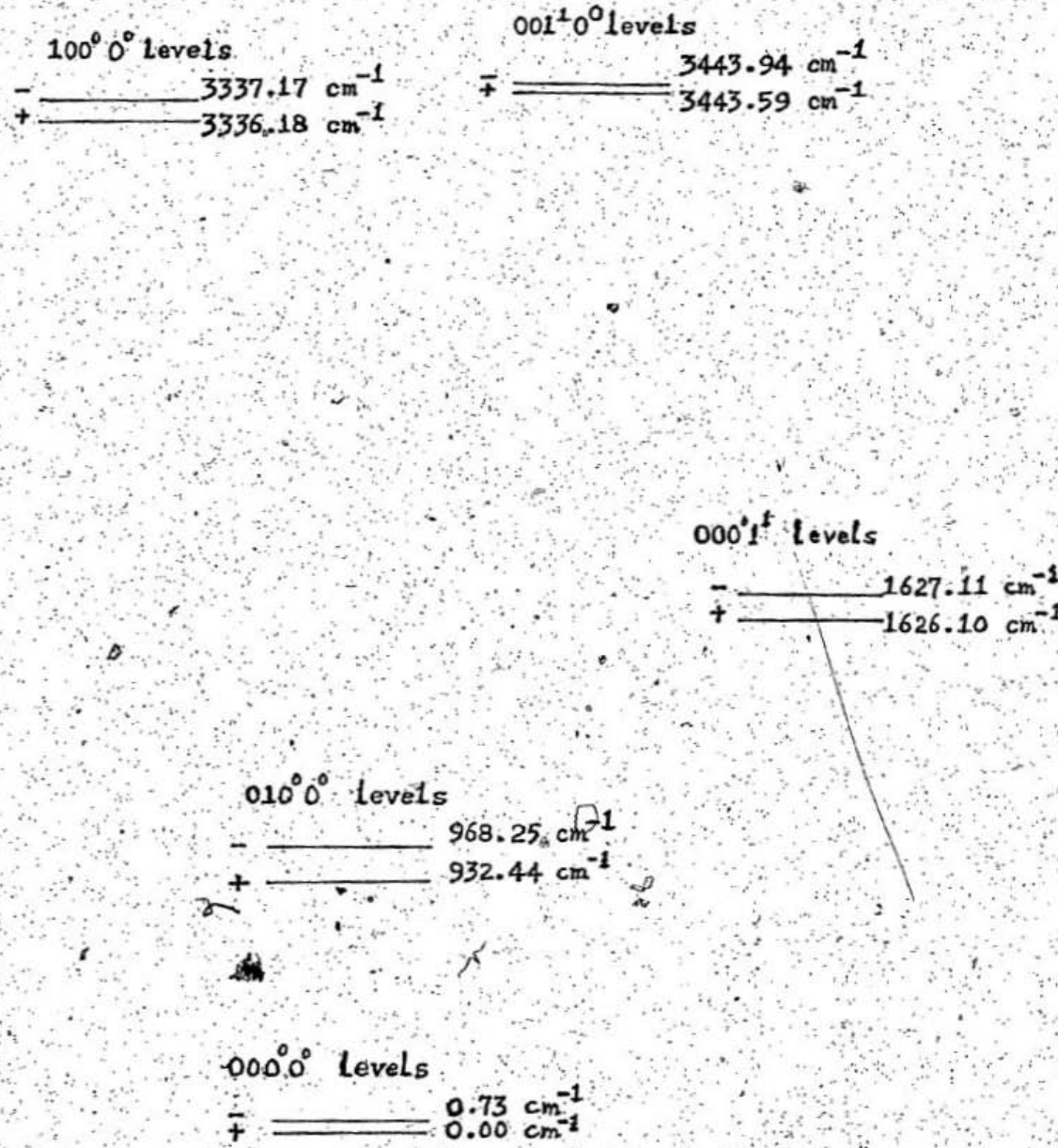

Fig. 1.3 Energy level diagram for inversion splittings of different modes of vibration of $N^{14}H_3$

CHAPTER II

EXPERIMENTAL APPARATUS AND TECHNIQUE

2.1 Description and Discussion of Components

A microwave spectrometer essentially consists of (1) a source of monochromatic radiation with proper frequency-range, (2) a frequency-monitor, (3) an absorption cell containing the gas under investigation, (4) a detector, and (5) a device for spectral presentation. In this section a brief description of these components will be given.

2.1a Sources

The microwave radiation sources employed here were two Watkins-Johnson Backward Wave Oscillators, model WJ 2020-2 and WJ 2019-1, using the X and J bands respectively. The J band has frequency range from 4.0 to 8.0 GHz and the X band, from 8.0 to 12.4 GHz. The power output from these oscillators is 50 to 100mW. These B.W. Oscillators were mounted in the Hewlett-Packard Sweep Oscillator, Model 8690 A. The frequency-sweep was controlled by varying the electrode voltage of the B.W.O. tube by means of a 50 K ohm ten-turn potentiometer, connected to the shaft of a 4 to 24 volts D.C. motor. It was possible to obtain a wide variety of slow sweep rates by varying the driving voltage of the motor or by adjusting Δf of the sweep oscillator.

2.1b Frequency Measurement

A portion of the microwave power output from the B.W. Oscillator is coupled out to the frequency measuring device by means of a 10 db-directional coupler The frequency is measured on a Hewlett-Packard Electronic Counter, Model 5245 L,

equipped with the Hewlett-Packard frequency converter (3 to 12.4 GHz), Model 5255 A.

The major portion of the microwave power goes to the absorption cell via variable attenuator and a series of waveguide sections.

2.1c The Absorption Cells

The absorption cells were made of ten-foot pieces of S-band waveguide of interior dimensions 2.840" x 1.340", with a central flat plate (called the Stark electrode) parallel to the broad faces of the guide and so perpendicular to the microwave electric field. In one of the cells the plate is supported by strips of teflon in which guiding grooves are milled (Fig. 2.1). In the other absorption cell the plate is supported on six equidistant pillars of insulating material. Connection to the Stark electrode is made by a brass rod through a hermetic seal in the side-wall of the cell, which terminates in a screw threaded into the plate. By mounting the Stark electrode parallel to the broad faces of the guide, interference with the propagating radiation is reduced to the minimum, as the microwave electric field in the dominant TE_{10} mode is always perpendicular to the electrode. Nevertheless, the presence of the electrode results in appreciable attenuation and also tends to produce reflections. The latter are reduced somewhat by tapering the ends of the electrode, as shown in Fig. 2.1a. The absorption cells are sealed at the ends with Mylar windows, supported on rubber 'O' rings. The cells are constructed of oversized waveguide so as to virtually eliminate saturation broadening. Tapered transition sections of waveguides are attached to the ends to facilitate further attachment of the appropriate X and J band equipment. The interior dimensions of the X and J band waveguides are 0.900" x 0.400" and 1.372" x 0.622", respectively. The

cut-off frequencies for the dominant TE_{10} mode for the S, J, and X band waveguides are 2.078 GHz, 4.301 GHz and 6.557 GHz respectively.

It is common practice to use oversized guide, such as S band guide, for the main absorption cell to avoid saturating the molecules with excessive radiation, (also to avoid excessive guide losses in the case where the frequencies exceed 20 gHz). Quoting from Walter Gordy, "Since there are no couplers, T-sections, slots, etc. in the absorption cell, it is possible to use oversized guide without exciting unwanted modes. ..... Here at Duke we have used S-band guide (3" x 1½") very effectively for absorption cells in the region from 3 to 5 mm wave-length. ..... In other regions oversized cells are desirable to avoid saturating the molecules with radiation."(29)

It is, of course, necessary to connect the different sized guides with horns, or tapered sections of guide, and this has been the practice in microwave spectroscopy for many years. In the case mentioned by Walter Gordy the ratio of the S-band width to that of the 3 to 5 mm band guide would have been 2.84"/0.11" = 25.8, while in this laboratory the ratio is only 2.84"/0.90" = 3.16, yet Gordy stated that they had "no more than the usual trouble with reflections".

The microwave power passes, as shown in Fig. 2.5 through a directional coupler, a variable attenuator, a series of tapered matching waveguide sections, and then into the absorption cell, which holds a small sample of the gas. The attenuators control the amount of micorwave power allowed to pass through the absorption cell, and also attenuate the unwanted reflected waves generated chiefly at the ends of the Stark electrode and at the windows. The directional coupler placed directly after the source does not provide any appreciable attenuation between source and detector, but provides 1% of the microwave power to the frequency meter for frequency measurement.

2.1d Vacuum System

The cells were directly connected to a vacuum system by an outlet through their broad sides about one third along their length. The vacuum system (Fig. 2.2) consisted of a number of stop-cocks and cold traps of glass. The vacuum system and the absorption cells were evacuated by a rotary oil pump (Welch Vacuum Pump, Model 1402). A liquid nitrogen trap was used to condense most of the gas in the cold trap before it reached the pump. The trapped gas was transferred to a glass bulb fitted with stop-cock and stored therin for future use. Pressure was measured with a Hastings Vacuum Gauge, Model SV-1, which was calibrated with a McLeod Gauge. The calibration curve is reproduced in Fig. 2.6.

2.1e Signal Modulation

If an electric field is applied to a polar molecule its absorption frequencies are shifted because of the Stark effect. If at some instant the B.W. Oscillator frequency coincides with that of an absorption line, and a periodic electric field is applied, then there will be a corresponding time variation in the power detected by the crystal, since the Stark components of the line are shifted relative to the source frequency. The switching can be done electronically at radio frequency, and the resulting modulation of the microwave power absorbed by the gas can then be detected by a radio receiver tuned to the modulating frequency. This is the principle of the Stark modulation spectrometer introduced by Hughes and Williams (18).

In addition to increasing sensitivity by avoiding low frequency noise, this method allows the detection of the absorption line, eliminating to a great extent the detection of the spurious signals arising out of mismatch in the microwave line.*

In the present experimental set up, the signal was amplitude modulated by a zero-based 100 K Hz square wave generator, manufactured by Industrial Components Incorporated. The voltage was continuously variable up to 2000 volts. The source oscillator was electrically swept over the absorption line at a rate which was slow compared to the modulation frequency, so that the absorption line was detected and displayed in the usual manner. In course of the sweep, when the oscillator frequency coincided with the frequency of some Stark line, the latter was detected and displayed inverted relative to the zero-field line. This was made possible by the use of a phase-sensitive detector. The Stark pattern was then used to identify the transition and evaluate the dipole moment.

*The amplifier is tuned to 100 KHz and the phase-sensitive detector used with a band width of either 1.0 or 0.1 Hz.

2.1f Detection

The output from the absorption cell was detected by Hewlett-Packard Crystal Detector, Model X424 or J424A (negative biased). The output of the crystal detector was fed into a preamplifier, and then to a receiver tuned to 100 KHz (both manufactured by Industrial Components Incorporated).

The crystal itself consists of a small piece of a semiconductor material, in contact with a fine tungsten whisker. Such a system behaves as a rectifier for current at microwave frequencies. The crystal is mounted on a holder whose outer casing is in contact with the waveguide walls. The inner conductor, to which the tungsten whisker is connected, leads across the waveguide, and so acts as the antenna for collecting microwave radiation, and the rectified output signal passes to the coaxial B.N.C. connector. The assemply of the X424A crystal detector is shown in Fig. 2.3.

2.1 g Display

For the display of the output signal from the 100 KHz receiver either a Hewlett-Packard 7035A X-Y recorder or a 7100B strip chart recorder was used. For the preliminary search of the absorption lines the X-Y recorder , and for the final analysis of the lines the strip-chart recorder was used. The complete block diagram of the microwave spectrograph is shown in Fig.2.5.

2.2 Experimental Technique

2.2a Search of Lines

The absorption cell and the glassware were normally evacuated to a pressure of 0.002 torr. In fact, the pumping out operation was continued for

several days by intermittent heating of the guide to ensure that the absorption cell and the rest of the vacuum system were completely free from any trace of absorbed gases. Further, the absorption cell was flushed several times with 99.99% $^{14}NH_3$ gas supplied by Matheson of Canada Ltd. by letting in the gas through the inlet. Each flush was followed by evacuation of the vacuum system. This process was repeated several times to ensure that very little of any foreign gas remained in the absorption cell and the glass wares.

Finally, a fresh sample of ammonia gas from the bottle was introduced into the absorption cell until the pressure rose up to 1 torr. Then the excess of the gas was removed from the cell by pumping it out and cooling in the trap until the pressure went down to the optimum level, i.e., to 0.01 torr.

Using the formula given by Schnabel et al. (15), an empirical spectrum was generated. The intensities of these lines at 100°C were also calculated. After raising the temperature of the guide to about 90°C, search for those lines whose theoretical intensities were of the order of 2×10^{-9} cm^{-1}, was made on a slow-sweep chart recorder. The temperature could not be raised further, as the seals in the absorption cell started leaking at higher temperatures.

2.2b Identification of Reflection Resonance-Lines

To identify the resonance-lines within the guide, the absorption cell was highly evacuated with intermittent heating so as to leave little trace of $^{14}NH_3$ gas in the vacuum system. The output voltage of the crystal was directly fed to the X-Y recorder, and again a sweep was taken at the steps of 100 MHz for the frequency range 4.0 to 12.4 GHz as done previously with the gas in the cells. Many lines reappeared with diminished intensity. These were, possibly, the resonance lines within the guide. As a further check on the nature of the origin of these lines, the experiment was repeated after raising the temperature of the guide by 50° to 60°C. These lines appeared again, but were displaced to the lower frequency side by an amount, which depended on the thermal expansion of the guide. As explained below, this frequency-shift due to temperature-variation is the characteristic associated with the resonance lines only. In this manner, the resonance lines within the guide were unambiguously identified and eliminated from the list for further investigation.

2.2c Shifting the Resonance Lines by Heating the Guide

One of the most serious problems in microwave spectroscopy is that of distinguishing absorption due to the material under study from the unwanted resonances set up within the waveguide system itself. Such standing waves arise from reflections between slight discontinuities in the waveguide

particularly at the coupling joints, windows, etc. These resonances overlap and obscure the Stark lines as well.

Working on the idea suggested by Dr. R. Tipping a method of moving the resonance lines to lower frequency was devised. The resonant frequency is given by

$$f = \frac{nv}{2L}$$

where v = velocity of the microwaves in the guide,

n = an integer,

L = length of the absorption cell.

When the absorption cell is heated, its length increases to

$$L' = L(1 + \alpha\Delta T),$$

where α = the temperature-coefficient of the material of the guide

ΔT = increase in temperature.

Therefore, the frequency of the resonance line changes to

$$f' = \frac{nv}{2L'} = \frac{nv}{2L(1 + \alpha\Delta T)}.$$

Thus, the frequency-shift $\Delta f = f' - f$.

$$= -\frac{nv}{2L}\left(1 - \frac{1}{1 + \alpha\Delta T}\right)$$

$$= -\frac{f \cdot \alpha\Delta T}{1 + \alpha\Delta T}$$

$$= -f \cdot \alpha\Delta T$$

As a typical example, let f = 8000 MHz, α (brass) = 19×10^{-6}, $\Delta T = 50^{\circ}C$, then Δf = -7.6 MHz. Thus, by raising the temperature of the guide, the resonance lines could be moved by a considerable amount to lower frequency side, whereas the absorption lines due to gases showed no such shift. This method was used not only to distinguish resonances from the absorption lines,

but also to forestall the obscuring of the Stark lines caused by these unwanted signals overlapping the wanted lines.

2.2d Voltage Calibration of Stark Cell

In spite of the utmost care in the design of the Stark modulation cell, the distance between the septum and the walls of the guide may not remain unchanged throughout its length, causing a variation in the electric field and the consequent uncertainty in the precision in the knowledge of the field strength. The average value of the field may be obtained by calibration with a substance whose dipole moment is known accurately. For voltage calibration of the guide here, carbon oxysulphide ($^{16}O\ ^{12}C\ ^{32}S$) was used as calibrant (μ in the ground state = .7149 D). The second order Stark shift of the ground state $0 \rightarrow 1$ transition (ν_o = 12162.97 MHz) was measured for different voltages and the electric field-strength (volts/cm) was calculated from the formula

$$E = \frac{1}{\mu} \sqrt{\frac{\nu_o \Delta\nu}{0.1351}}$$

where $\Delta\nu$ = Stark shift in MHz and μ = 0.7149D. A graph was plotted between the voltmeter reading V and the electric field strength E. This was done for both the guides. The calibration-curves are reproduced in Fig. 2.7.

2.2e Analysis of the Lines

For accurate measurement of frequencies of the absorption lines and the resolution of Stark lines, the output frequency-variation was controlled by a 50 K ohm ten-turn potentiometer, slowly driven by a 4 to 24 volts D.C. motor via a worm gear. By keeping the driving voltage at 20 volts and maintaining Δf at 200 MHz, a sweep rate of 0.1 to 0.2 MHz per minute was obtained. The

crystal current, which is also a measure of the signal strength, was kept at 120 μa. The bandwidth of the 100 KHz receiver was selected to be 0.1 Hz . The display of the output signal from the 100 KHz receiver was made on the strip chart recorder, the paper speed being maintained at 0.2 inch per minute. The voltage scale usually chosen was 250 mV full scale deflection.

2.2f Calibration of the Frequency-Meter

Using the ground state 0→1 rotational transitional frequency of OCS as the frequency standard, the HP frequency-meter was calibrated. The average result of the 96 samples was 12162.970 MHz. The theoretical value is 12162.984* MHz which is calculated using Costain's value of 36488.8128 MHz for the J = 2→3 lines of OCS and the Landholt-Bornstein value for D of 1.31×10^{-3} MHz. The weighted average for the ratio of the theoretical frequency and the observed frequency is 1.0000011. The correction to the observed frequencies is +0.014 MHz, which is less than the r.m.s. error of ±0.0225 MHz. Hence in the present work no corrections were applied to the frequency-meter readings. It will be noted that only one standard frequency is needed, because this is sufficient to calibrate the crystal in the frequency-meter.

---

* The frequency of a rotational line is given by the formula,

$$\nu = 2B(J+1) - 4D(J+1)^3,$$

where J is the rotational quantum number of the lower state. Obviously, for the 0→1 transition , J=0.

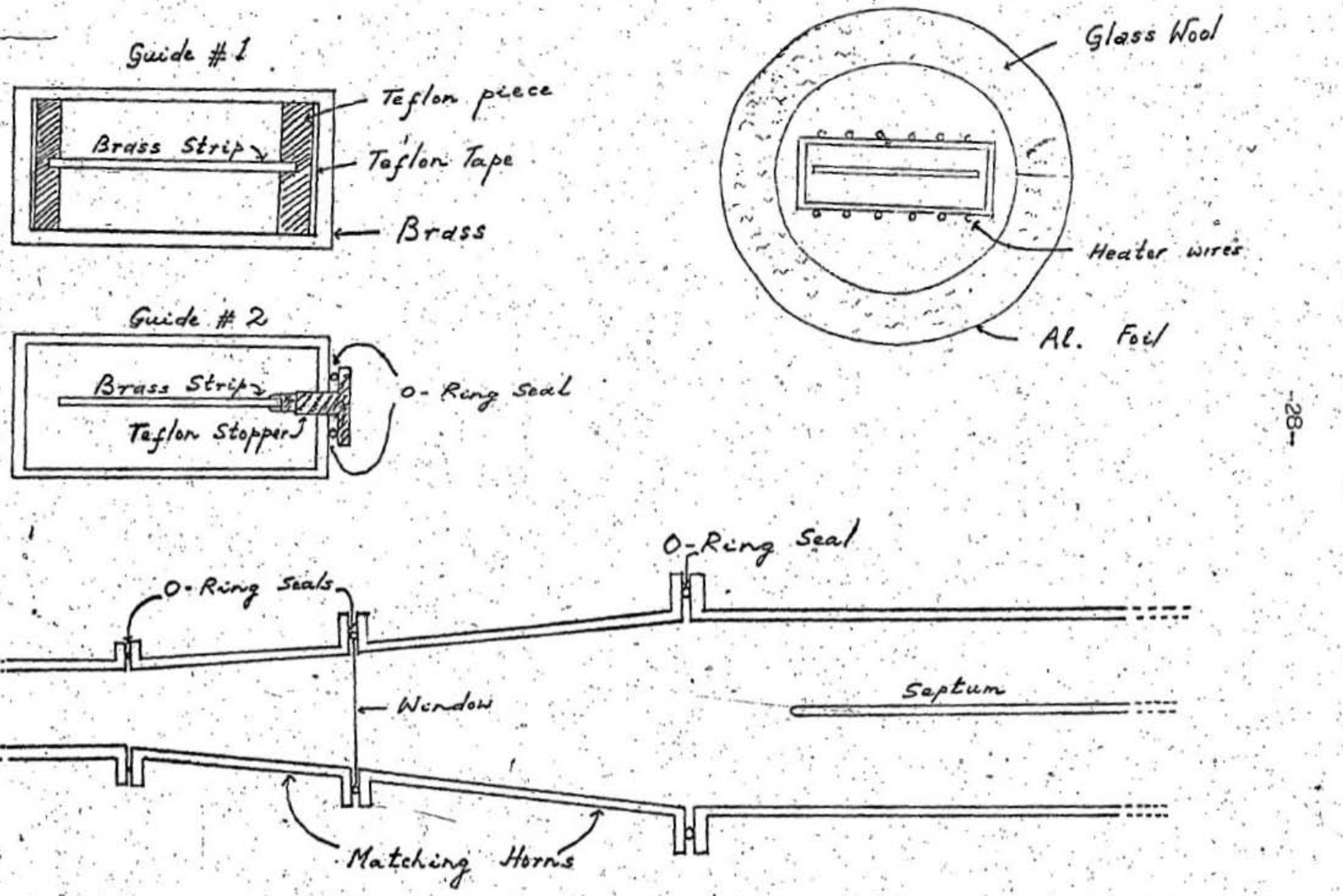

Fig. 2.1 Absorption Cells

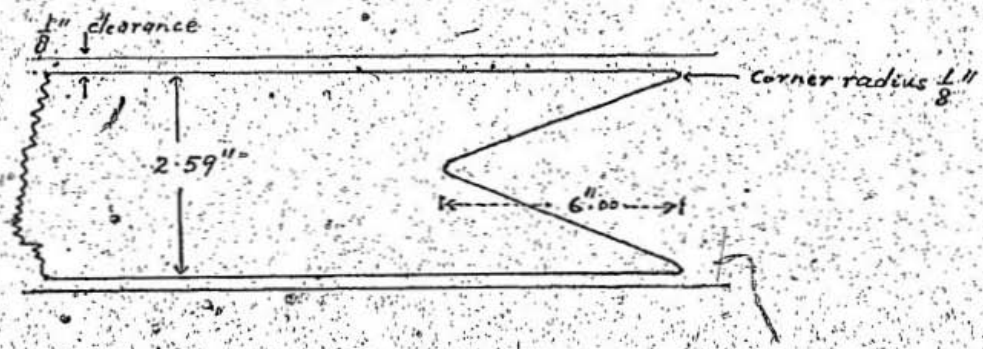

Fig. 2.1a View of the end of the Septum

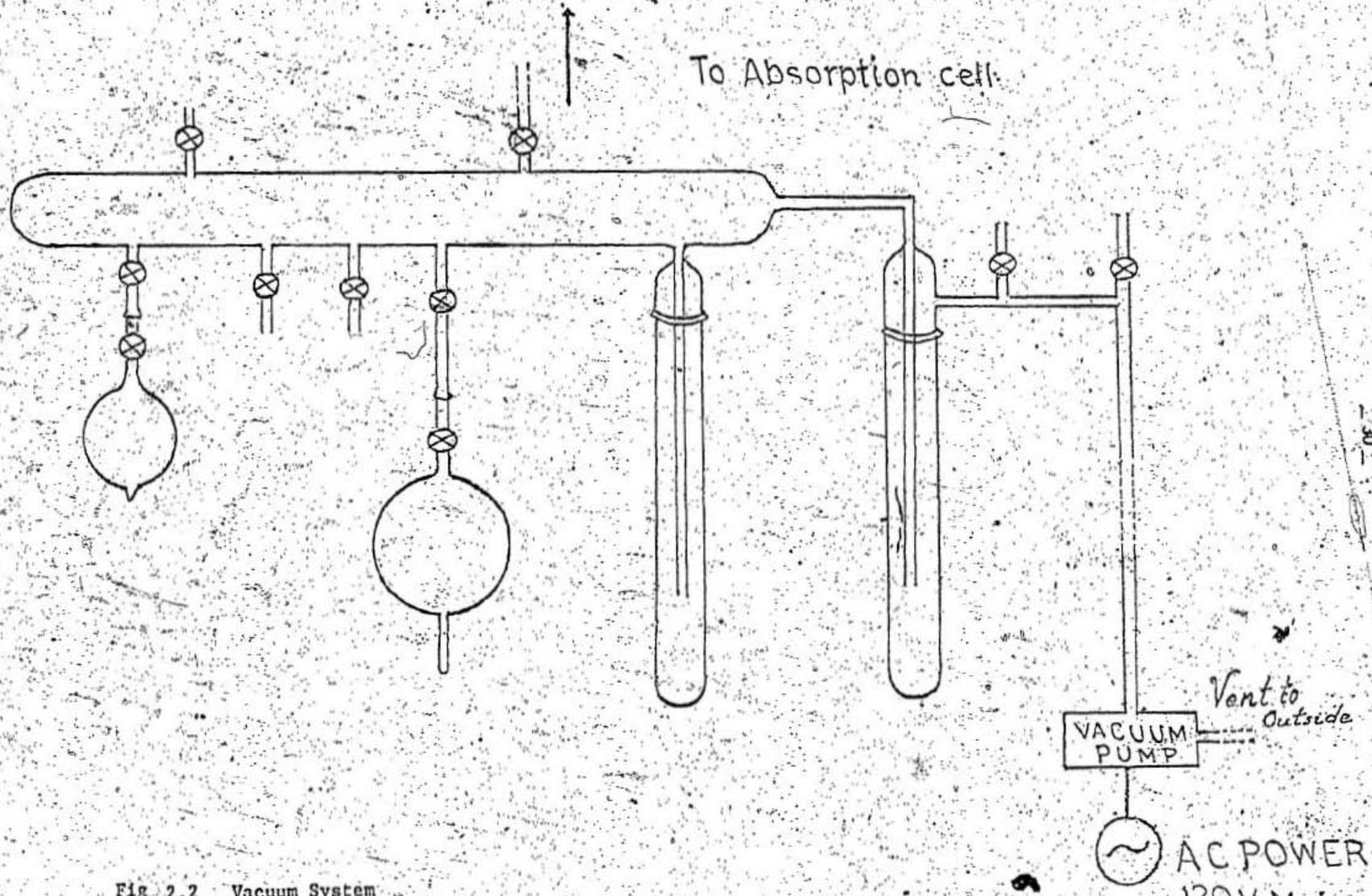

Fig. 2.2 Vacuum System

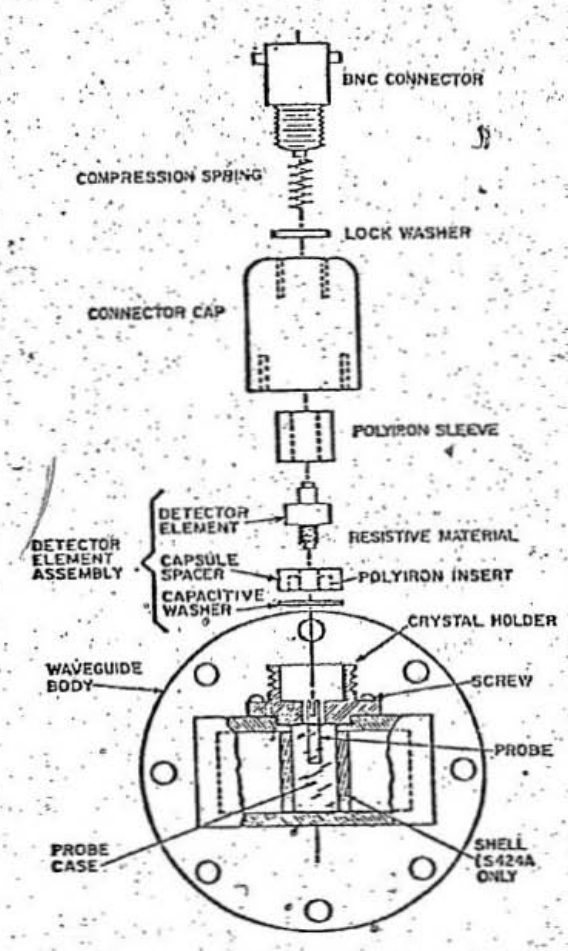

Fig. 2.3. Complete assembly of X424A Crystal detector.

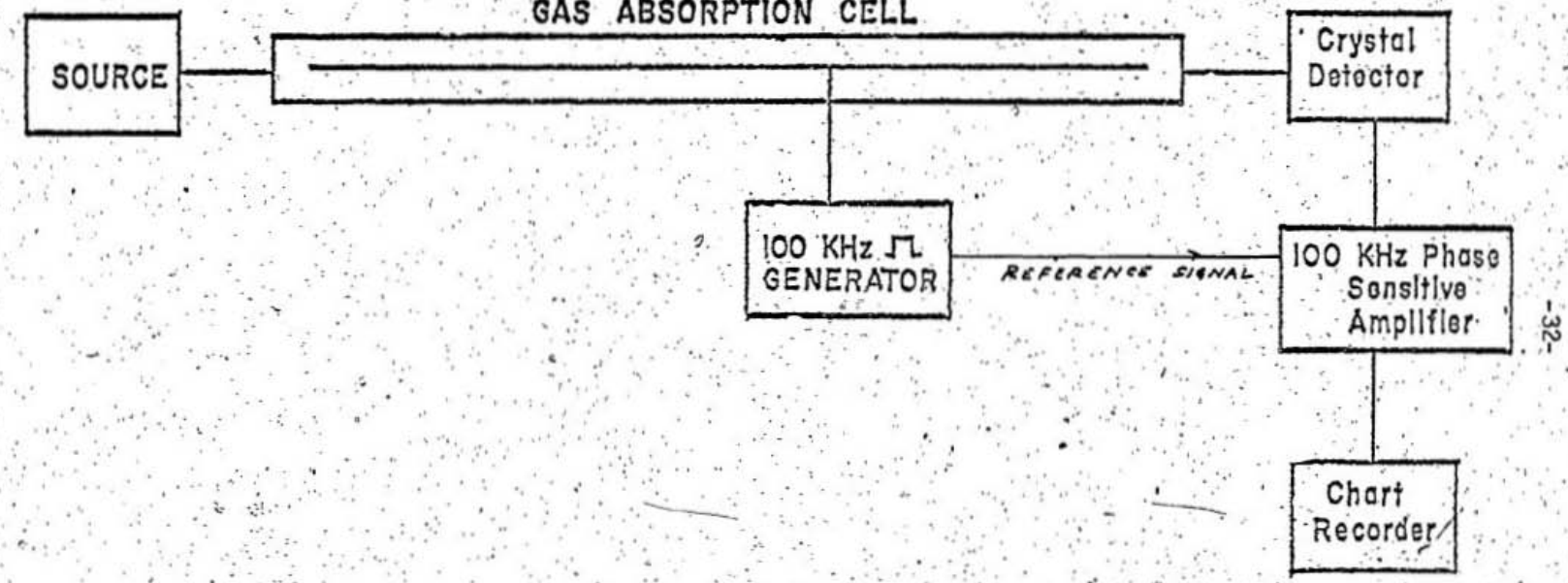

Fig. 2.4. Block diagram of Stark modulation microwave spectrometer.

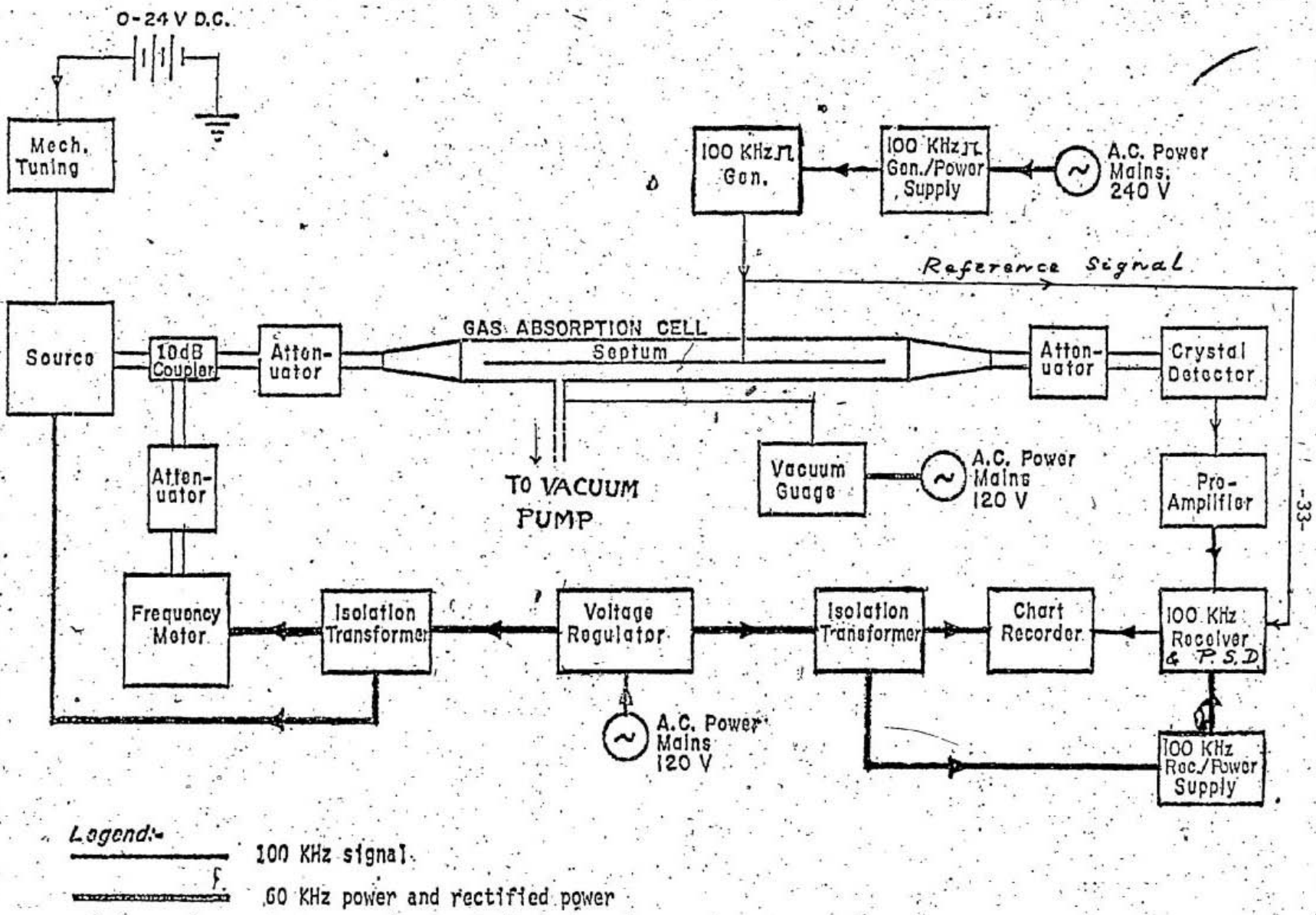

Fig. 2.5. Complete block diagram of the Stark-modulated microwave spectrometer electronic gear.

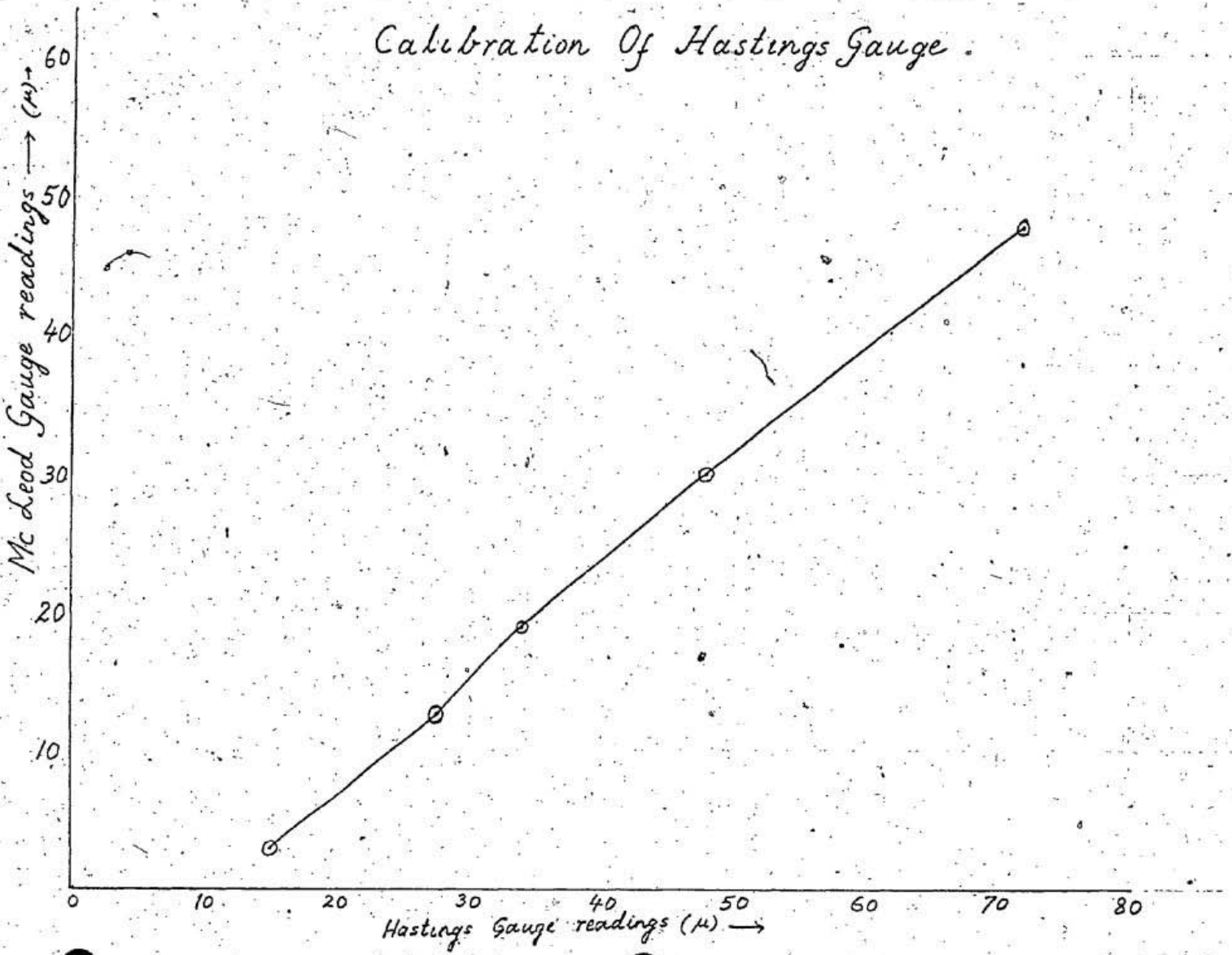

Fig 2.6 Calibration of Hastings Gauge

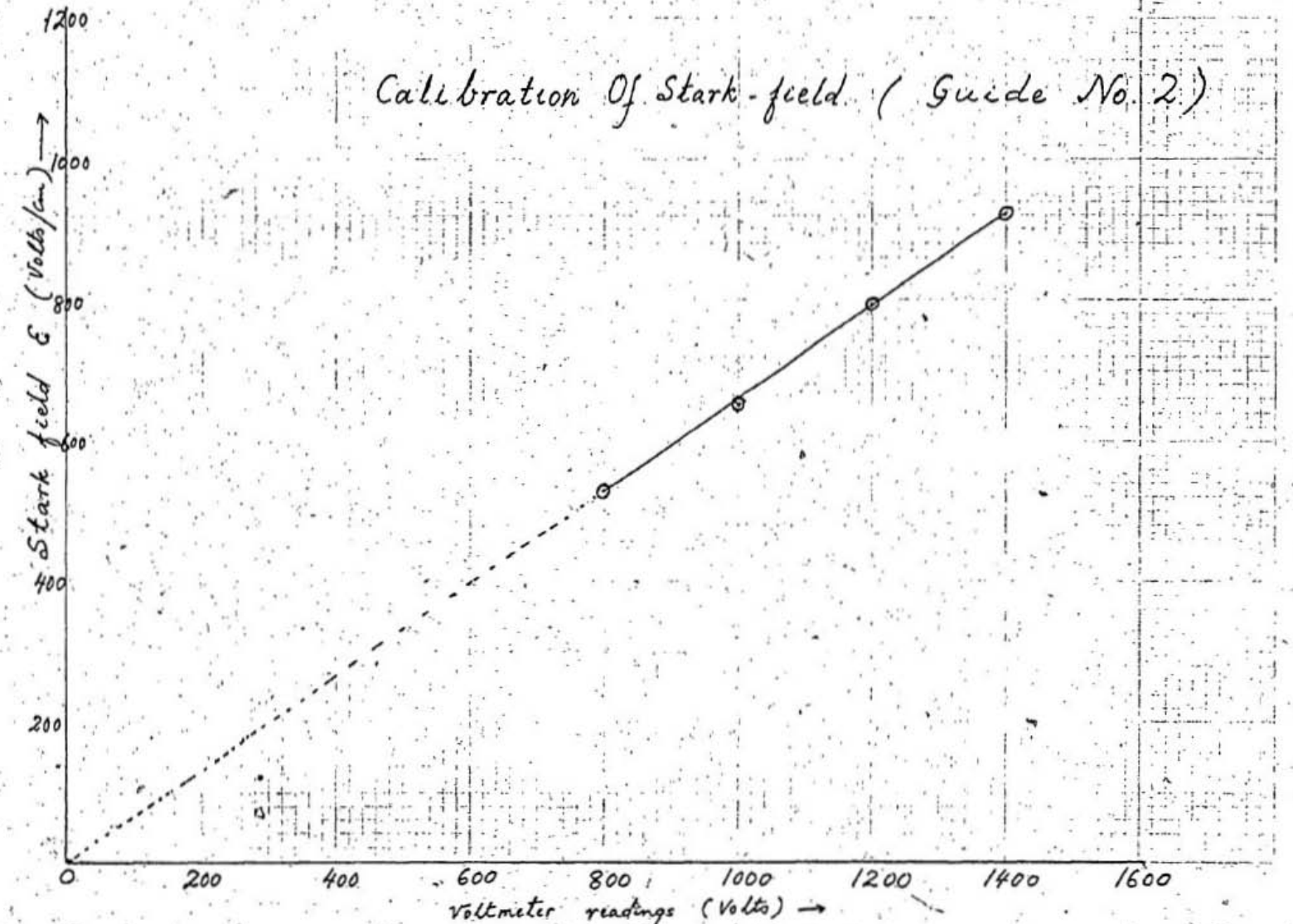

Fig. 2.7 Calibration of Stark field

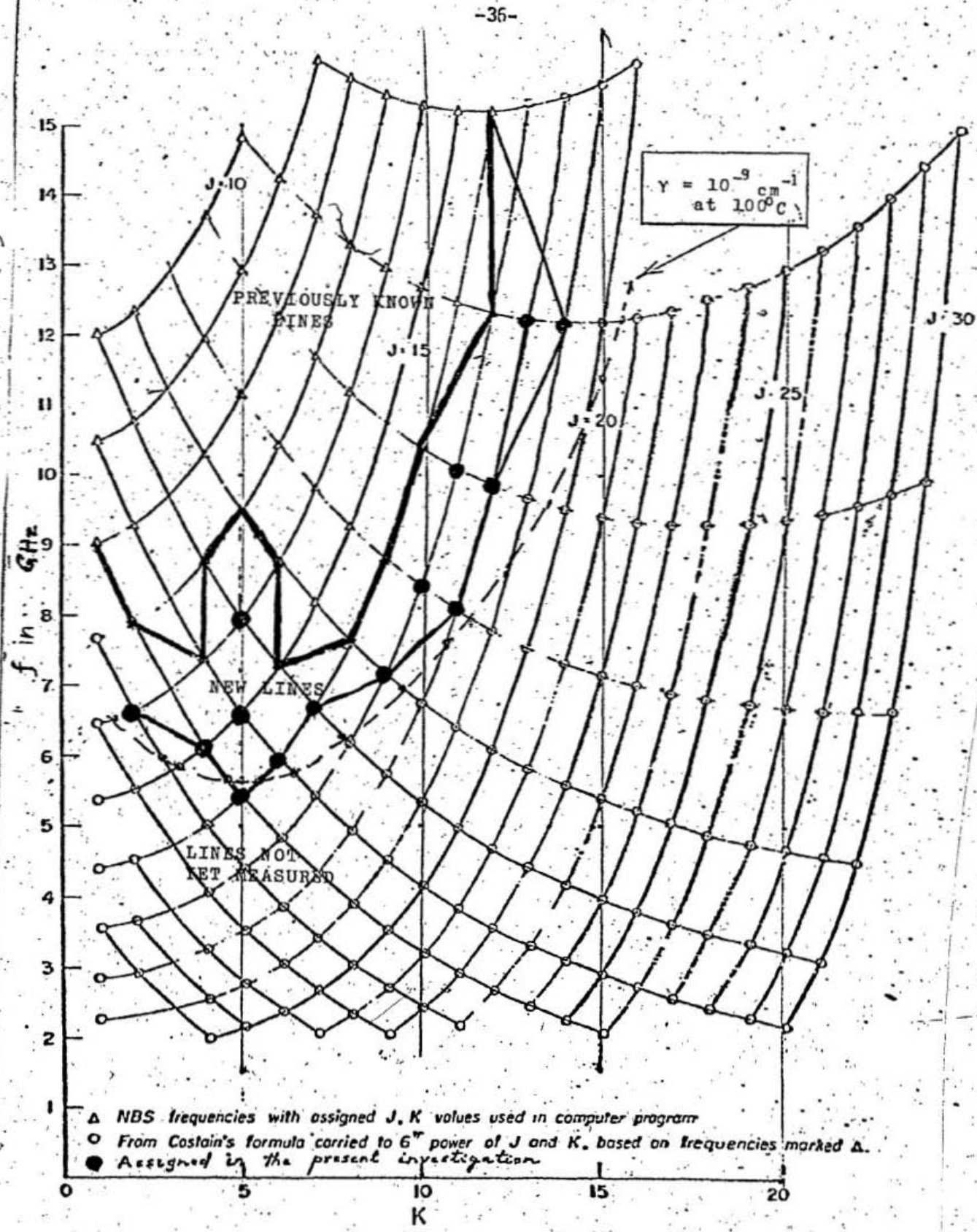

Fig. 2.8 Chart showing the rotational fine structure of the inversion spectrum of $^{14}NH_3$

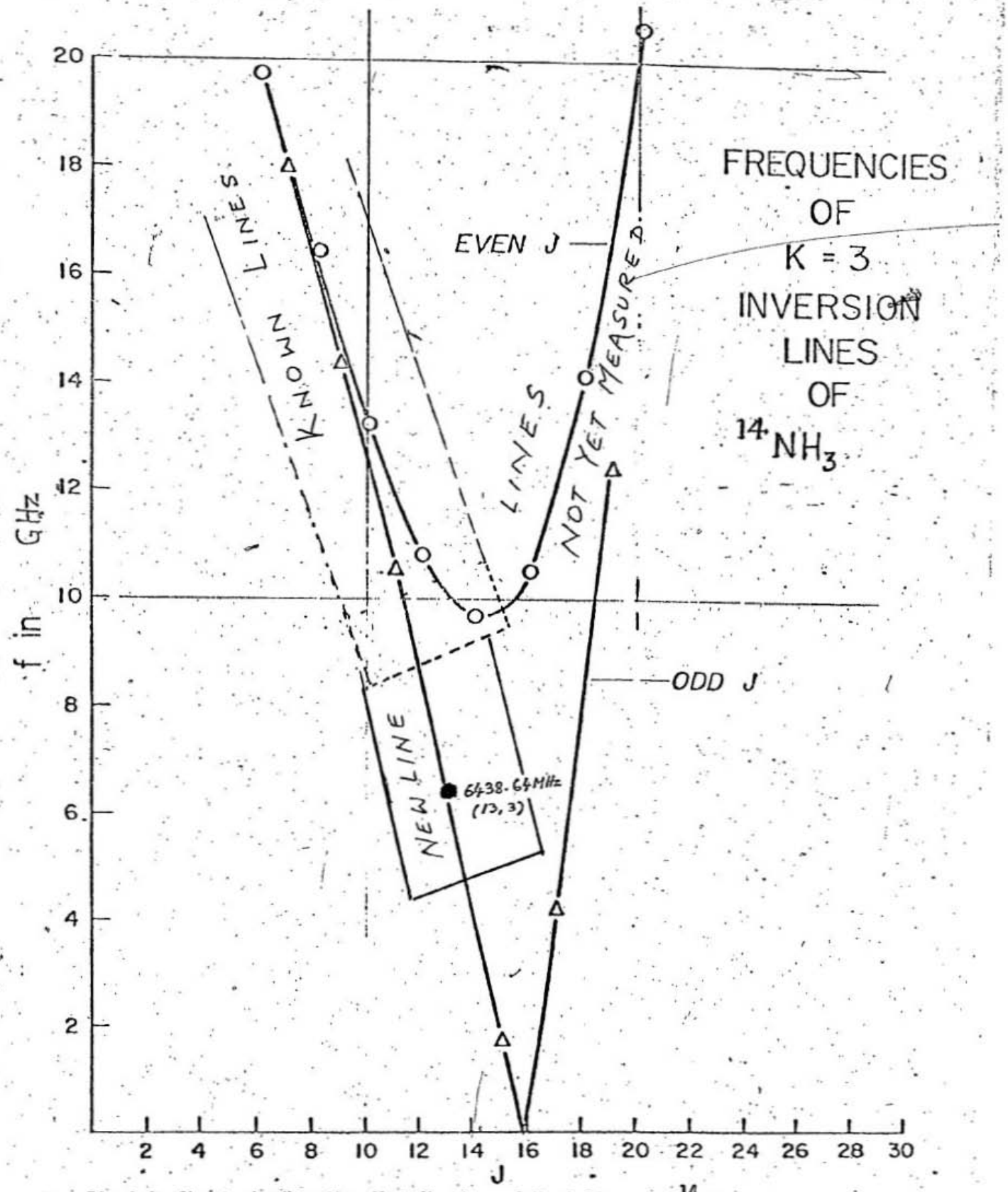

Fig.2.9 Chart showing the distribution of K= 3 lines of $^{14}NH_3$

CHAPTER III

RESULTS AND DISCUSSIONS

3.1 Ground State Inversion Lines of $^{14}NH_3$

As a result of careful investigations 15 new ground state inversion lines of $^{14}NH_3$, including one K = 3 and one K = 6 lines, were observed. The frequencies of the newly observed lines were accurately measured by taking the average of a number of observations at the peak of the absorption lines in the up and down slow sweeps. The results are given in the Table 3.1 and the Figures 2.8 and 2.9.

Corrections were applied for K = 3 and K = 6 lines, using the values of the rotation-vibration function determined in this laboratory (26) as well as that given by Schnabel et al. (15) in the Nielsen and Dennison's formula (16).

The corrections for K = 3 are expressed as

$$\delta\nu' = (-1)^J \alpha_J J(J+1)\,(J(J+1)-2)(J(J+1)-6)$$

with $\alpha_J = 3.74044 \times 10^{-4} - 6.097 \times 10^{-6}\,(J-3)$ MHz (Schnabel)

or, $\alpha_J = 3.57582 \times 10^{-4}\,\left[1 - \frac{J(J+1)}{1475.63}\right]$ MHz (Arthur G. Earle.)

The corrections for K = 6 are expressed as

$$\delta\nu'' = (-1)^{J+1}\, 1.24 \times 10^{-14}\, \phi(J) \text{ MHz} \qquad \text{(Schnabel)}$$

where $\phi(J) = J(J+1)(J(J+1)-2)(J(J+1)-6)(J(J+1)-12)(J(J+1)-20)(J(J+1)-30)$

The assignments of the newly observed lines were made on the basis of the empirical formula developed by Constain (14) and later by Schnable et al. (15). Further, the Stark shifts of the lines 6438.64 MHz and 7969.32 MHz are consistent with the theoretical values, which confirms the correctness of the assignments.

Because the J values ranged from 13 to 19 in these lines, it was difficult to resolve the separate Stark components in their Stark patterns. However, as can be seen Figures 3.12 and 3.14, the position of the outer component, with $M_J = J$, can be estimated within ±0.15 MHz, defining the outer limit of the Stark lines at the Stark voltage used. The square of the dipole moment can then be found by using the formula for the Stark shift of Ammonia, given in section 1.6, with M = J.

The outer limits of the Stark lines of 6438.64 MHz and 7969.32 MHz at different voltages were observed and the dipole moment was calculated from each observation. The average value of the dipole moment is 1.472 ± 0.002 D which is in good agreement with the value 1.475 ± 0.0006 D obtained by Pujio Shimizu (19) by Stark spectroscopy using CO_2 and N_2O lasers. The results of the Stark analysis of these lines are given in Tables 3.2 and 3.3. The frequencies of the outer limits of the Stark lines were plotted against the Stark voltages. All the points lie on straight lines. The graphs are shown in Figures 3.1 and 3.3. Due to high values of J and low intensities of these lines the individual Stark lines could not be resolved. As a check that these lines were due to the gas $^{14}NH_3$ slow sweeps were taken after pumping out the gas for one hour maintaining the other conditions as before. The intensities of the lines reduced to approximately 1/10 of the original ones.

3.2 J = 0→1 Rotational Transitions of Carbonyl Sulphide

Nine lines of Carbonyl Sulphide were observed, accurately measured and assigned. The assignements of the vibrational quantum numbers and isotopic constituents were made on the basis of the previous works reported in NBS monograph 70, Volume IV, for J = 1→2, 2→3 and 3→4 transitions and also on the basis of the values of the constants given in the book by Landolt-Bornstein (20).

The triplet structure due to the quadrupole moment of ^{33}S nucleus in the 0→1 transition was completely resolved. Using the value of the quadrupole coupling constant (eqQ) = -29.07 MHz obtained by Eshback et al. (21) and the centre of gravity ν_0 = 12009.793 MHz the calculated line positions agree with those observed within the experimental error of 0.02 MHz.

From Stark analysis, the value of dipole moment of carbonyl sulphide for different isotopic forms and different vibrational states was obtained. The results of the Stark analysis are given in tables 3.5 and 3.13. The graphs of the Stark shifts vs. Stark voltages are shown in the figures 3.3 and 3.11.

The lower frequency scales in the Fig. 3.12 through 3.26 correspond to the sweeps taken after the $^{14}NH_3$ gas was pumped out for about one hour.

TABLE 3.1

GROUND STATE INVERSION LINES OF $^{14}NH_3$

Assignment J	K	Observed frequency ν_{obs} (MHz)	Theoretical frequency ν_{theo} (MHz) Schnabel[b]	MUN[c]	$\Delta_{schn.}$[a]	Δ_{MUN}
13	3	6 438.64	6 440.16	6 437.84	-1.52	-0.84
14	2	6 640.23	6 640.06	6 640.25	+0.17	+0.02
14	5	7 969.32	7 969.28	7 969.32	+0.04	+0.00
15	4	6 123.37	6 123.36	6 123.48	+0.01	-0.11
15	5	6 621.15	6 621.05	6 621.14	+0.10	-0.01
16	5	5 433.50	5 433.32	5 433.27	+0.18	-0.23
16	6	5 973.93	5 973.64	5 974.04[e]	+0.29	-0.11
16	7	6 690.45	6 690.34	6 690.42	+0.11	-0.03
17	9	7 152.30	7 151.89	7 152.21	+0.41	+0.09
17	10	8 426.86	8 426.43	8 426.91	+0.43	-0.05
17	11	10 098.47	10 098.15	10 098.54	+0.32	-0.07
18	11	8 084.48	8 083.63	8 084.49	+0.85	-0.01
18	12	9 853.07	9 852.22	9 853.02	+0.85	-0.29
18	13	12 211.81	12 211.31	12 212.01	+0.50	- .21
19	14	12 168.54	12 167.31	12 169.73	+1.23	-1.19

a $\Delta = \nu_{obs} - \nu_{theo}$

b See Appendix I.

c See Appendix II.

d This frequency is the 4th power expansion of $J(J+1)$ and K^2.

e This result followed by using the second formula on page 38 for α_J. and the uncorrected frequency 8245.282 MHz. from Appendix II incalculating the J = 13, K = 3 frequency. The corrections for the J = 16, k = 6 line was based on Schnabel's correction, (15).

TABLE 3.2

STARK SHIFT FOR ν_o = 6438.64 MHz of $^{14}NH_3$

Stark Voltage (Volts)	Max. Stark Shift (MHz)	μ (Debye)	Average μ (Debye)
800	2.15	1.461	
1 000	3.40	1.492	
1 200	4.95	1.472	1.473±.008
1 400	6.65	1.472	
1 600	8.80	1.472	
1 700	9.90	1.470	
1 800	11.50	1.473	

TABLE 3.3

STARK SHIFT FOR ν_o = 7969.32 MHz of $^{14}NH_3$

Stark Voltage (Volts)	Max. Stark Shift (MHz)	μ (Debye)	Average μ (Debye)
500	1.67	1.474	
600	2.40	1.472	
700	3.26	1.471	1.472±0.003
800	4.26	1.471	
900	5.40	1.472	

TABLE 3.4

ROTATIONAL 0→1 LINES OF CARBONYL SULPHIDE

Isotopic Species	Vib. State	Hyperfine F	Hyperfine F'	Observed Freq. (MHz)	Calculated Freq. (MHz)
O C S	0 0 0			12162.97	12162.984
	1 0° 0			12126.74	12126.64
	0 2° 0			12200.38	12200.36
$O^{13}C$ S	0 0 0			12123.88	12123.767
O C ^{33}S	0 0 0	3/2	3/2	12003.96	12003.949
	0 0 0	5/2	3/2	12011.29	12011.246
	0 0 0	1/2	1/2	12017.05	12017.060
O C ^{34}S	0 0 0			11865.70	11865.627
^{18}O C S	0 0 0			11409.65	11409.645

{Fermi pair

TABLE 3.5

STARK SHIFT OF ν_o = 12162.97 MHz of OCS (CALIBRATION OF STARK FIELD) μ = 0.7149 DEBYE (Ref. 22)

Stark Voltage (Volts)	$\Delta\nu$ (MHz)	E (Volts/cm)
800	1.58	527.56
1 000	2.40	650.20
1 200	3.59	795.23
1 400	4.82	921.45

TABLE 3.6

STARK SHIFT OF ν_o = 12126.74 MHz OF OCS (10^o0)

Stark Voltage (Volts)	$\Delta\nu$ (MHz)	μ (Debye)	Average μ (D)
800	1.55	0.707	
1 000	2.42	0.717	0.709±0.006
1 200	3.45	0.6998	
1 400	4.79	0.712	

TABLE 3.7

STARK SHIFT OF ν_o = 12200.38 MHz OF OCS (02^o0)

Stark Voltage (Volts)	$\Delta\nu$ (MHz)	μ (D)	Average μ (D)
800	1.49	0.695	
1 000	2.38	0.713	0.699±0.008
1 200	3.37	0.694	
1 400	4.53	0.694	

TABLE 3.8

STARK SHIFT OF ν_o = 12123.88 MHz OF $O^{13}CS$

Stark Voltage (Volts)	Δν (MHz)	μ (D)	Average μ (D)
800	1.68	0.736	
1 000	2.45	0.721	
1 200	3.50	0.705	0.719±0.011
1 400	4.84	0.715	

TABLE 3.9

STARK SHIFT OF ν_o = 12003.96 MHz OF $OC^{33}S$

Stark Voltage (Volts)	Δν (MHz)	μ (D)	Average μ (D)
800	1.30	0.644	
1 000	2.00	0.648	0.635±0.015
1 200	2.90	0.638	
1 400	3.55	0.609	

TABLE 3.10

STARK SHIFT OF ν_o = 12011.29 MHz OF $OC^{33}S$

Stark Voltage (Volts)	Δν (MHz)	μ (D)	Average μ (D)
800	1.20	0.619	
1 000	1.80	0.615	0.614±0.006
1 200	2.60	0.605	
1 400	3.65	0.618	

TABLE 3.11

STARK SHIFT OF ν_o = 12017.05 MHz OF $OC^{33}S$

Stark Voltage (Volts)	Δν (MHz)	μ (D)	Average μ (D)
800	1.20	0.619	
1 000	1.75	0.607	0.608±0.006
1 200	2.55	0.605	
1 400	3.48	0.603	

TABLE 3.12

STARK SHIFT OF ν_o = 11865.70 MHz OF $OC^{34}S$

Stark Voltage (Volts)	Δν (MHz)	μ (D)	Average μ (D)
800	1.72	0.737	
1 000	2.60	0.735	0.726±0.011
1 200	3.65	0.712	
1 400	5.00	0.719	

TABLE 3.13

STARK SHIFT OF ν_o = 11409.65 MHz OF ^{18}OCS

Stark Voltage (Volts)	Δν (MHz)	μ (D)	Average μ (D)
800	1.75	0.728	
1 000	2.75	0.741	0.726±0.010
1 200	3.81	0.713	
1 400	5.28	0.724	

TABLE 3.14

ELECTRIC DIPOLE MOMENTS OF THE ISOTOPIC SPECIES OF CARBONYL SULPHIDE IN DIFFERENT VIBRATIONAL STATES

Isotopic Species	Vib. State	μ^a (relative) (Present Work)	μ (relative) (Previous work)	Ref.
O C S	0 0 0	1.0000	1.00000	(23)
	1 0 0	0.9917		
	0 2^o 0	0.9778		
O ^{13}C S	0 0 0	1.0057		
O C ^{33}S	0 0 0	0.8659[b]		
O C ^{34}S	0 0 0	1.0155		
^{18}O C S	0 0 0	1.0155		

a In the present work the dipole moment of the 0→1 ground state rotational transition line of OCS was taken to be 0.7149 D (Ref. 22).

b Averaged from the three quadrupole lines.

Graph for plotting second order Stark Shifts

$\nu_0 = 6438.64$ MHz of $^{14}NH_3$ (00°00)

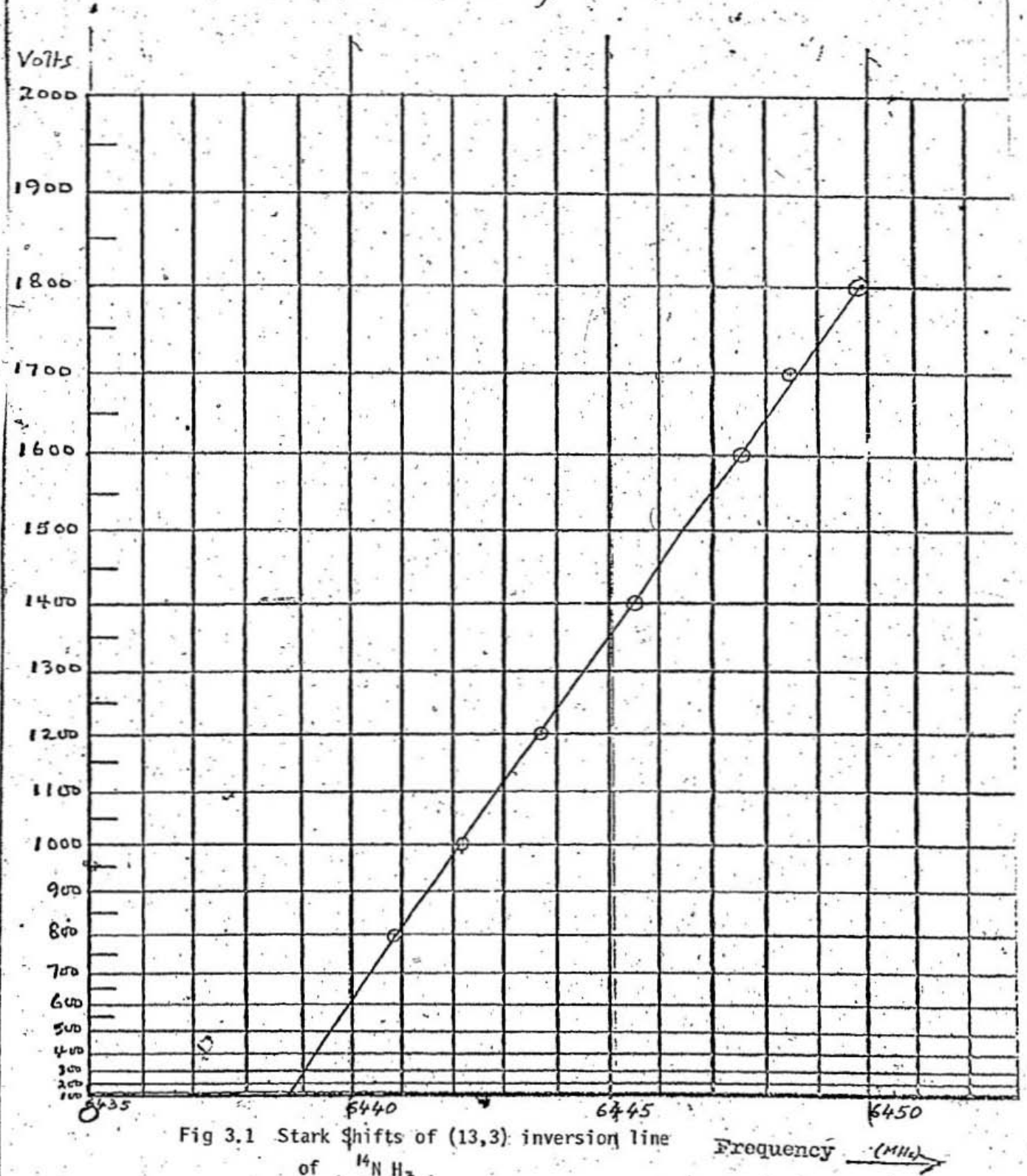

Fig 3.1 Stark Shifts of (13,3) inversion line of $^{14}N\,H_3$

Graph for plotting second order Stark Shifts

$\nu_0 = 7969.32$ MHz of $^{14}NH_3$

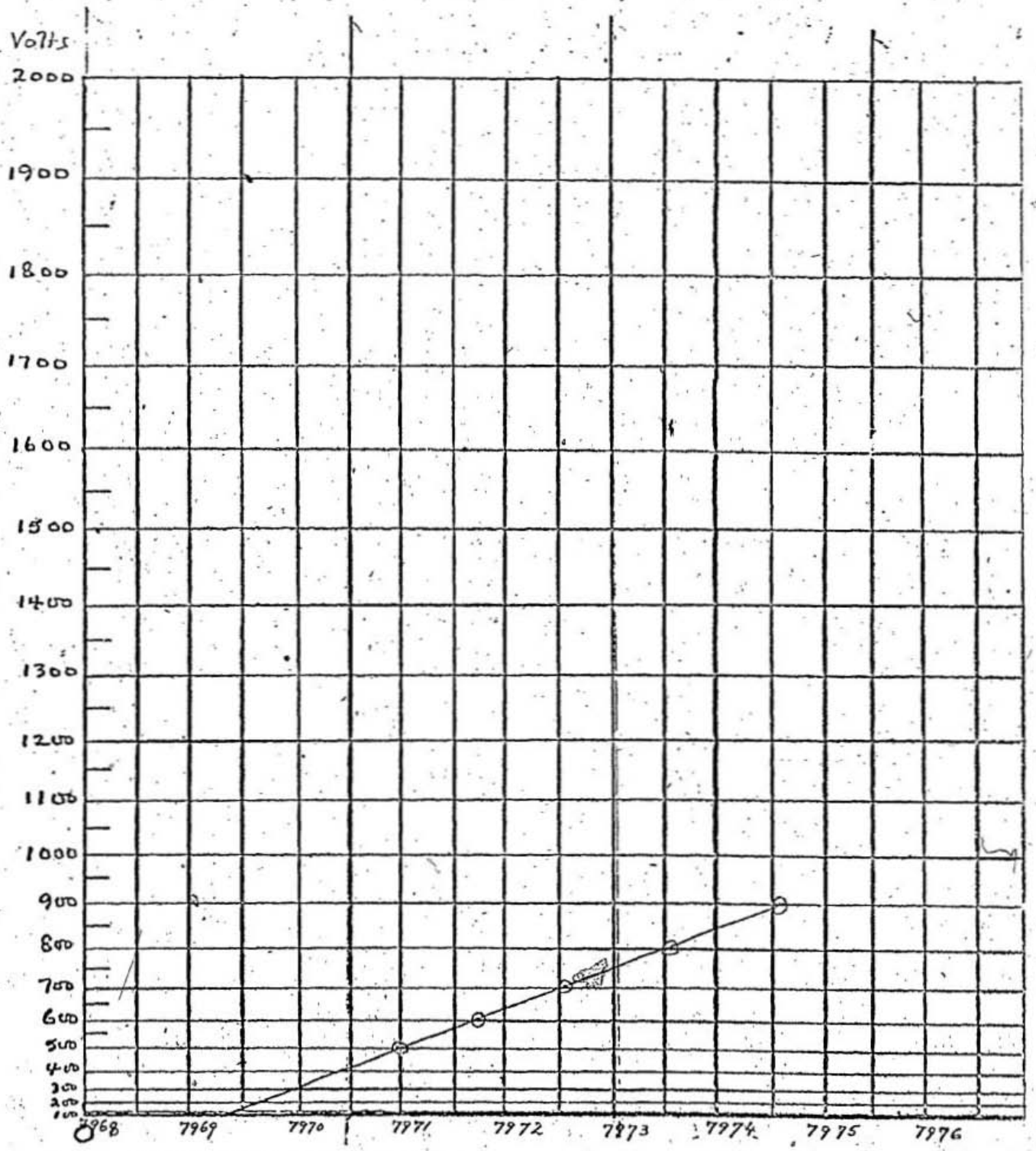

Fig 3.2 Stark shifts of (14,5) inversion line Of $^{14}NH_3$

Graph for plotting second order Stark Shifts

$\nu_0 = 12162.97$ MHz of OCS (000)

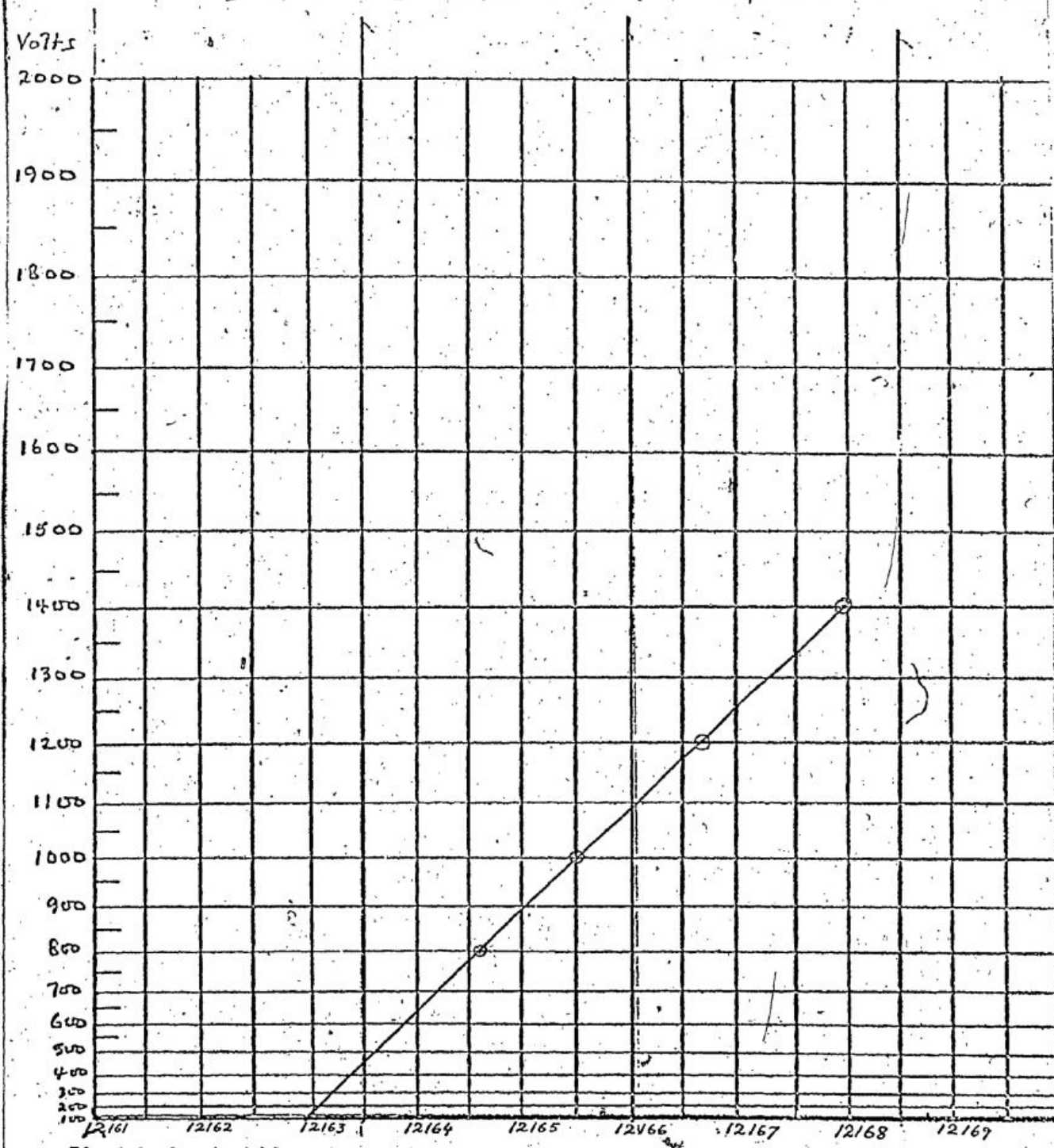

Fig 3.3 Stark shifts of 0→1 rotational line of OCS in the (000) state

Graph for plotting second order Stark Shifts

ν_0 = 12126.74 MHz of OCS (10°0)

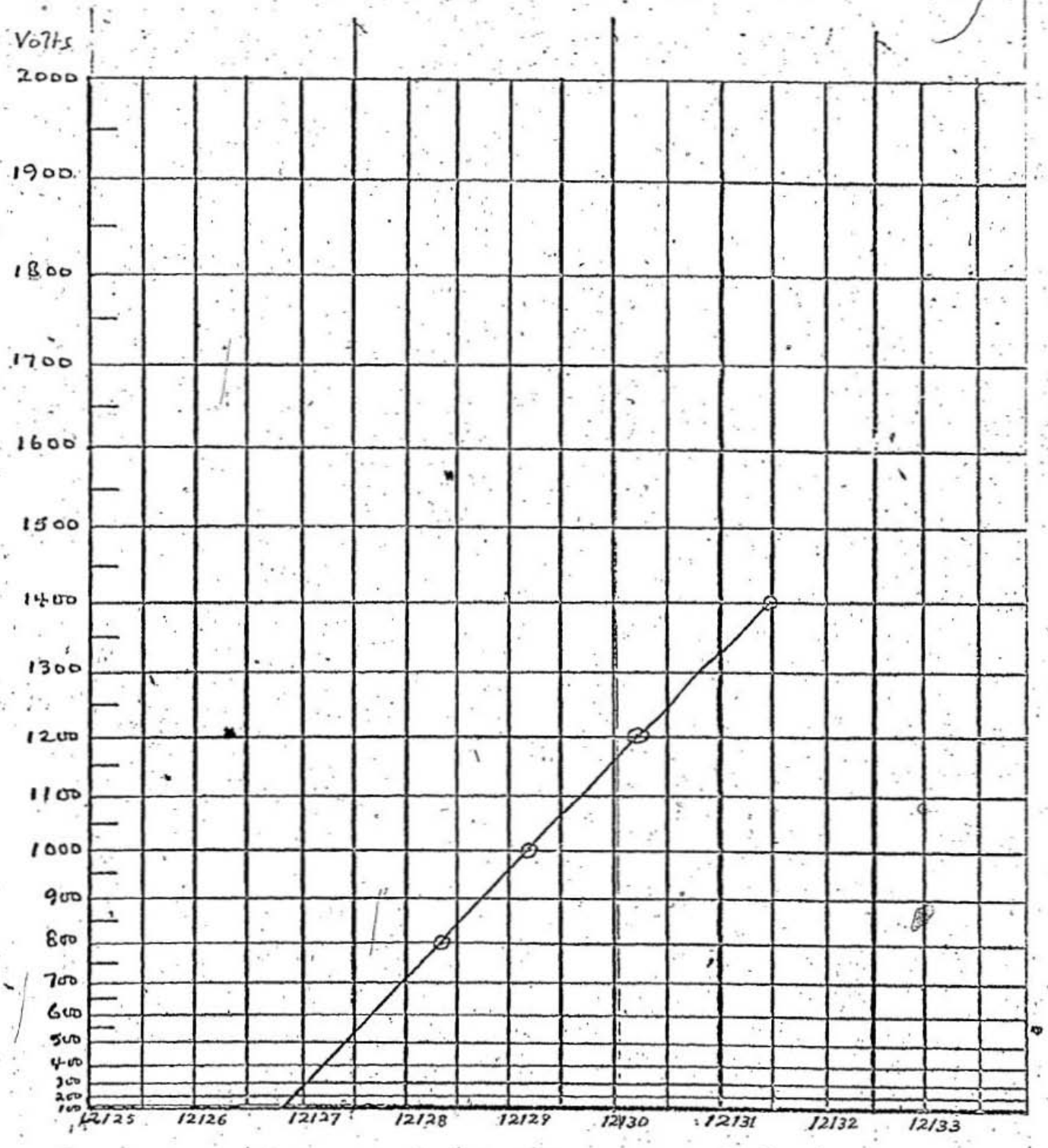

Fig 3.4 Stark shifts of 0→1 rotational line of OCS in the (10^0 0) state

Graph for plotting second order Stark Shifts

ν_0 = 12200.38 MHz. of OCS ($02^{\circ}0$)

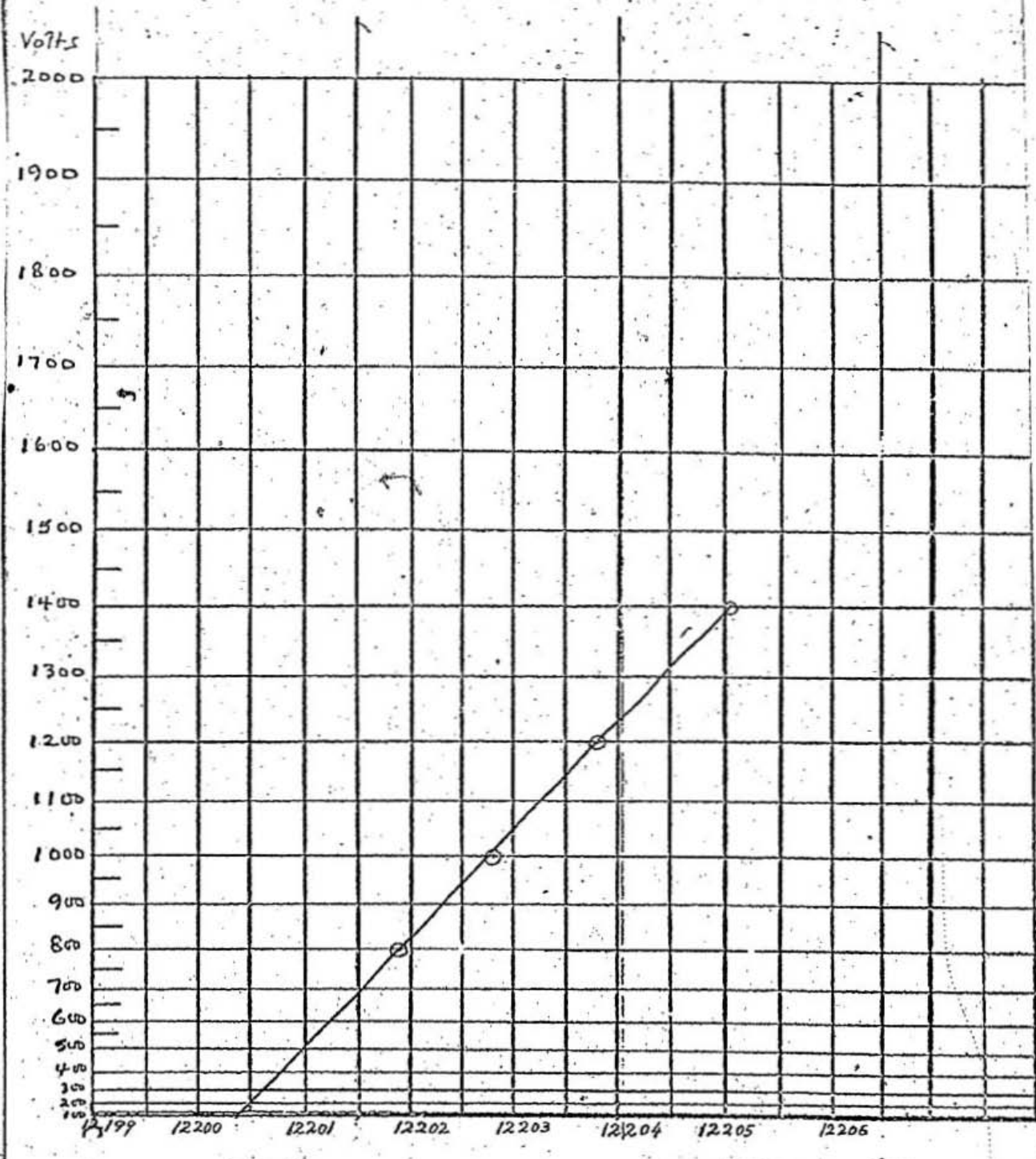

Fig 3.5 Stark shifts of 0→1 rotational line of OCS in the ($02^{\circ}0$) state

Graph for plotting second order Stark Shifts

ν_0 = 12123.76 MHz of $O^{13}CS$

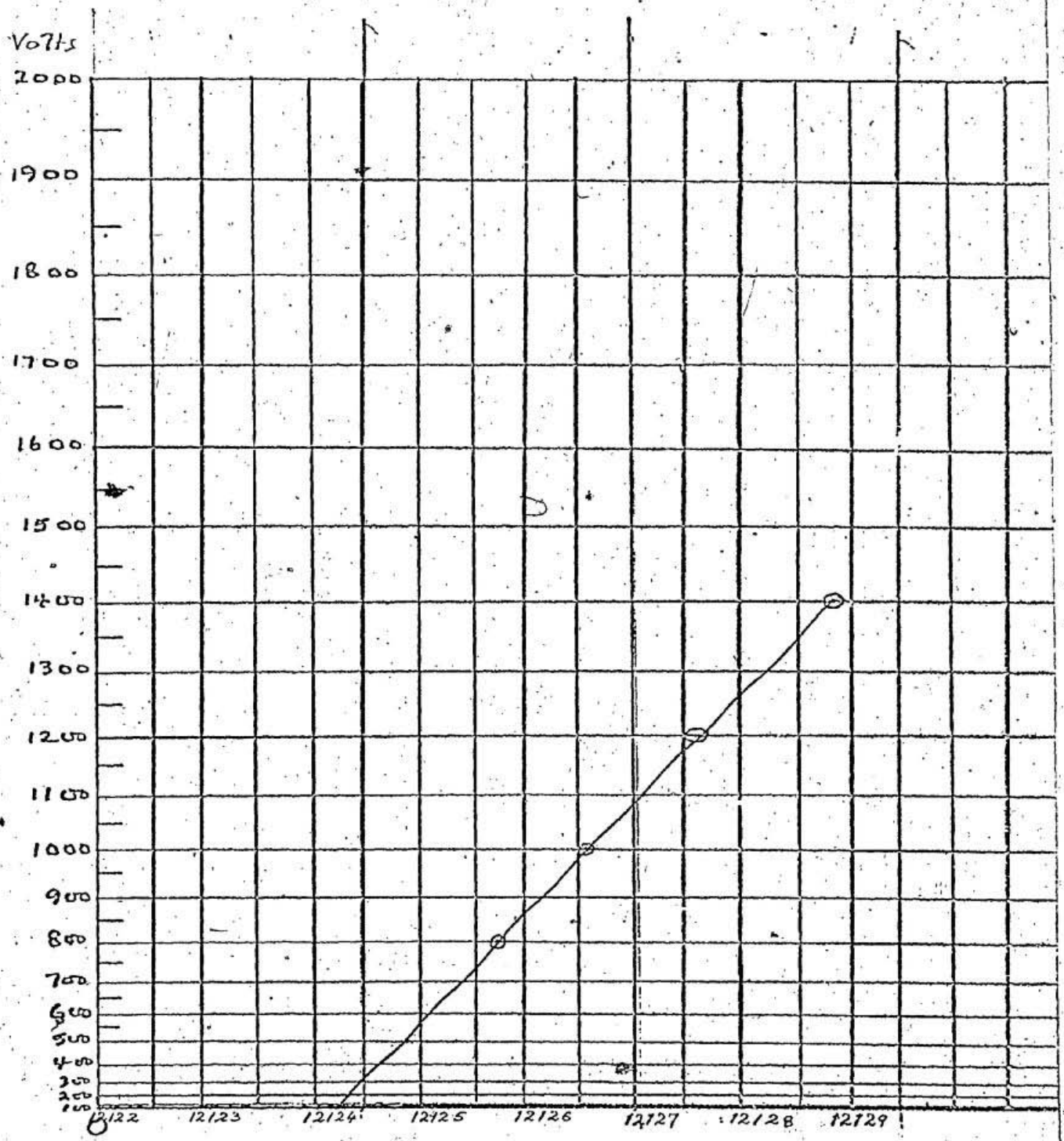

Fig 3.6 Stark shifts of 0→1 rotational line of $O^{13}CS$ in the (000) state

Graph for plotting second order Stark Shifts

$\nu_o = 12003.96$ MHz of $OC^{33}S$

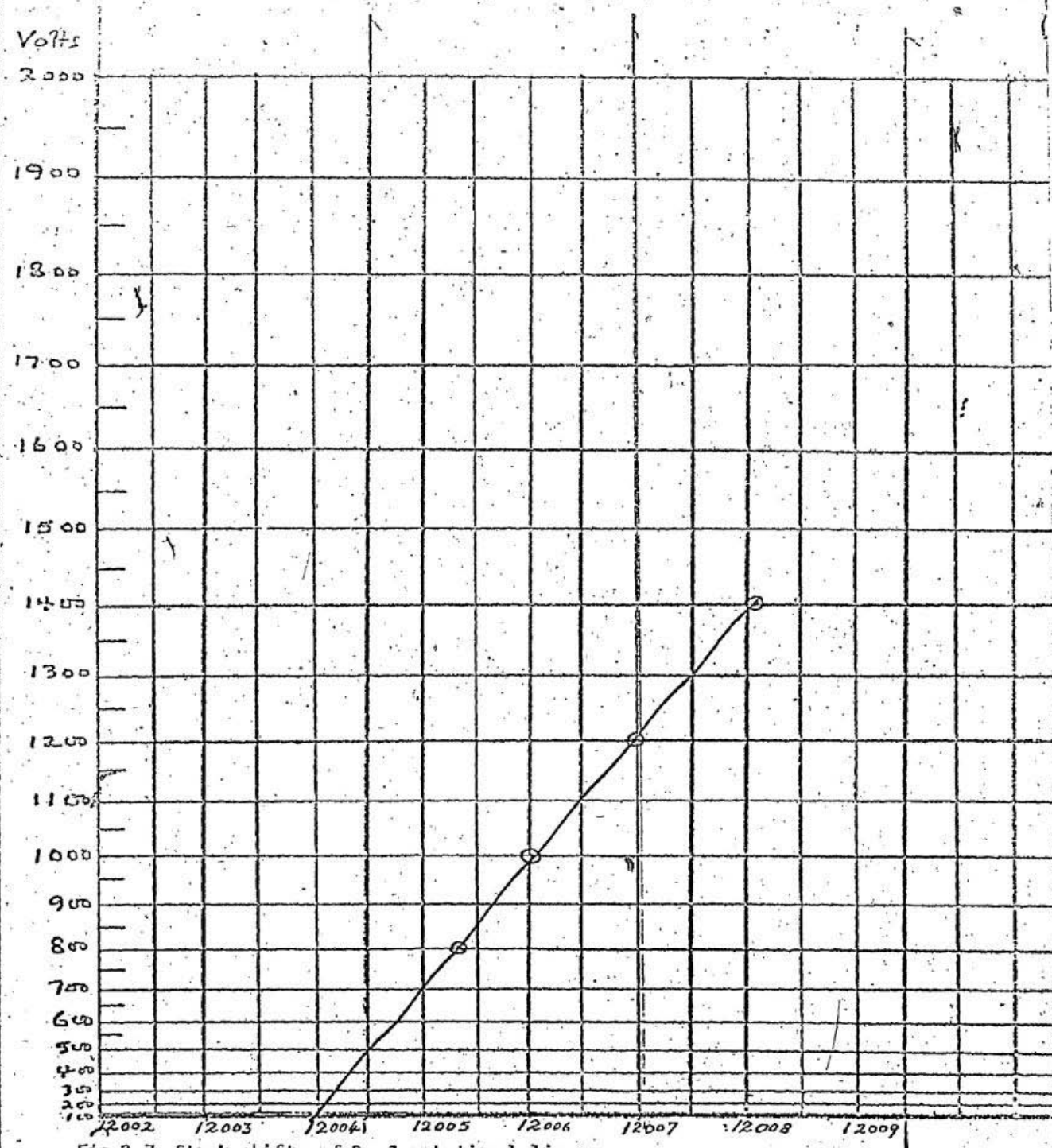

Fig 3.7 Stark shifts of 0→1 rotational line of $OC^{33}S$ in the (000) state (lower component)

Graph for plotting second order Stark Shifts

$\nu_0 = 12011.29$ MHz of $OC^{33}S$

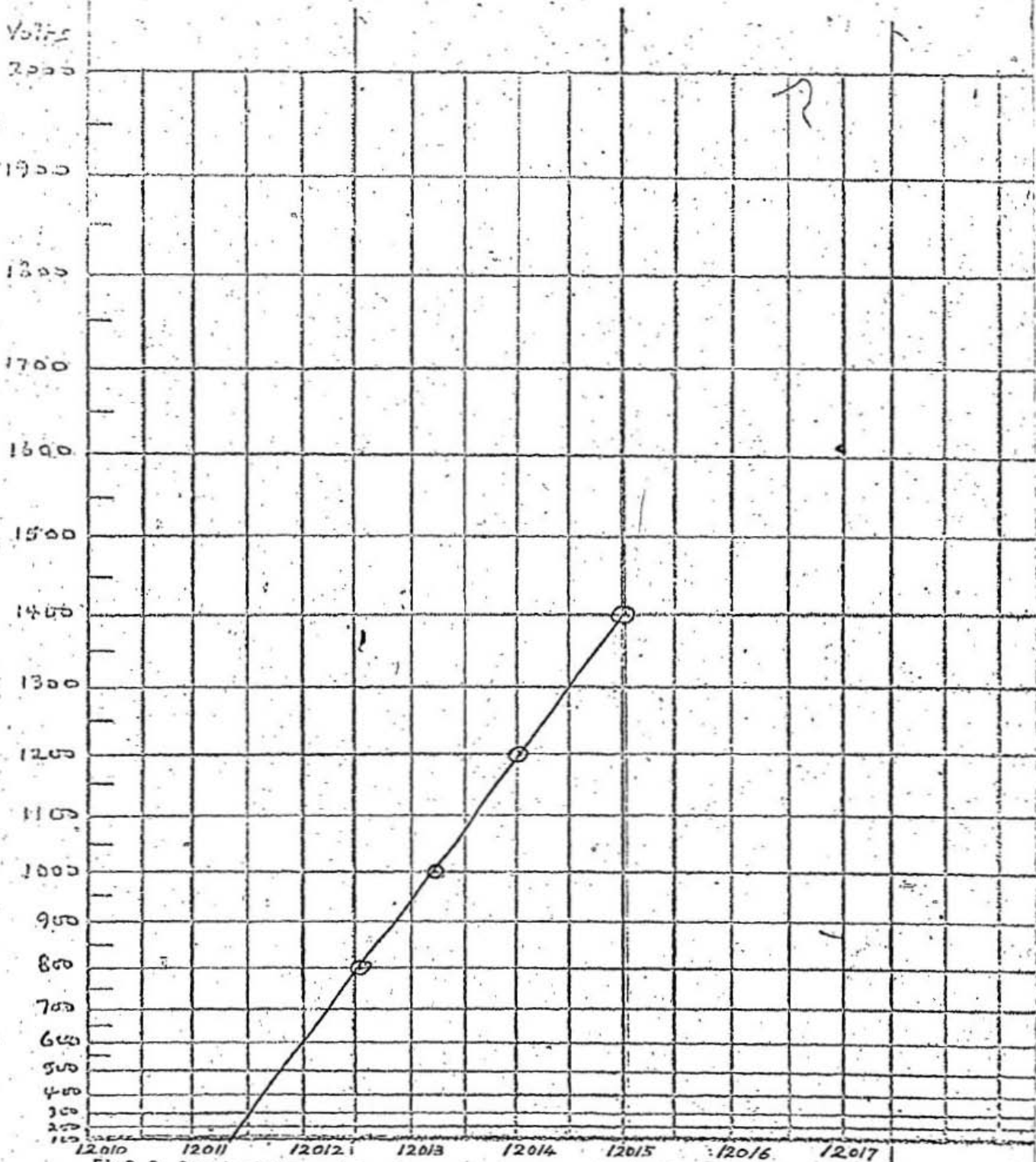

Fig3.8 Stark shifts of 0→1 rotational line of $OC^{33}S$ in the (000) state. (middle component)

Graph for plotting second order Stark Shifts

ν_0 = 12017.05 MHz of $OC^{33}S$

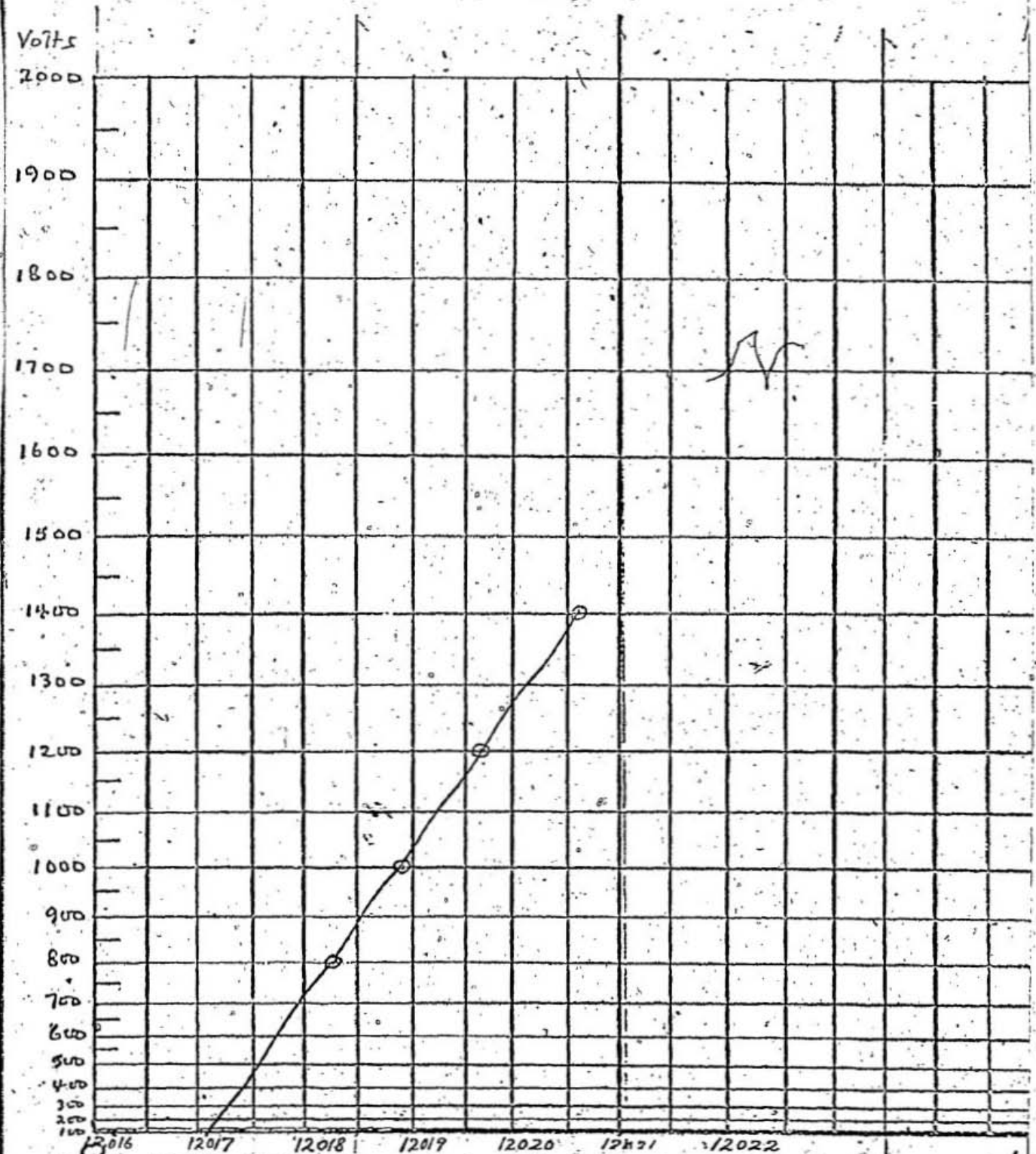

Fig 3.9 Stark shifts of 0→1 rotational line of $OC^{33}S$ in the (000) state (upper component)

Graph for plotting second order Stark Shifts

ν_0 = 11865.70 MHz of $OC^{34}S$

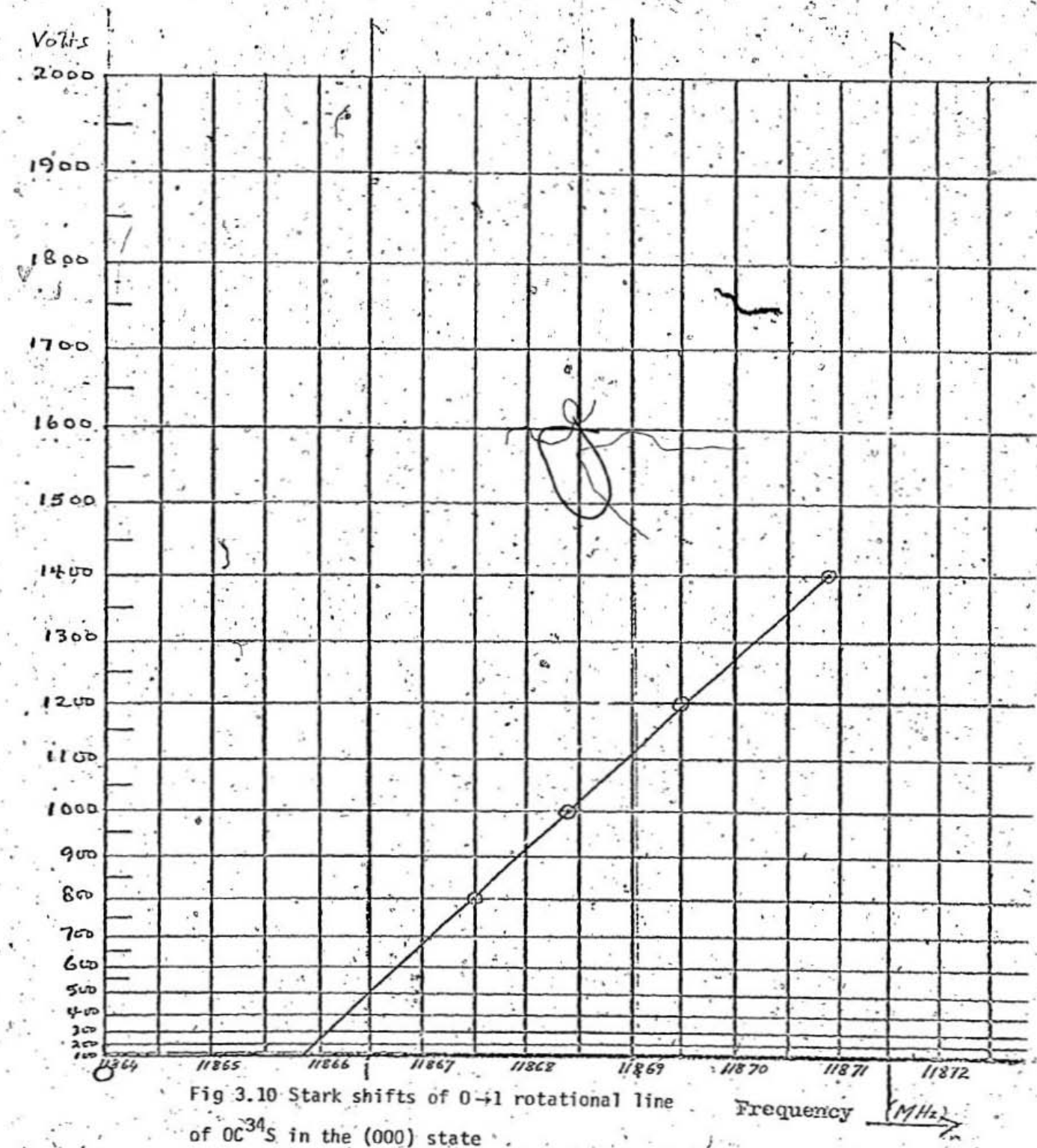

Fig 3.10 Stark shifts of 0→1 rotational line of $OC^{34}S$ in the (000) state

Graph for plotting second order Stark Shifts

ν_0 = 11409.65 MHz of ^{18}OCS

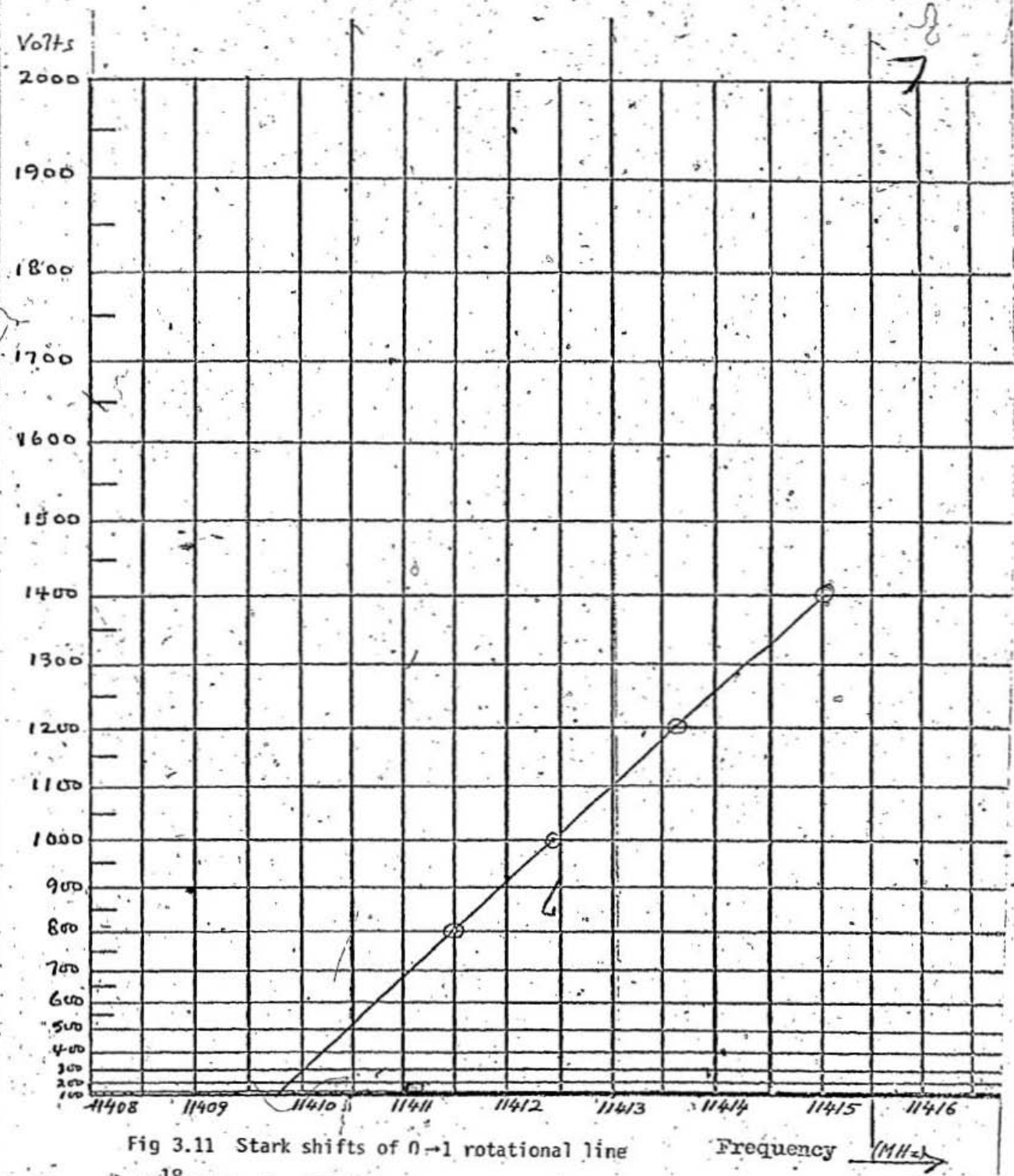

Fig 3.11 Stark shifts of 0→1 rotational line of ^{18}OCS in the (000) state.

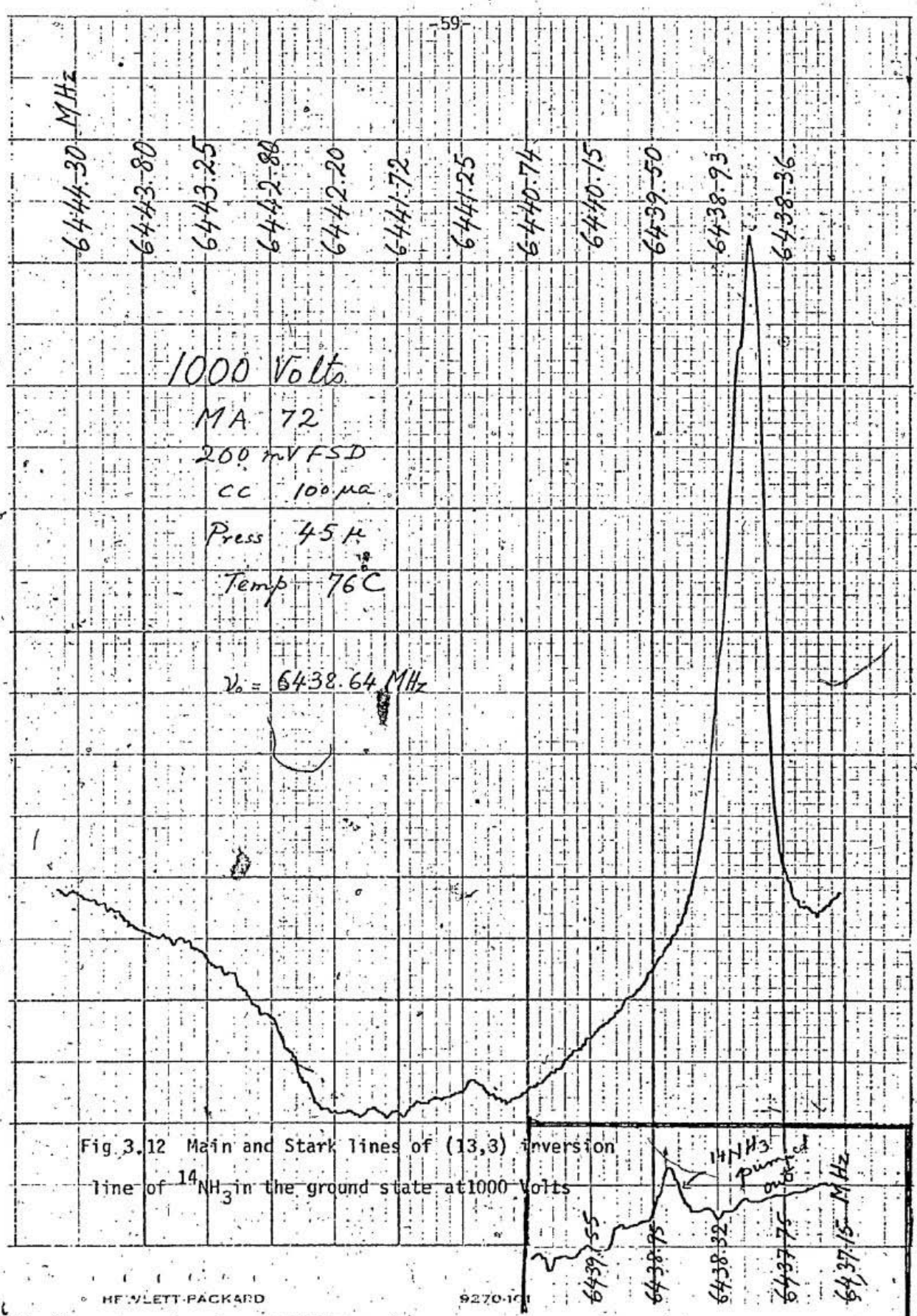

Fig. 3.12 Main and Stark lines of (13,3) inversion line of $^{14}NH_3$ in the ground state at 1000 volts

Fig. 3.13 (14,2) inversion line of $^{14}NH_3$ in the ground state

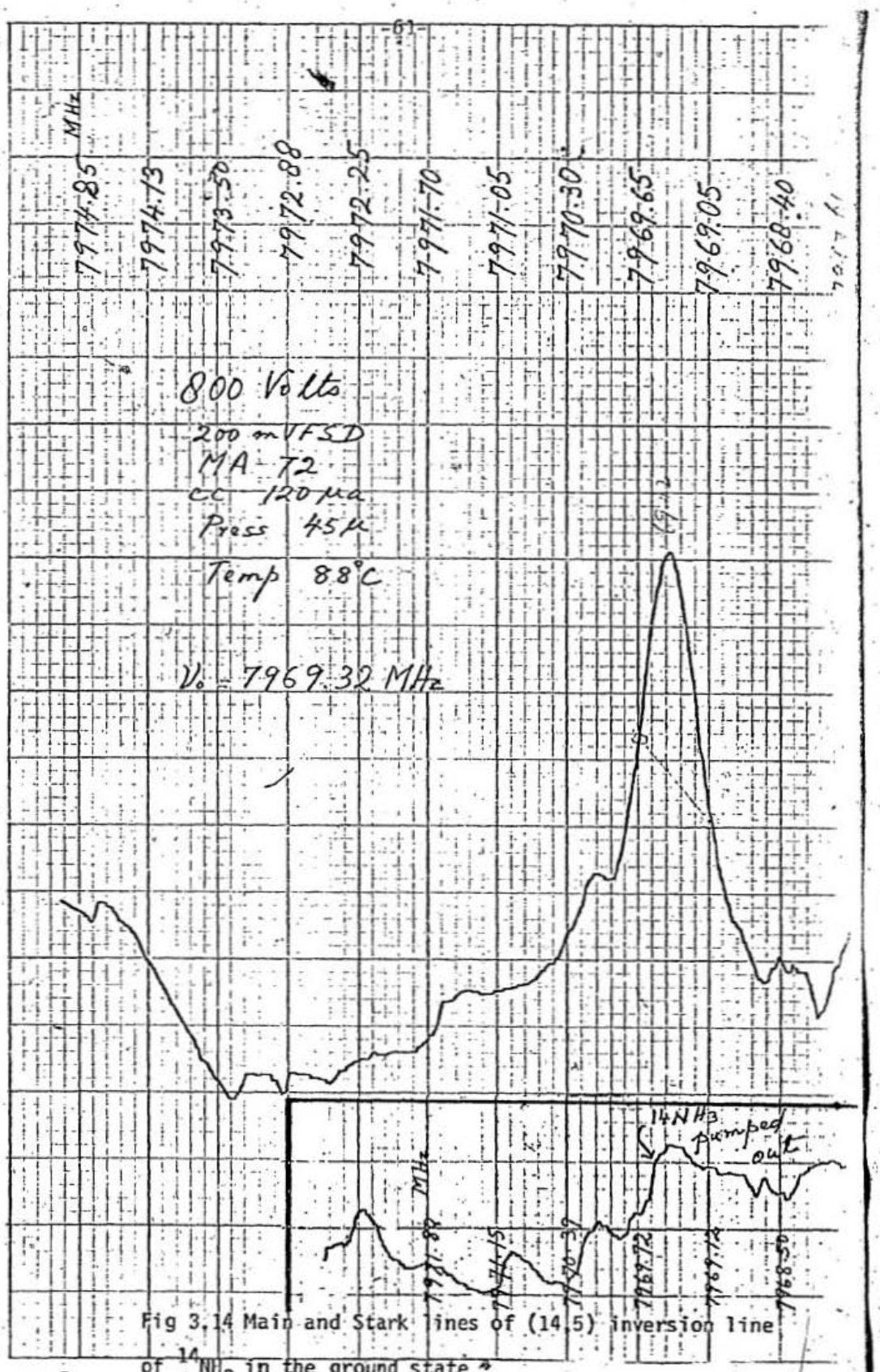

Fig 3.14 Main and Stark lines of (14,5) inversion line of $^{14}NH_3$ in the ground state.

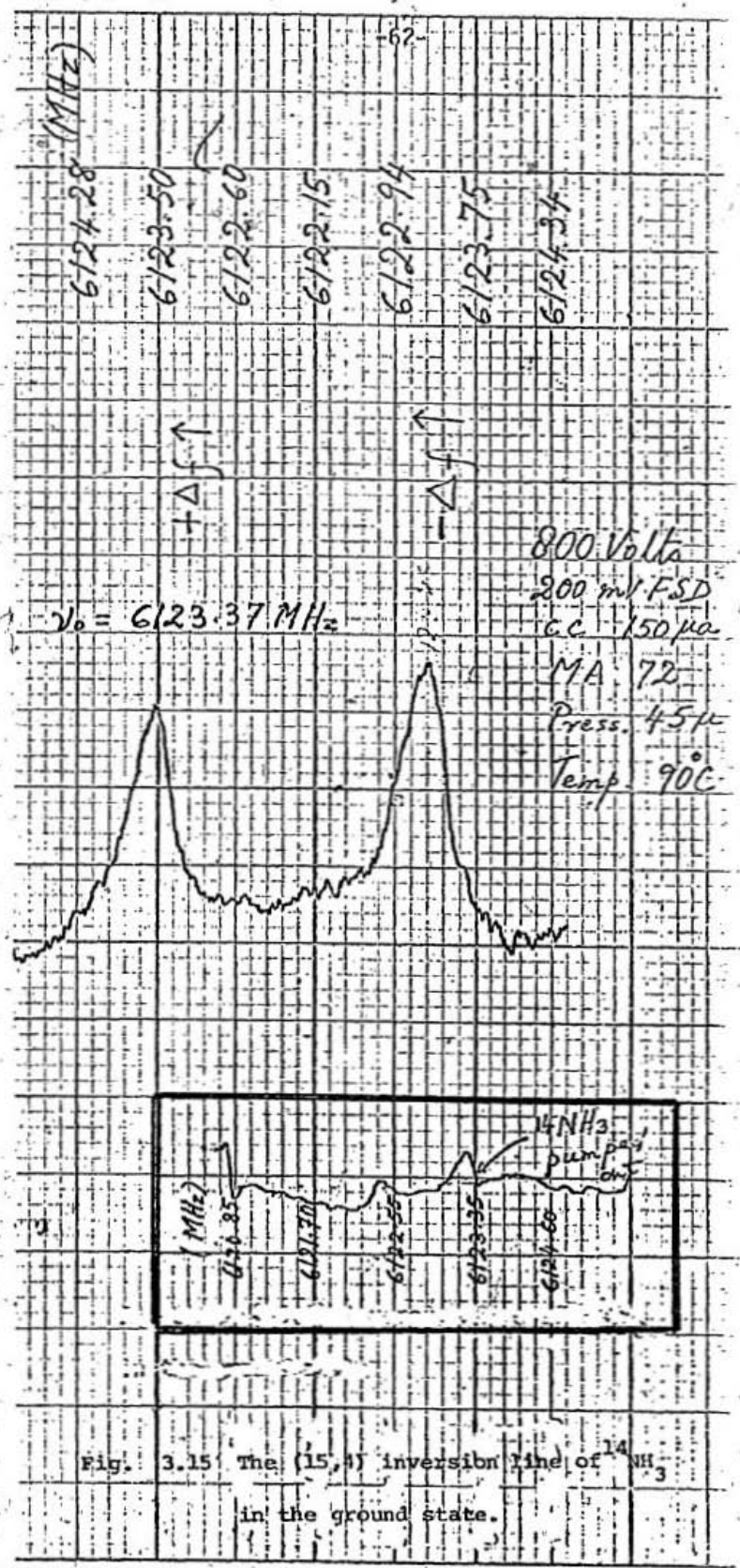

Fig. 3.15 The (15,8) inversion line of $^{14}NH_3$ in the ground state.

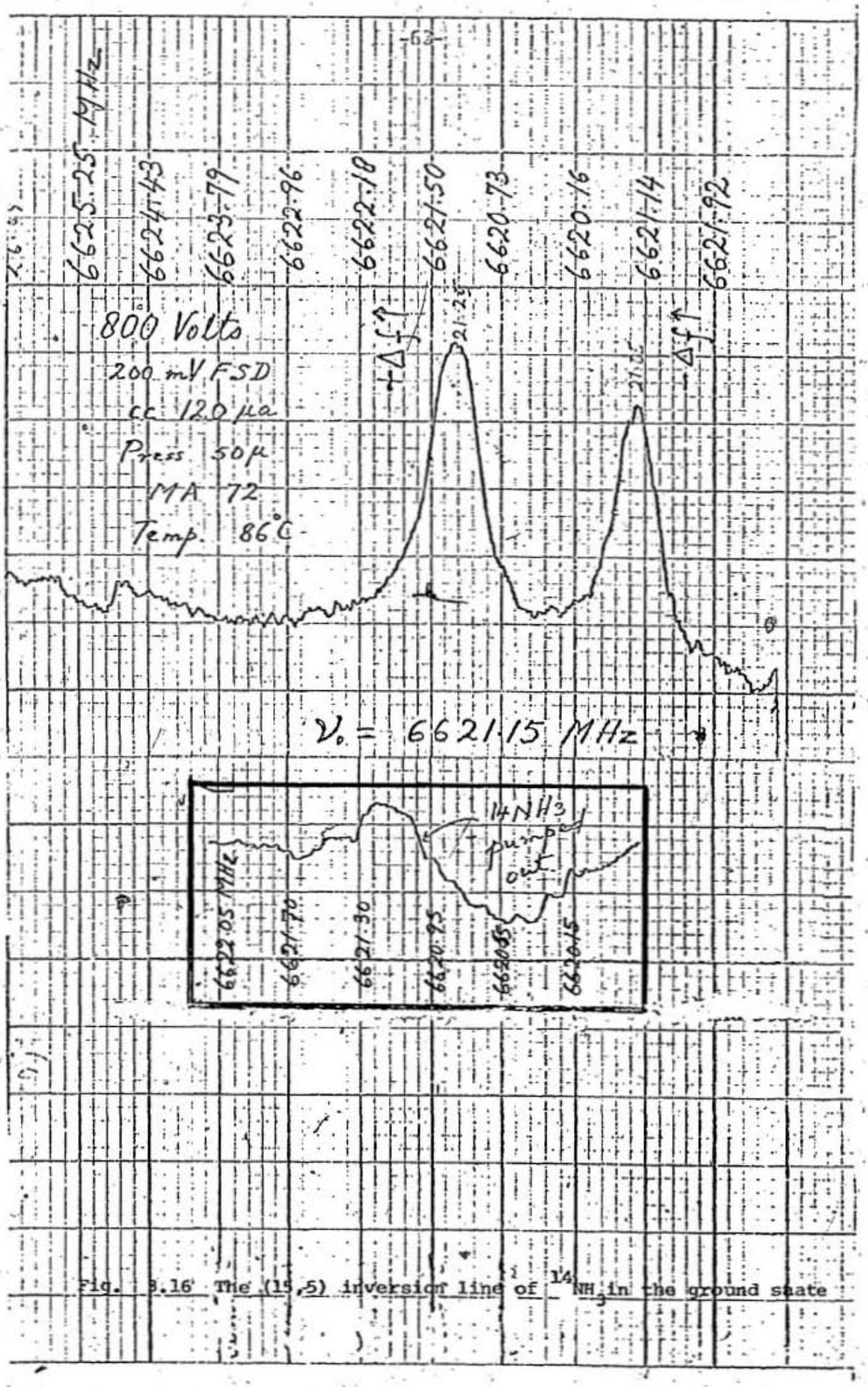

Fig. 3.16 The (15,5) inversion line of $^{14}NH_3$ in the ground state

Fig. 3.17 The (16,5) inversion line of $^{14}NH_3$ in the ground state

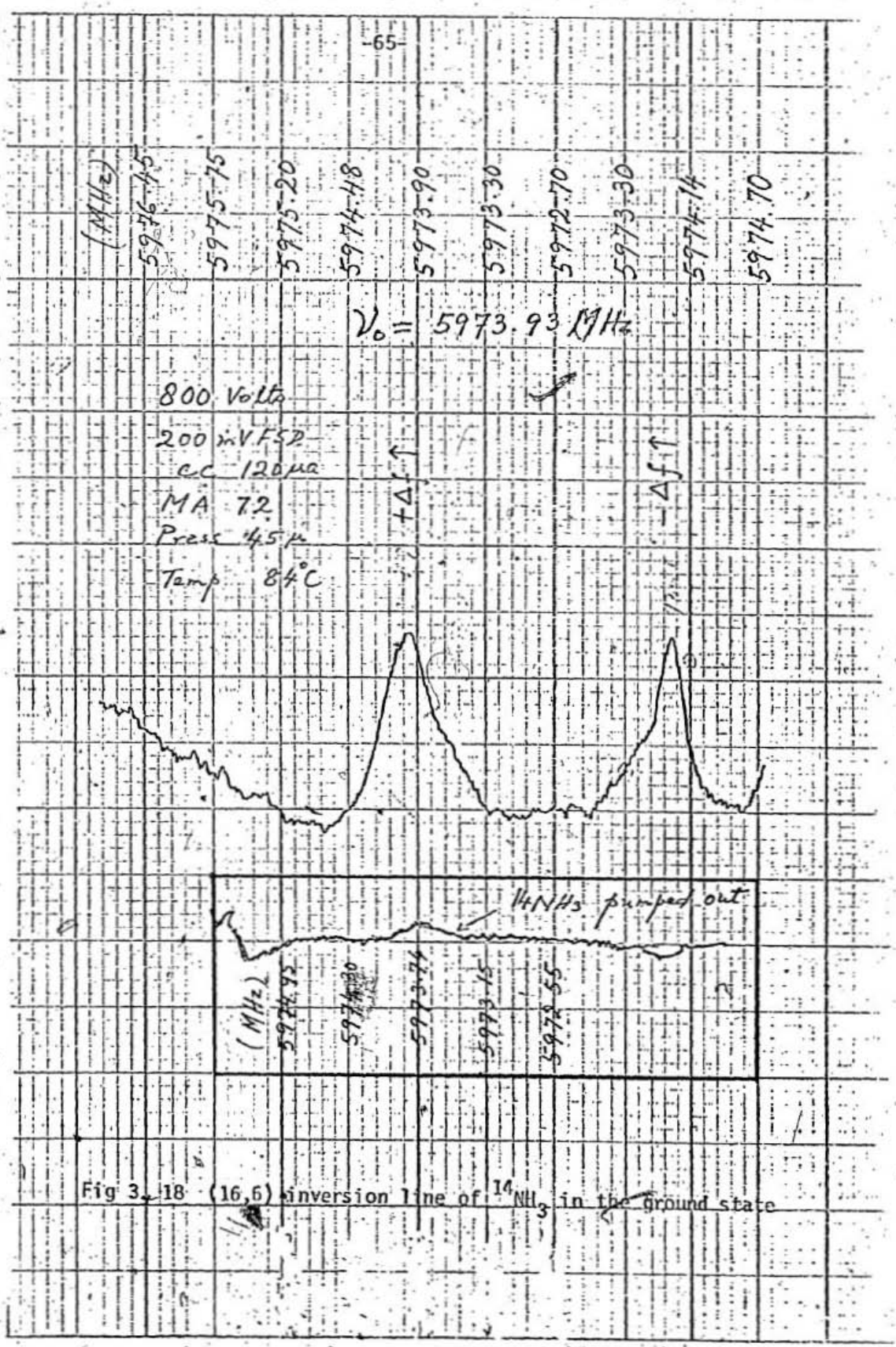

Fig 3. 18 (16,6) inversion line of $^{14}NH_3$ in the ground state

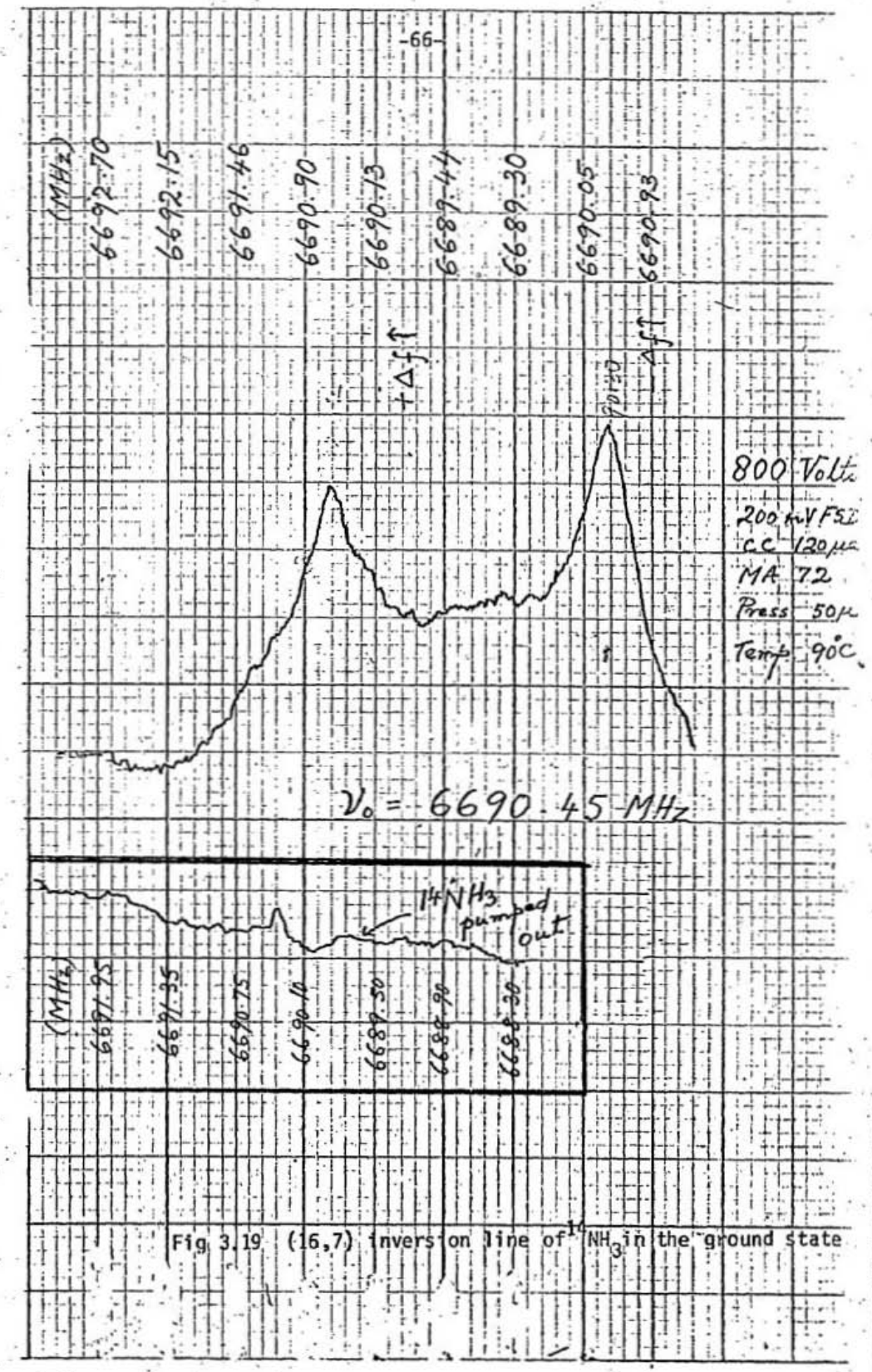

Fig 3.19 (16,7) inversion line of $^{14}NH_3$ in the ground state

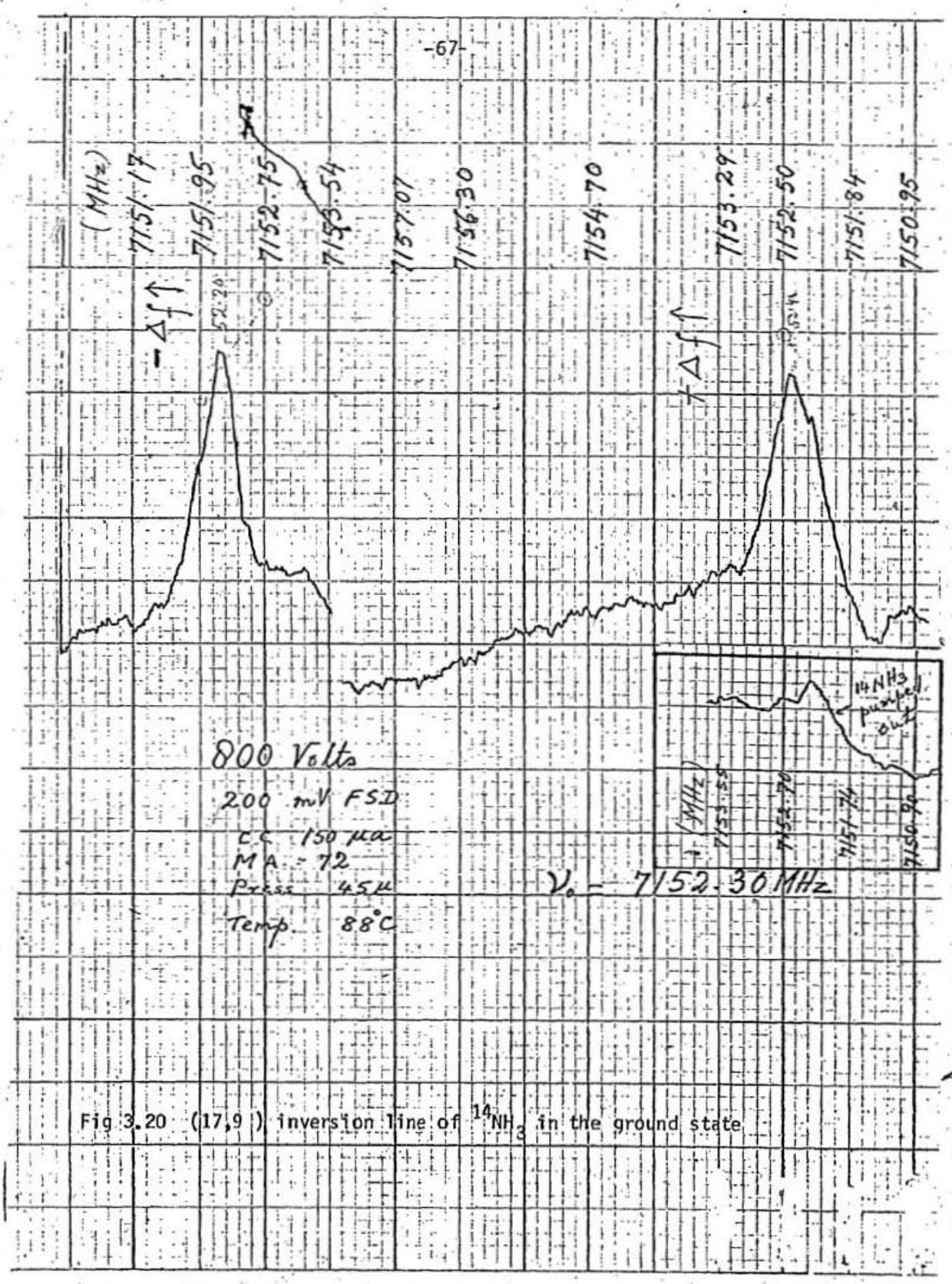

Fig 3.20 (17,9) inversion line of $^{14}NH_3$ in the ground state

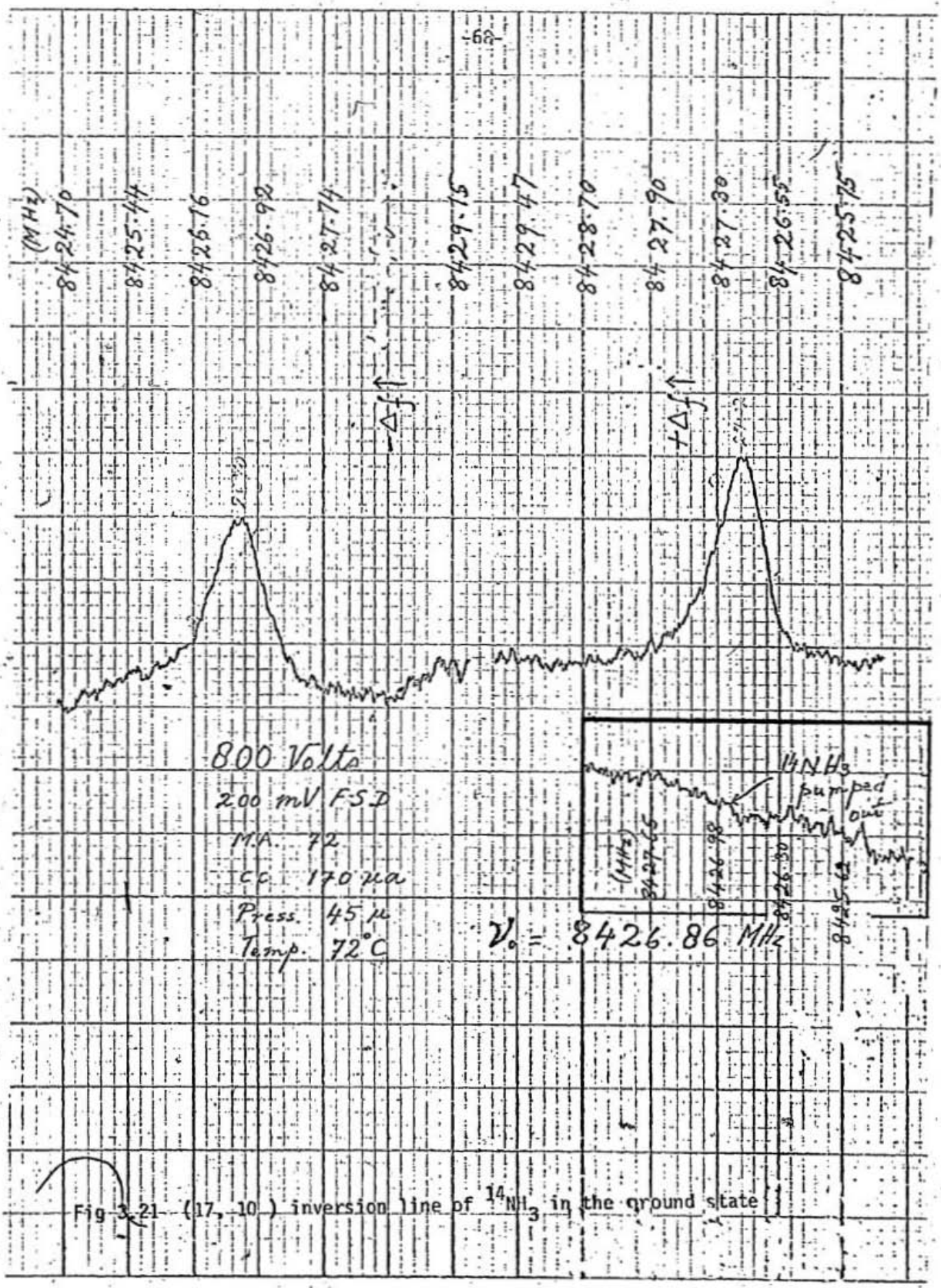

Fig 3.21 (17, 10) inversion line of $^{14}NH_3$ in the ground state

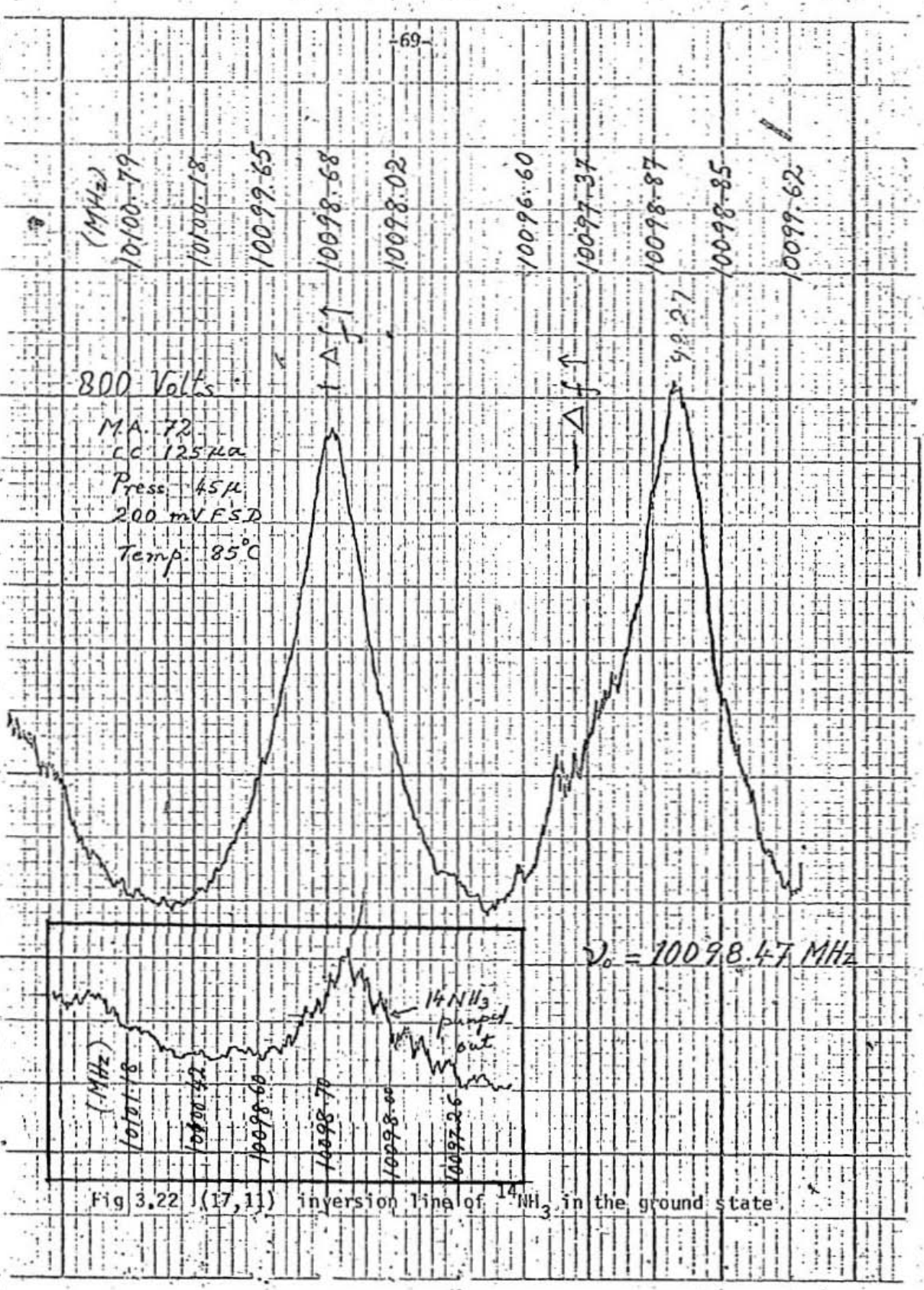

Fig 3.22 (17,11) inversion line of $^{14}NH_3$ in the ground state.

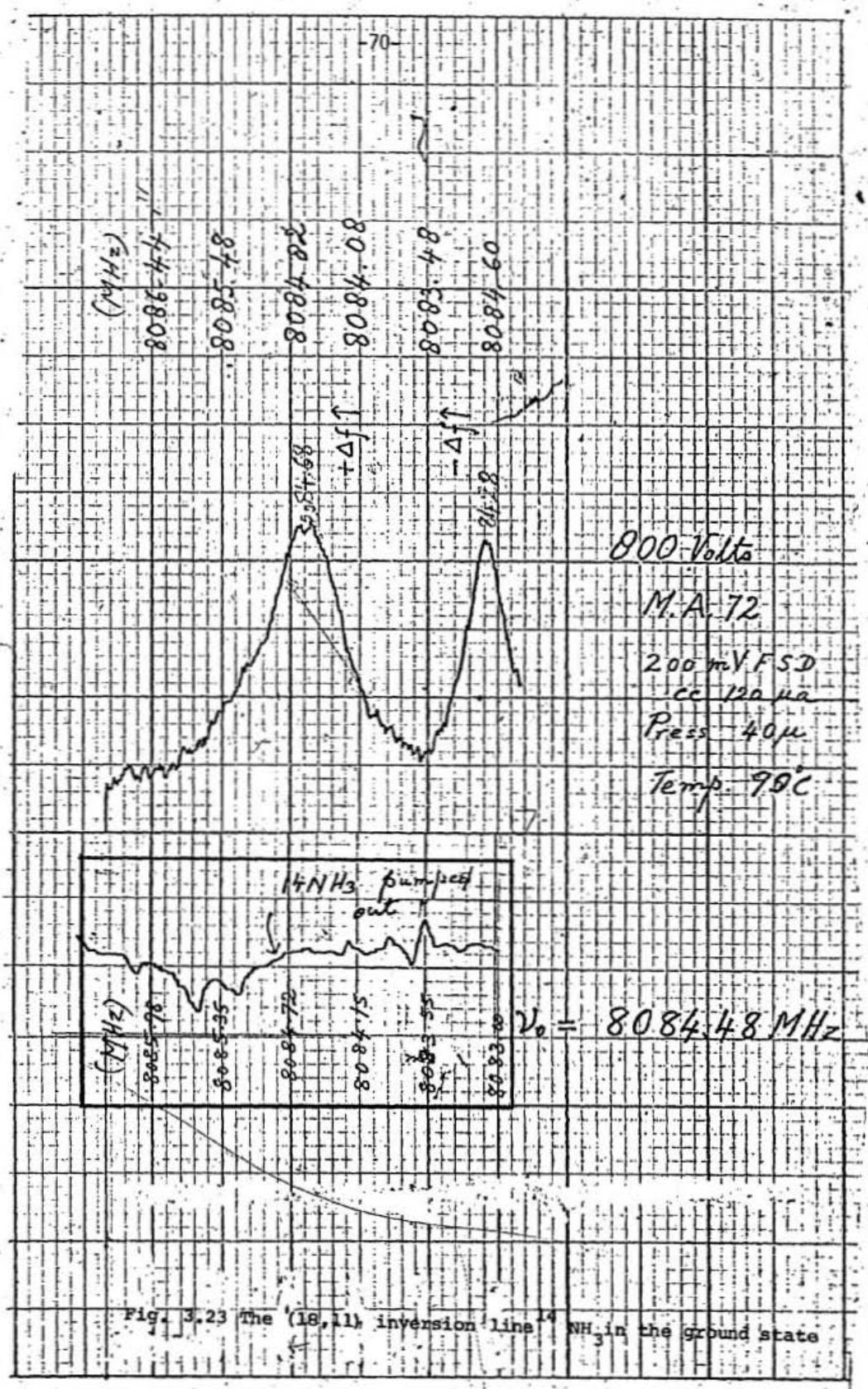

Fig. 3.23 The (18,11) inversion line $^{14}NH_3$ in the ground state

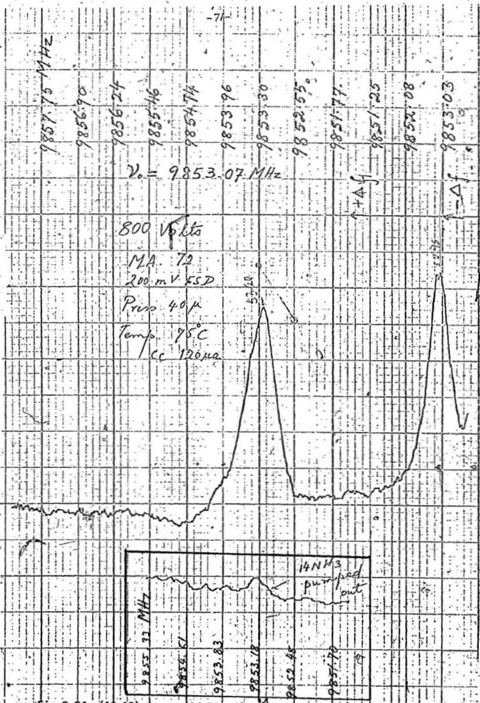

Fig 3.24 (18,12) inversion line of $^{14}NH_3$ in the ground state

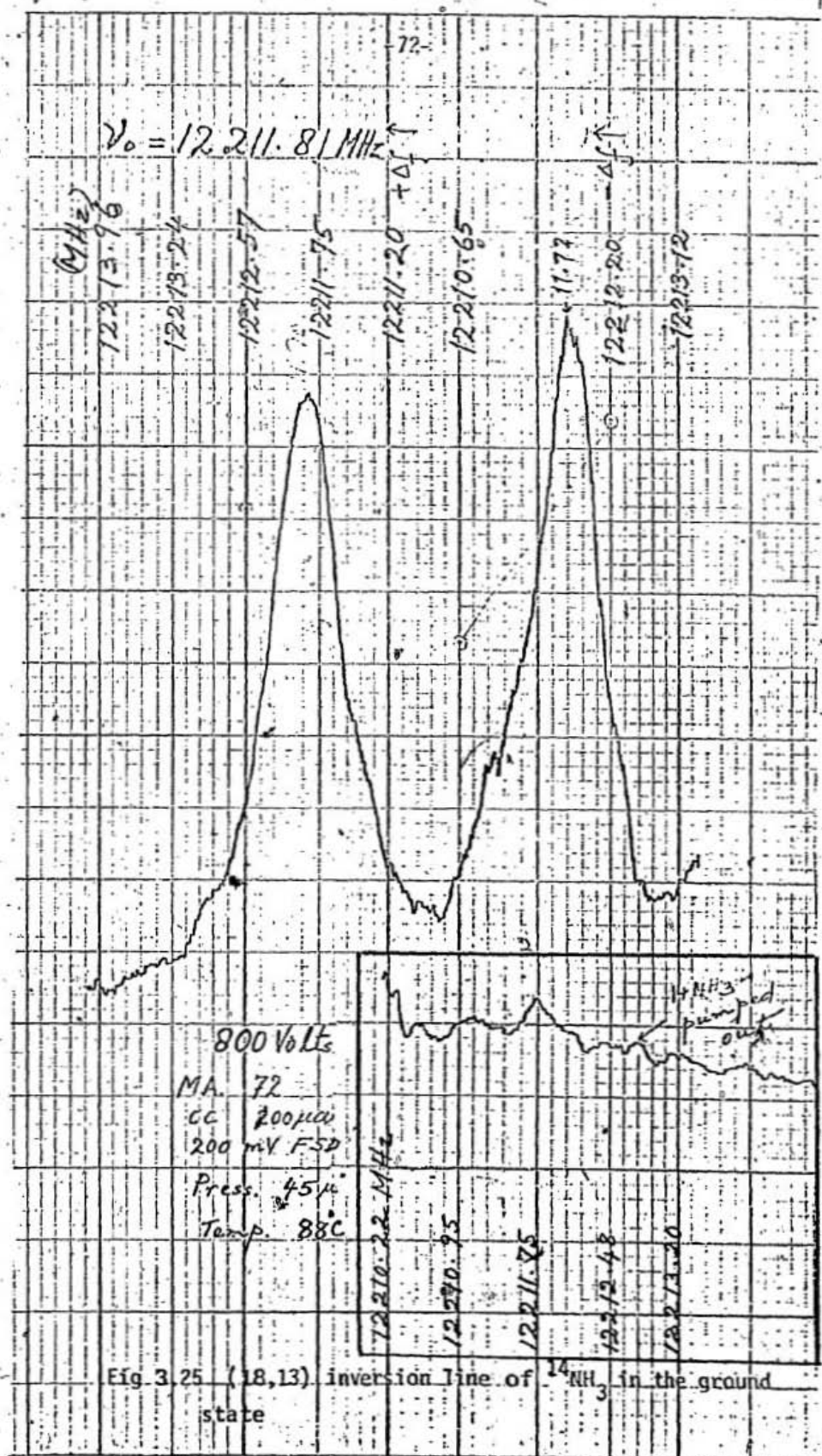

Fig 3.25 (18,13) inversion line of $^{14}NH_3$ in the ground state

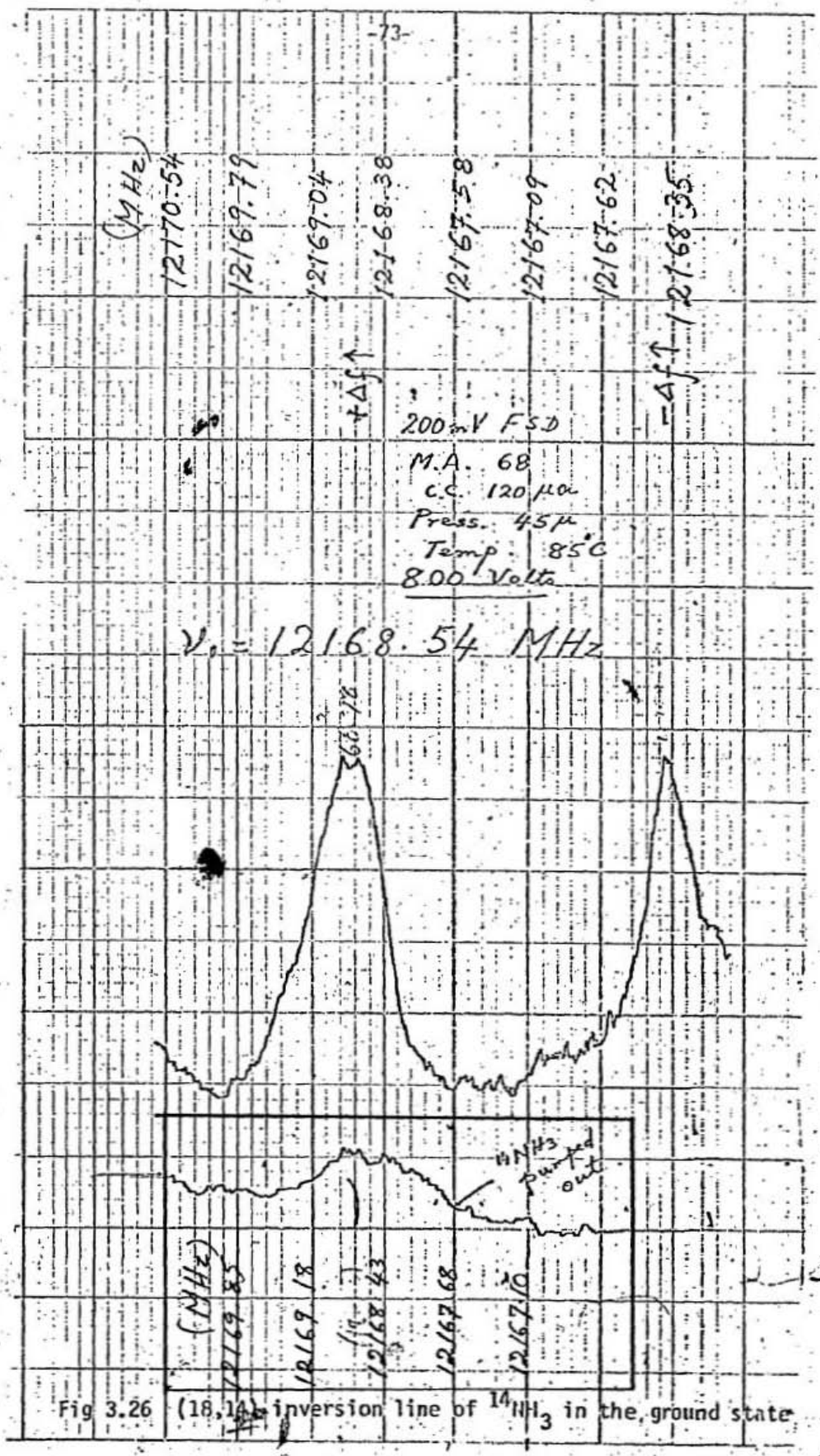

Fig 3.26 (18,18) inversion line of $^{14}NH_3$ in the ground state

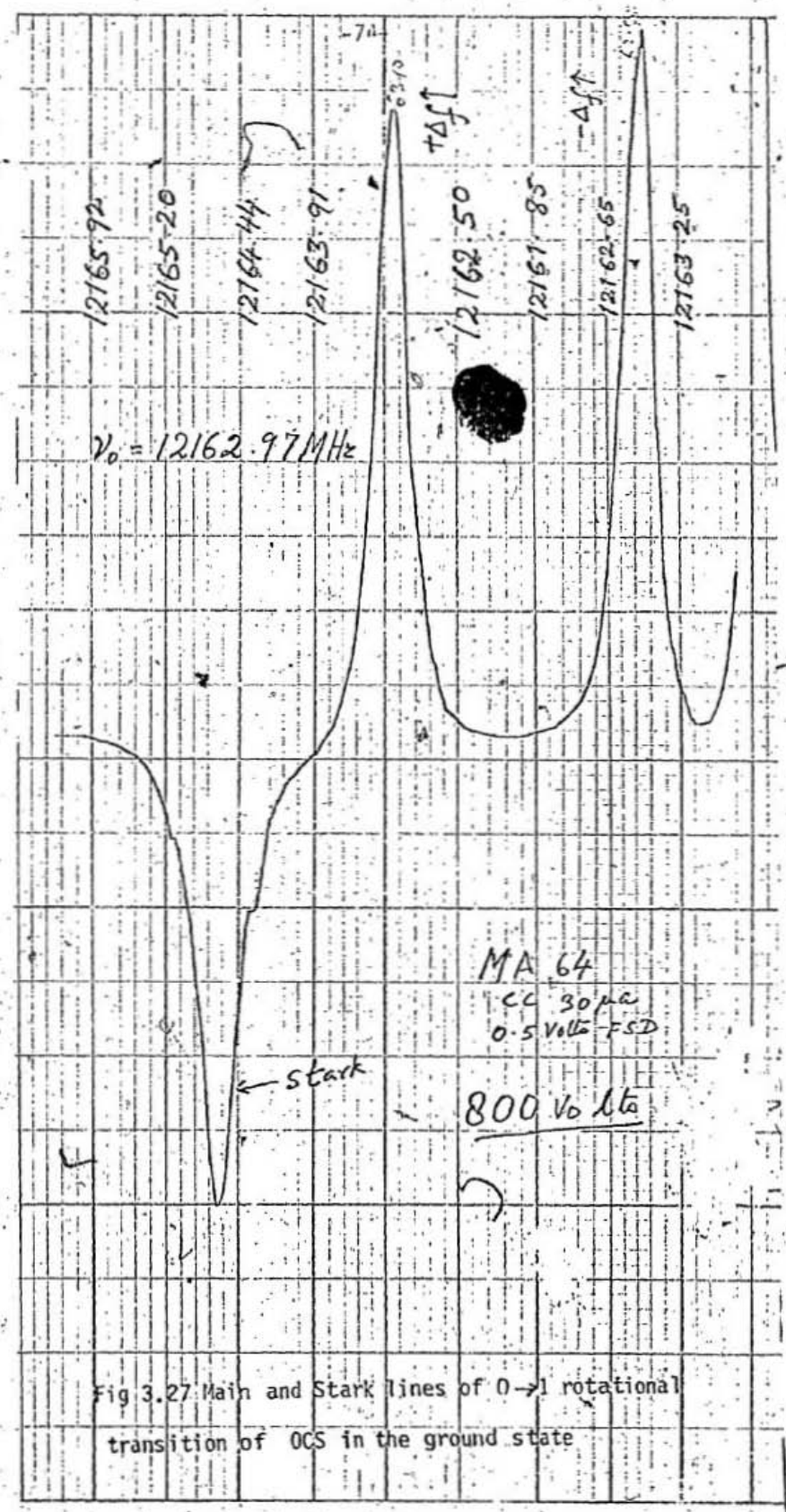

Fig 3.27 Main and Stark lines of 0→1 rotational transition of OCS in the ground state

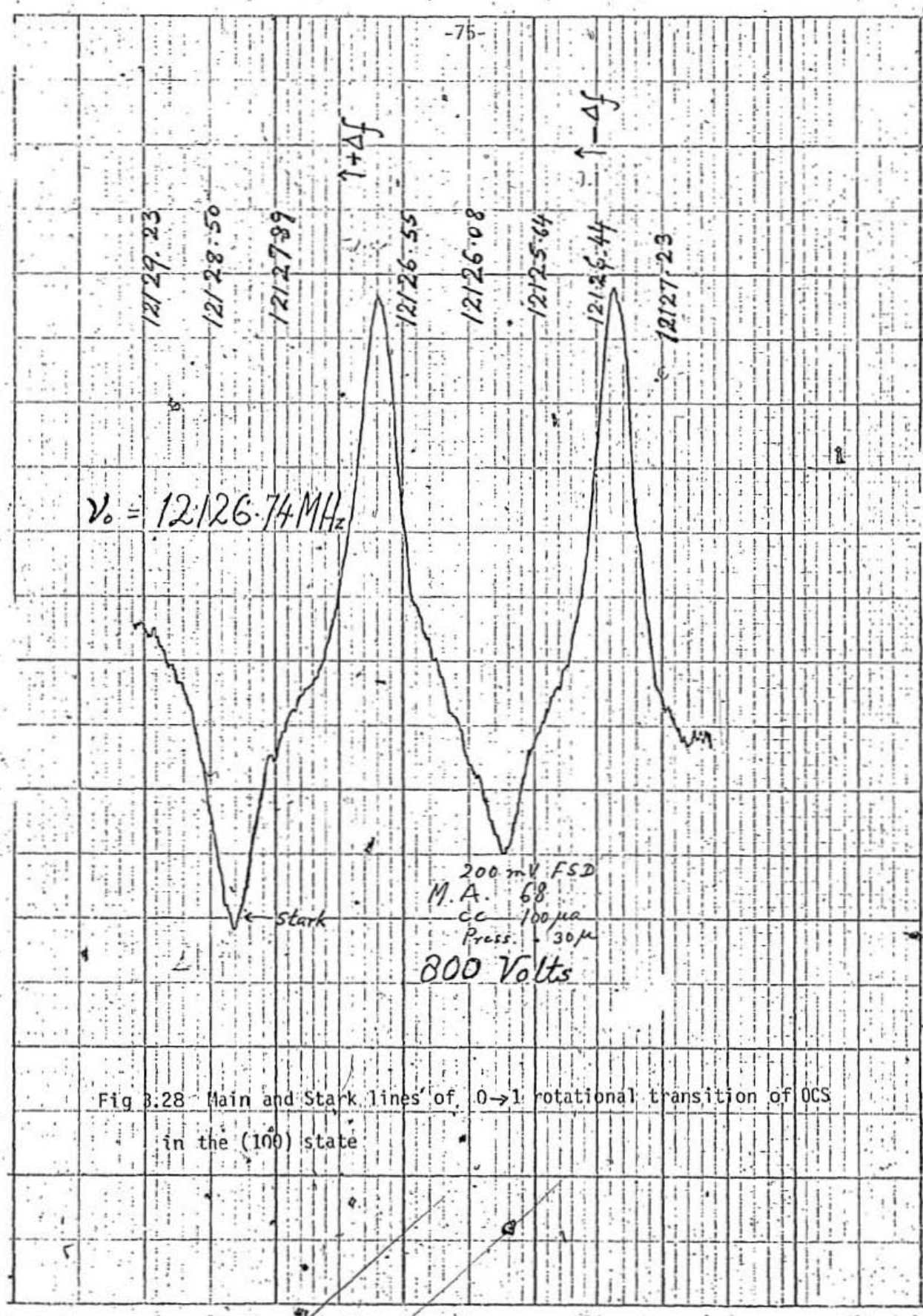

Fig 3.28 Main and Stark lines of 0→1 rotational transition of OCS in the (100) state

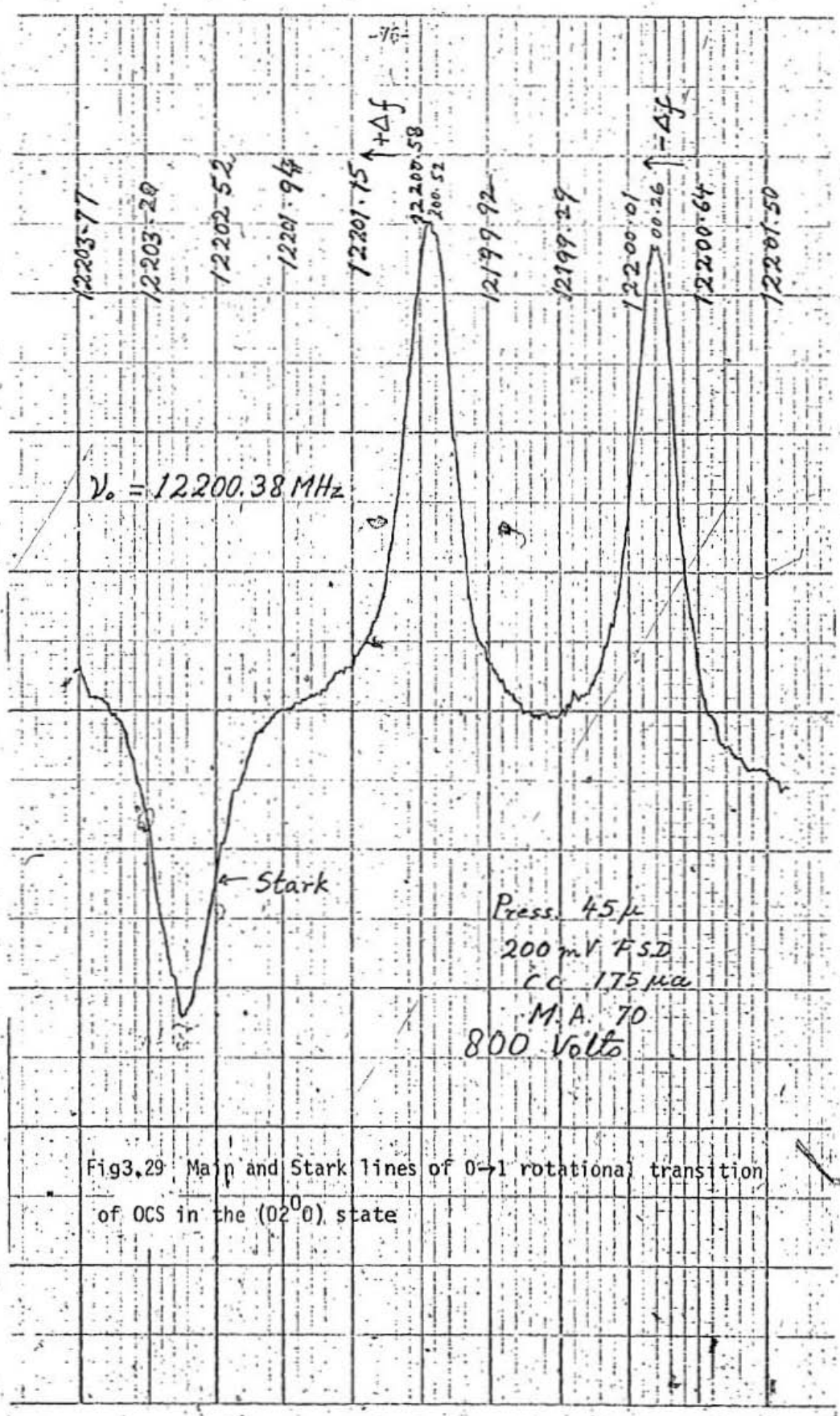

Fig3.29 Main and Stark lines of 0→1 rotational transition of OCS in the $(02^{0}0)$ state

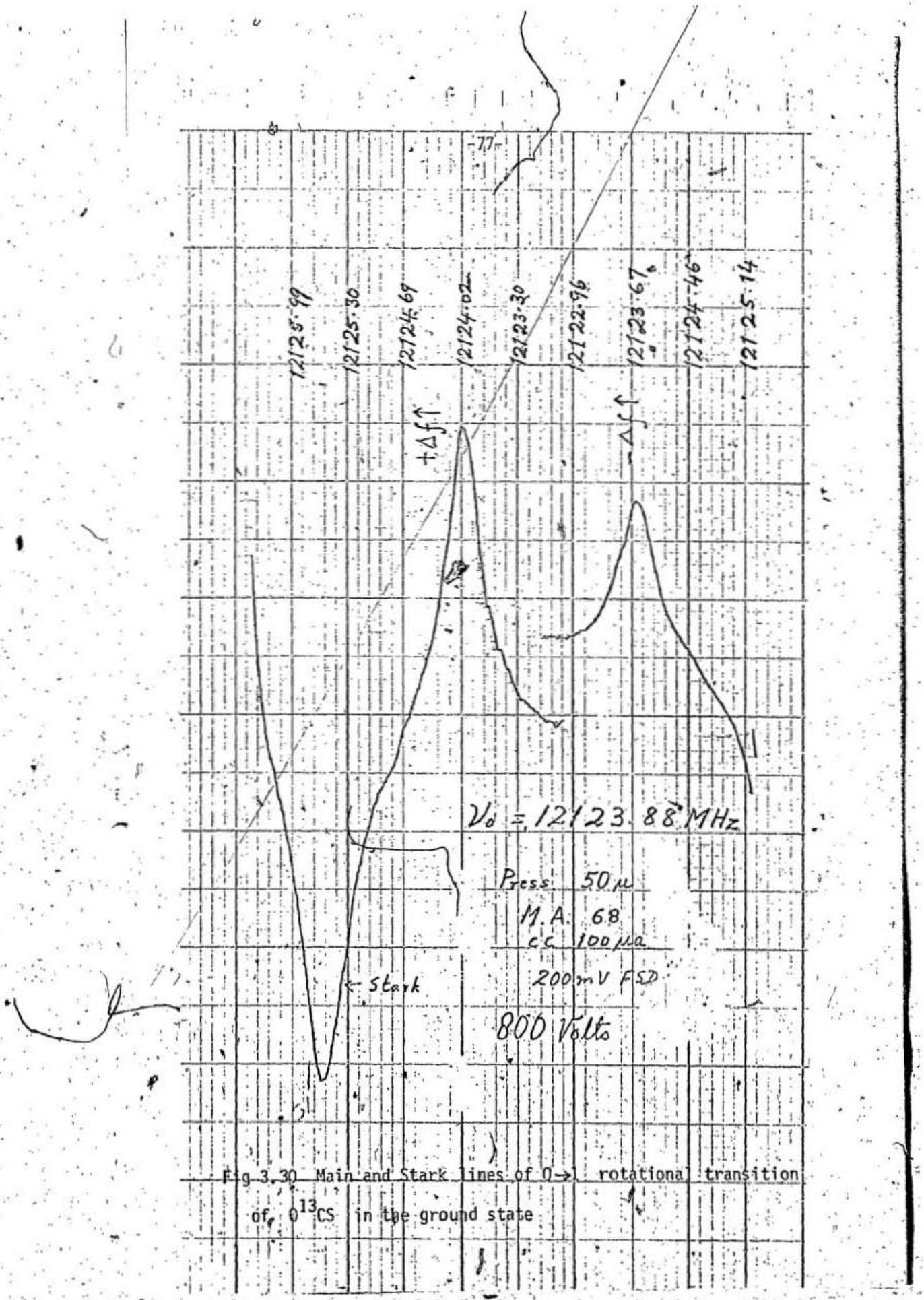

Fig 3.30 Main and Stark lines of 0→1 rotational transition of $O^{13}CS$ in the ground state

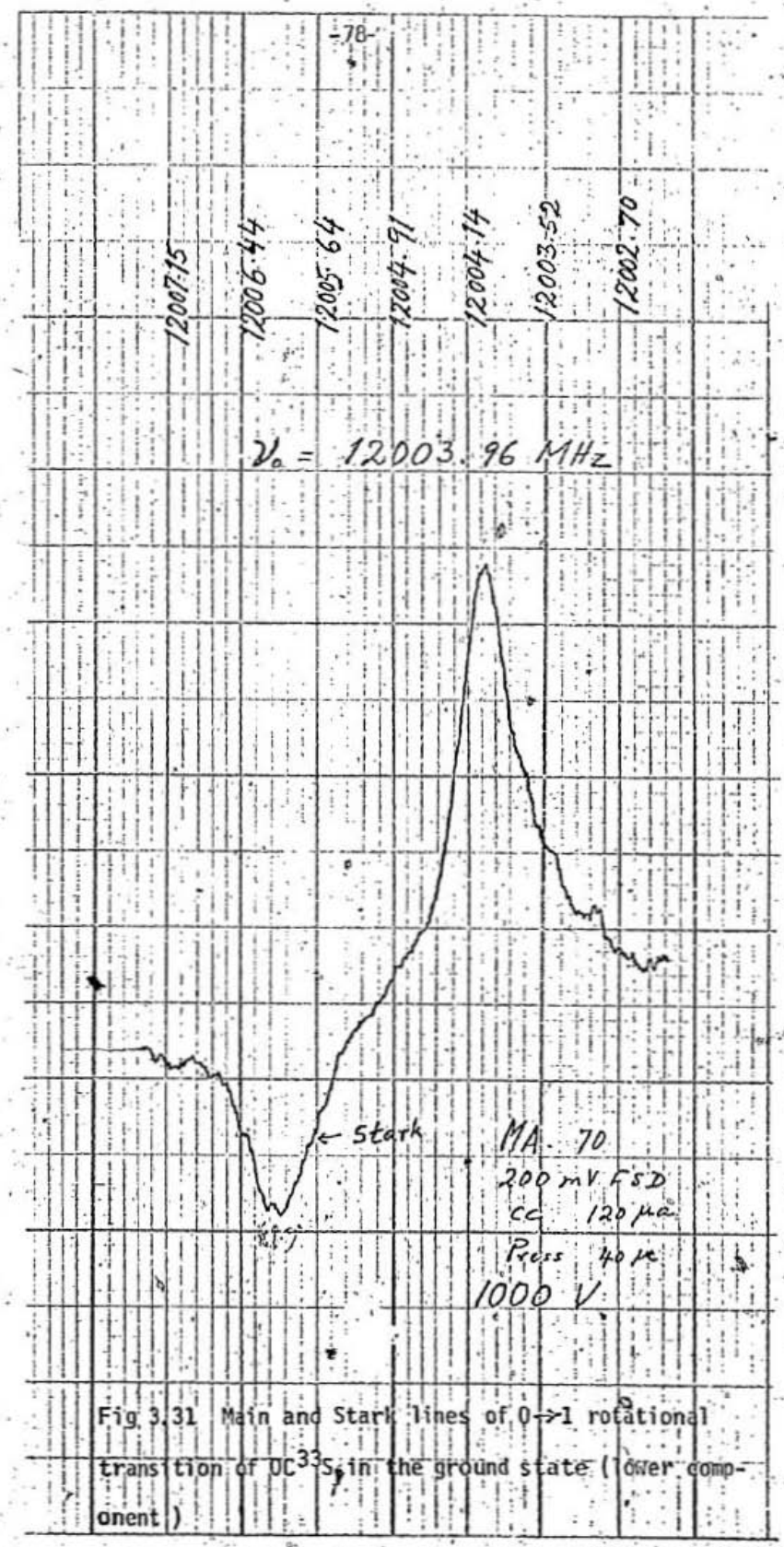

Fig 3.31 Main and Stark lines of 0→1 rotational transition of $OC^{33}S$ in the ground state (lower component)

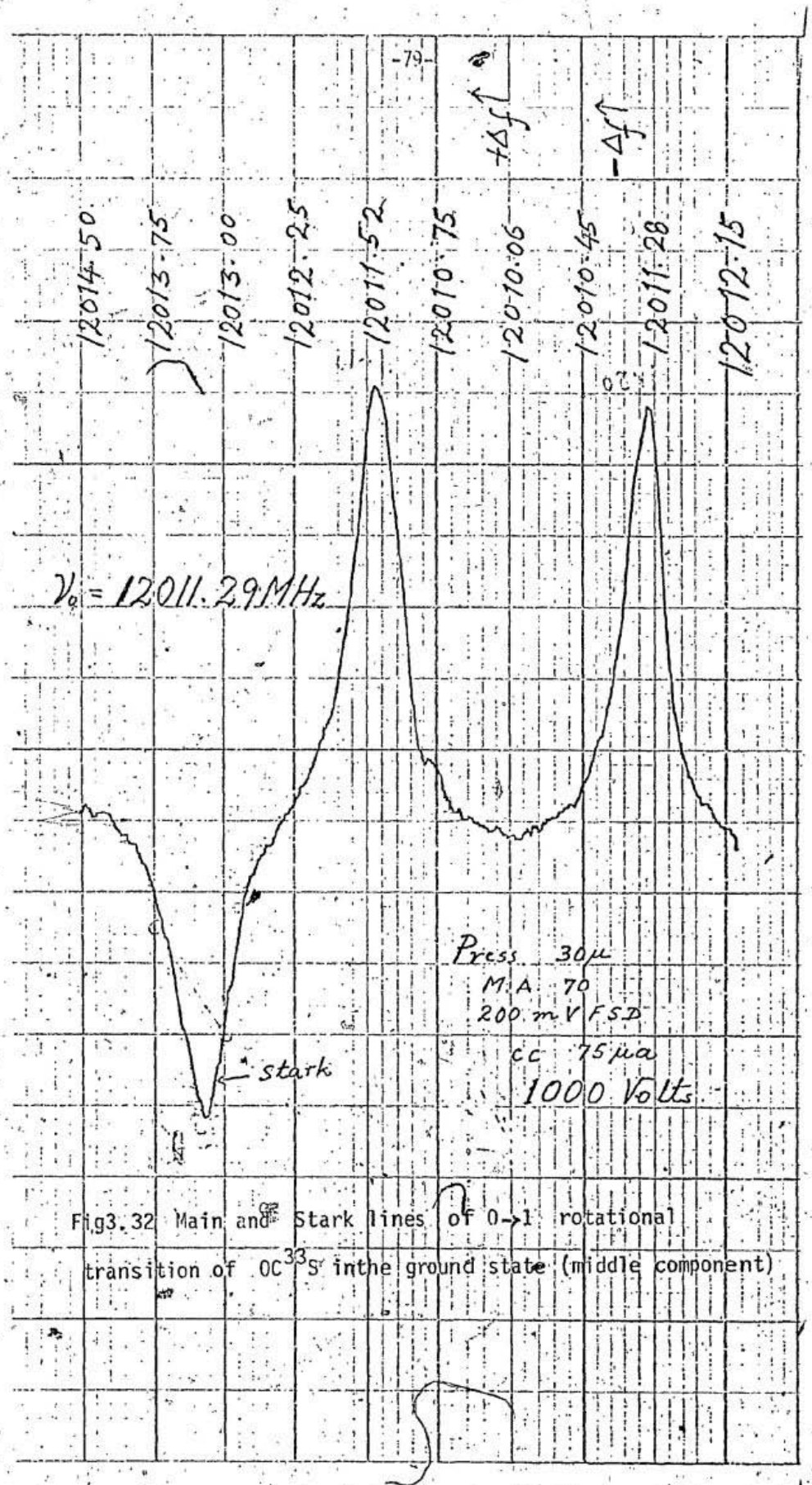

Fig3.32 Main and Stark lines of 0→1 rotational transition of $OC^{33}S$ inthe ground state (middle component)

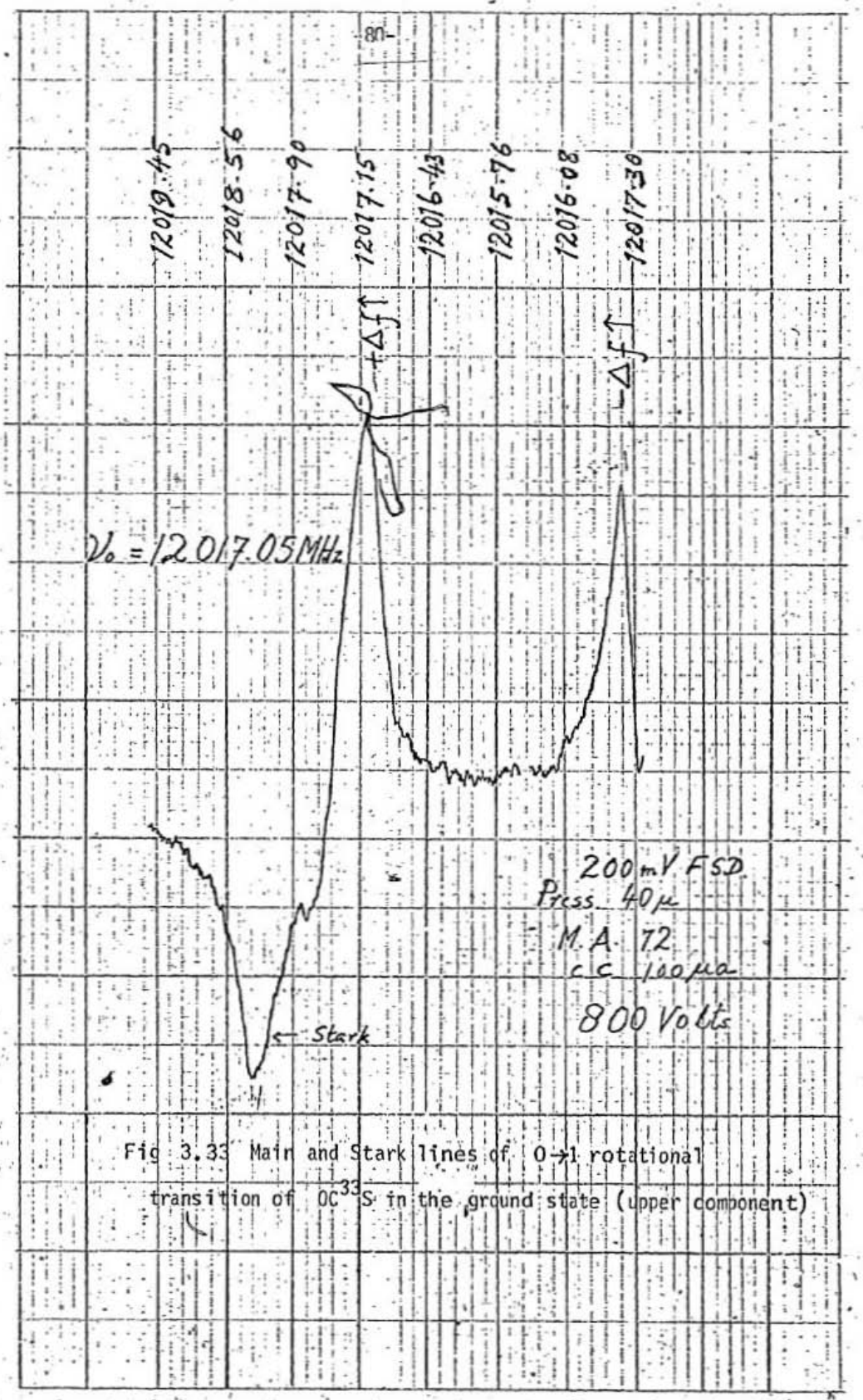

Fig 3.33 Main and Stark lines of $0 \rightarrow 1$ rotational transition of $OC^{33}S$ in the ground state (upper component)

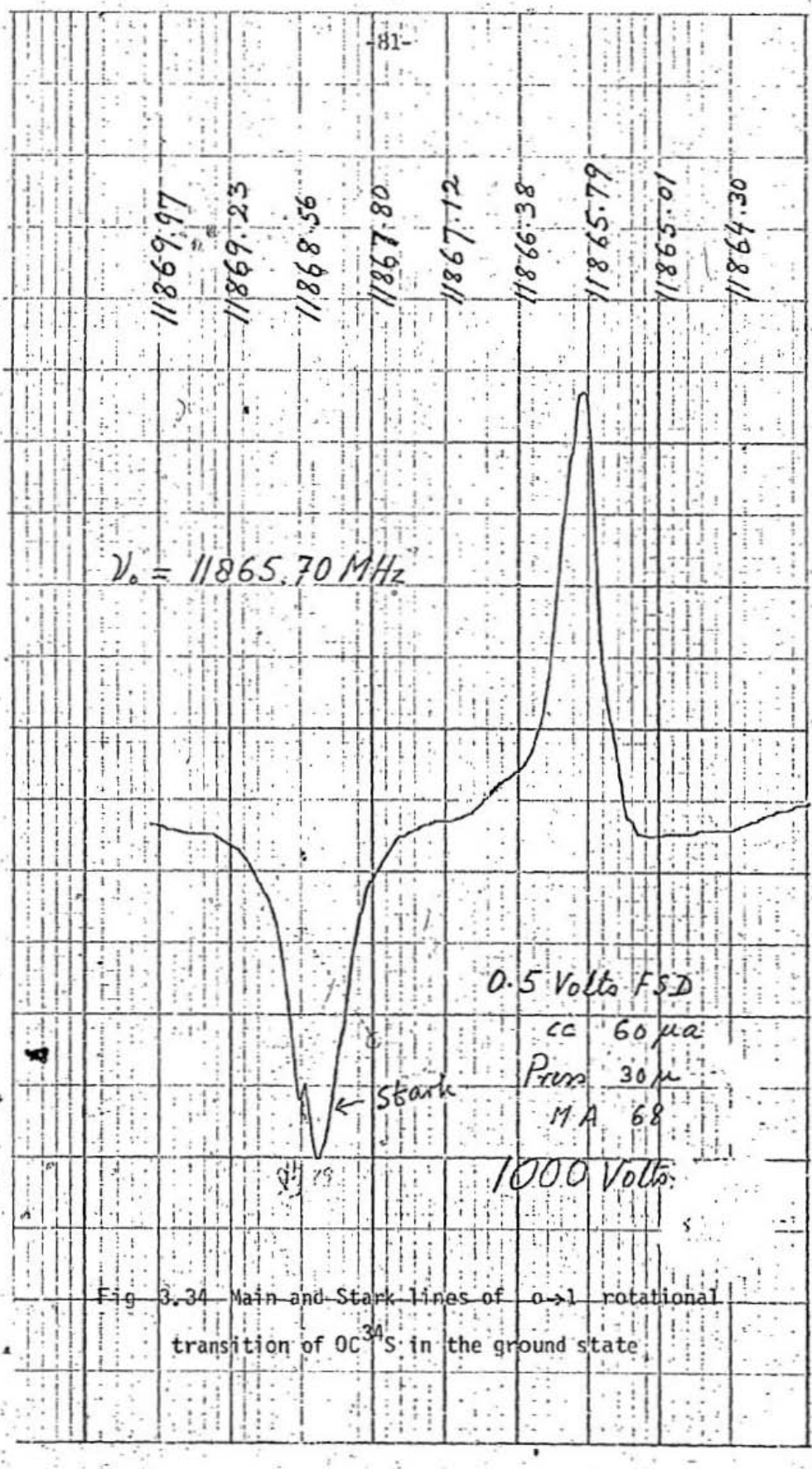

Fig 3.34 Main and Stark lines of o→1 rotational transition of $OC^{34}S$ in the ground state

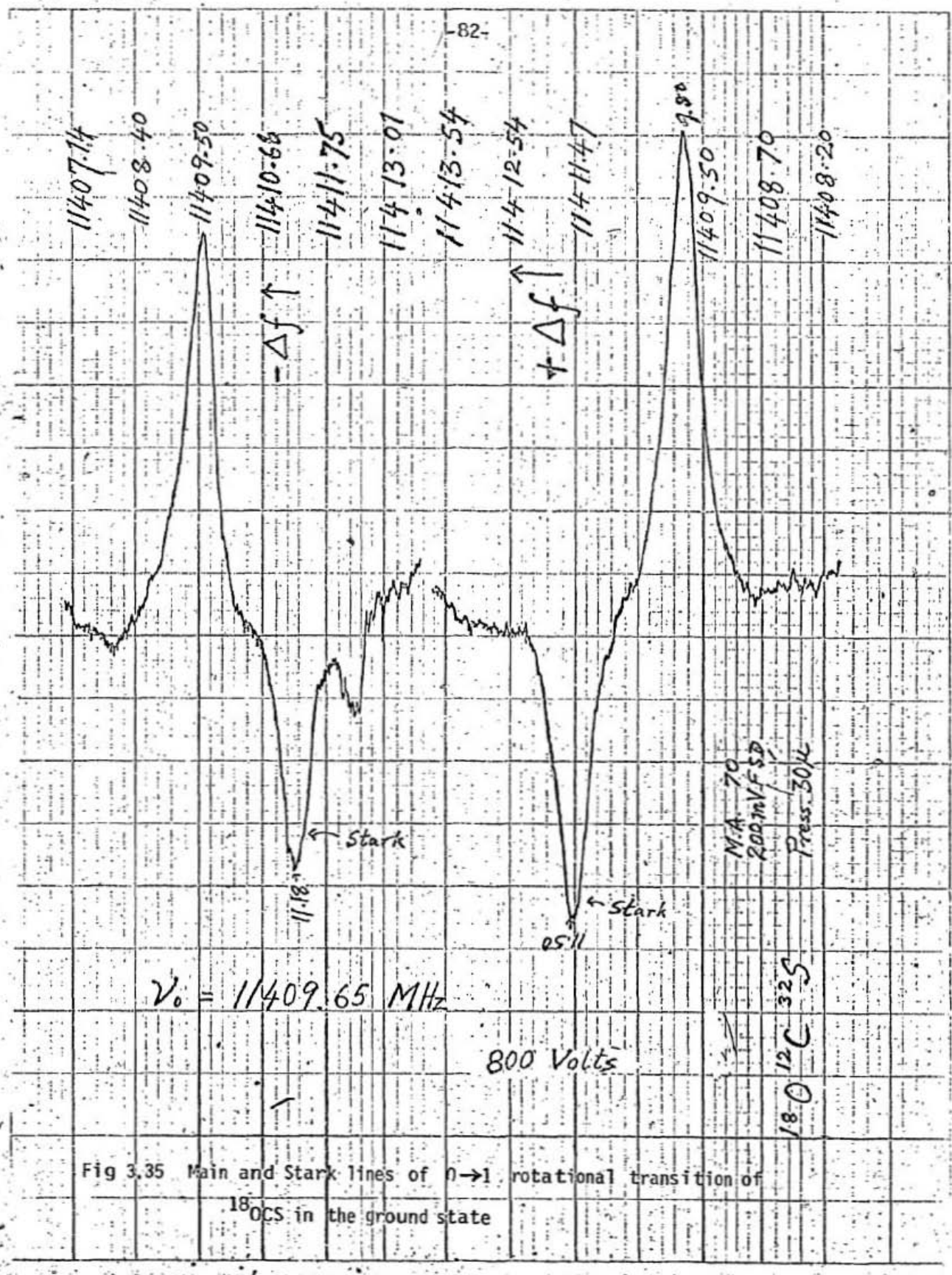

Fig 3.35 Main and Stark lines of 0→1 rotational transition of ^{18}OCS in the ground state

3.3 Summary of Results

Fifteen new ground state inversion lines of $^{14}NH_3$ were observed, accurately measured and assigned. The results of the Stark analysis of two of these lines confirmed the assignments, which are mainly based on the extrapolation of the empirical formula of Schnabel et al. and the computations by G. Pederson and Paul Gillard of MUN. The dipole moment computed from the Stark shifts of these two lines is 1.472 ± 0.002 D, which is in good agreement with the value of 1.475 ± 0.006 D reported by Fujio Shimizu (19) recently. The r.m.s. deviation of the predicted frequencies from the observed frequencies is ±0.64 MHz with Schnabel's formula and ±0.36 MHz with MUN computations. The agreement between the theoretical frequencies from the semi-empirical formulae of Schnabel et al. for K = 3 and K = 6 lines and the observed frequencies is good in view of the large shift for J = 13 and K = 3.

Nine 0→1 rotational transitions of carbonyl sulphide were observed, accurately measured and assigned. Two of them were identified as Fermi pair and three of them constituted a triplet due to the quadrupole action of the ^{33}S nucleus. The r.m.s. deviation between the calculated and observed frequencies is ±0.014 MHz, which is less than the experimental error of ±0.023 MHz. From the Stark analysis the relative dipole moments of (100) and ($02^{0}0$) vibrational states of OCS and (000) state of ^{18}OCS, $O^{13}CS$, $OC^{33}S$ and $OC^{34}S$ were determined. The results are given in Table 3.14. The following points are to be noted.

1. The dipole moment of OCS is less in the vibrational states than in the ground state. It is 0.825% less in (100) state

and 2.224% in the ($02^{\circ}0$) state. The value of the dipole moment in the ($01^{\circ}0$) state is reported to be 1.53% less than that in the ground state by Reinartz et al. (24).

2. The variation of the dipole moment with isotopic substitution is also appreciable. The substitution of ^{18}O, ^{13}C and ^{34}S in OCS increases the dipole moment by 1.83%, 0.294%, and 1.413%, respectively. However, there is a large decrease of 12.44% in the value of the dipole moment by isotopic substitution of ^{33}S, which has the quadrupole constant of 29.07 MHz.

A variation of dipole moment with vibrational state is intuitively reasonable, since the molecular structure and the charge distribution differ from those in the ground state. The dipole moment variation can be treated approximately by considering the change of the effective bond length with vibrational quantum number. The change in the dipole moment depends not only on the bending or change in the relative directions of O-C and C-S bonds, but also on the electronic wave functions involved in each bond due to vibration. Since each isotopic species has slightly different vibrational energy the variation of dipole moment with isotopic substitution is also reasonable.

BIBLIOGRAPHY

(1) G. Herzberg, Molecular Spectra and Molecular Structure II, D. Van Nostrand Co., Inc., 1968.

(2) D.M. Dennison and G.E. Uhlenbeck, Phys. Rev. 41, 313 (1932).

(3) M.F. Manning, J. Chem. Phys. 3, 136 (1935).

(4) R.R. Newton and L.H. Thomas, J. Chem. Phys. 16, 310 (1948).

(5) C.C. Costain and G.B.B.M. Sutherland, J. Phys. Chem. 56, 321 (1952).

(6) J.D. Swalen and James A. Ibers, J. Chem. Phys. 36, 1914 (1962).

(7) R.J. Damburg and R. Kh. Propin, Chem. Phys. Letters 14, 82 (1972).

(8) Timothy D. Davis and Ralph E. Christoffersen, Chem. Phys. Letters 20, 317 (1973).

(9) William T. Weeks, Karl T. Hecht, and David M. Dennison, J. Mol. Spectrosc. 8, 30 (1962).

(10) W.S. Benedict and Earl K. Plyler, Can. J. Phys. 35, 1235 (1957).

(11) V. Spirko, J.M.R. Stone, and D. Papousek, J. Mol. Spectrosc. 60, 159 (1976).

(12) B. Bleany and R.P. Penrose, Nature 157, 339 (1946).

(13) H.Y. Sheng, E.F. Barker, and D.M. Dennison, Phys. Rev. 60, 786 (1941).

(14) C.C. Costain, Phys. Rev. 82, 108 (1951).

(15) E. Schnabel, T. Torring, and W. Wilke, Z. Physik 188, 167 (1965).

(16) H.H. Nielsen and D.M. Dennison, Phys. Rev. 72, 1101 (1947).

(17) D.K. Coles, and W.E. Good, Phys. Rev. 70, 979 (1946).

(18) R.H. Hughes, and E.B. Wilson Jr., Phys. Rev. 71, 562 (1947).

(19) Fujio Shimizu, J. Chem. Phys. 51, 2754 (1969).

(20) Landolt and Bornstein, Molecular constants from microwave spectroscopy, II/4, Springer-Verlag, New York, 1967.

(21) J. R. Eshbach, R. E. Hillger and M. W. P. Strandberg, Phys. Fev. 85, 532 (1952).

(22) H. A. Dijkerman and G. Ruitenberg, Chem. Phys. Letters 3, 172 (1969).

(23) F. H. De Leeuw and A. Dymanus, Chem. Phys. Letters 7, 288 (1970); Chem. Phys. Letters 3, 172 (1969).

(24) J. M. L. J. Reinartz, W. L. Meerts and A. Dymanus, Chem. Phys. Letters 16, 576 (1972).

(25) A. Battaglia, A. Gozzini and E. Polacco, Arch, Des Sciences, 13, 171, (1960); W. H. Flygare, W. Huttner, and P. D. Foster, J. Chem. Phys., 50, 1714, (1969); M. Redon and M. Fourrier, Chem. Phys. Letters, 17, 1,114 (1972); R. M. Lees, J. Mol. Spectrosc., 69, 225, (1968).

(26) Arthur G. Earle, The Microwave Spectra of Tertiary Butyl Chloride and Tertiary Butyl Bromide, M.Sc. Thesis, Memorial University of Newfoundland, 1974.

(27) W. Gordy, W. V. Smith, R. F. Trambarolo, Microwave Spectroscopy, Dover, 1953, 15

(28) H. S. Muenter, J. Chem. Phys. 48, 4544, 1968.

(29) W. Gordy, Rev. Mod. Phys. 20, 671, 1948.

(30) Microwave Spectral Tables, NBS Monograph 70, Volume IV, pp. 369-371.

APPENDIX I. Schnabel, Torring and Wilke's formula for the ground State inversion lines of $^{14}NH_3$

$$\begin{aligned}\nu = \nu_o \exp\big(& A_1 Y + A_2 Y^2 + A_3 Y^3 + A_4 Y^4 + A_5 Y^5 \\ & + A_6 X + A_7 X Y + A_8 X Y^2 + A_9 X Y^3 + A_{10} X Y^4 \\ & + A_{11} X^2 + A_{12} X^2 Y + A_{13} X^2 Y^2 + A_{14} X^2 Y^3 \\ & + A_{15} X^3 + A_{16} X^3 Y + A_{17} X^3 Y^2 \\ & + A_{18} X^4 + A_{19} X^4 Y \\ & + A_{20} X^5 \big)\end{aligned}$$

where $X = J(J+1)$ and $Y = K^2$

$\nu_o = 23\ 785.877_4$ MHz

$A_1 = 8.89166044 \times 10^{-3}$

$A_2 = 6.82956601 \times 10^{-7}$

$A_3 = 3.66026044 \times 10^{-9}$

$A_4 = 1.02312849 \times 10^{-11}$

$A_5 = 2.08517390 \times 10^{-14}$

$A_6 = -6.37113219 \times 10^{-3}$

$A_7 = -2.04826749 \times 10^{-6}$

$A_8 = -9.19702558 \times 10^{-9}$

$A_9 = -3.17220556 \times 10^{-11}$

$A_{10} = -7.44622471 \times 10^{-14}$

$A_{11} = 9.73962594 \times 10^{-7}$

$A_{12} = 7.66861022 \times 10^{-9}$

$A_{13} = 3.48189589 \times 10^{-11}$

$A_{14} = 1.04852978 \times 10^{-13}$

$A_{15} = -2.07544023 \times 10^{-9}$

$A_{16} = -1.57805504 \times 10^{-11}$

$A_{17} = -7.15251973 \times 10^{-14}$

$A_{18} = 2.39229413 \times 10^{-12}$

$A_{19} = 2.33418889 \times 10^{-14}$

$A_{20} = -2.95350627 \times 10^{-15}$

APPENDIX II. MUN Computations (G. Pedersen and P. Gillard, Private Communication)

Fit to the fourth power of X and Y in the Costain-Schabel's formula

$$\nu_4 = \exp\left(A_1' + A_2' X + A_3' Y + A_4' X^2 + A_5' XY + A_6' Y^2 + A_7' X^3 + A_8' X^2 Y + A_9' XY^2 + A_{10}' Y^3 + A_{11}' X^4 + A_{12}' X^3 Y + A_{13}' X^2 Y^2 + A_{14}' XY^3 + A_{15}' Y^4 \right)$$

where $X = J(J+1)$ and $Y = K^2$

$A_1' = 10.07624$

$A_2' = -6.351096 \times 10^{-3}$

$A_3' = 8.868682 \times 10^{-3}$

$A_4' = 7.361310 \times 10^{-7}$

$A_5' = -1.511275 \times 10^{-6}$

$A_6' = 4.125797 \times 10^{-7}$

$A_7' = -7.878753 \times 10^{-10}$

$A_8' = 3.191010 \times 10^{-9}$

$A_9' = -4.325049 \times 10^{-9}$

$A_{10}' = 1.976797 \times 10^{-9}$

$A_{11}' = -7.947429 \times 10^{-13}$

$A_{12}' = 4.238329 \times 10^{-13}$

$A_{13}' = 5.284553 \times 10^{-12}$

$A_{14}' = -1.012030 \times 10^{-11}$

$A_{15}' = 6.082239 \times 10^{-12}$

These coefficients were obtained by least squares fitting to the frequencies and quantum numbers of forty-three lines ranging in frequency from 7617.90 MHz, (J=14, K=4) to 15933.32 MHz, (J=11, K=7) taken from the Microwave Spectral Tables, (Vol. IV), (30). Lines with K=3 and K=6 were not used, because these need the corrections described on page 38.

Table of frequencies computed by G.Pedersen and Paul Gillard.

From $\nu = \exp S$, where S is a polynomial of degree 4 in the variables $J(J+1)$ and K^2.

J	K	frequency in MHz. ($^{14}N H_3$)
2	0	22883.134
2	1	23086.781
3	0	22029.266
3	1	22225.120
3	2	22823.294
3	3	23856.612
4	0	20941.785
4	1	21127.732
4	2	21695.626
4	3	22676.559
4	4	24125.598
5	0	19660.039
5	1	19834.335
5	2	20366.625
5	3	21285.972
5	4	22643.841
5	5	24519.063
6	0	18228.239
6	1	18389.559
6	2	18882.191
6	3	19732.951
6	4	20989.308
6	5	22723.939
6	6	25042.015
7	0	16692.864
7	1	16840.312
7	2	17290.558
7	3	18068.028
7	4	19215.940
7	5	20800.433
7	6	22917.146
8	0	15100.111
8	1	15233.222
8	2	15639.662
8	3	16341.398
8	4	17377.286
8	5	18806.752
8	6	20715.659
8	7	23225.236
9	0	13493.632
9	1	13612.338
9	2	13974.773
9	3	14600.448
9	4	15523.866
9	5	16797.759
9	6	18498.254
9	7	20732.716
10	0	11912.663
10	1	12017.255
10	2	12336.568
10	3	12887.731
10	4	13701.007
10	5	14822.624
10	6	16319.257
10	7	18284.830
10	8	20850.681
11	0	10390.674
11	1	10481.734
11	2	10759.724
11	3	11239.495
11	4	11947.283
11	5	12923.133
11	6	14224.752
11	7	15933.330
11	8	18162.228
12	0	8954.552
12	1	9032.904
12	2	9272.080
12	3	9684.815
12	4	10293.589
12	5	11132.694
12	6	12251.499
12	7	13719.378
12	8	15633.044
12	9	18127.461
13	0	7624.317
13	1	7690.948
13	2	7894.339
13	3	8245.282
13	4	8762.826
13	5	9476.006
13	6	10426.585
13	7	11673.178
13	8	13297.369
13	9	15412.794
13	10	18178.727
14	0	6413.284
14	1	6469.293
14	2	6640.251
14	3	6935.207
14	4	7370.123
14	5	7969.316
14	6	8767.729
14	7	9814.348
14	8	11177.251
14	9	12951.079
14	10	15268.168
14	11	18315.377
15	0	5328.608
15	1	5375.142
15	2	5517.175
15	3	5762.211
15	4	6123.482
15	5	6621.135
15	6	7284.096
15	7	8152.879

J	K	frequency in MHz.
15	8	9283.668
15	9	10754.489
15	10	12674.145
15	11	15195.842
15	12	18537.934
16	3	4728.106
16	4	5024.722
16	5	5433.274
16	6	5977.459
16	7	6690.423
16	8	7618.103
16	9	8824.131
16	10	10397.084
16	11	12461.330
16	12	15193.517
16	13	18848.149
17	5	4402.063
17	6	4843.565
17	7	5421.942
17	8	6174.357
17	9	7152.211
17	10	8426.908
17	11	10098.445
17	12	12308.393
17	13	15259.894
17	14	19249.147
18	8	4940.418
18	9	5724.242
18	10	6745.714
18	11	8084.494
18	12	9853.019
18	13	12212.012
19	10	5330.290
19	11	6390.569
19	12	7790.498
19	13	9656.166
19	14	12169.734
20	10	4154.328
20	13	7539.475